4.0 DEPOSIT PH

A quick screening test was performed on the deposits that remained on the TTS, FDB and TSP regions following the tube pulling operation. The purpose of this test was to determine if the crevice chemistry was highly acidic or highly caustic. This test simply involved lightly wetting a piece of pH paper (Hydrion pH 0.0-13.0, Lot 233713, expiration date: 12-01-2016) with deionized water and pressing it against the deposits of interest. The resulting color of the pH paper was then compared with the color chart that came with the paper.

In all cases, in all TSP region surfaces/deposits and at both TTS regions, the pH paper indicated a neutral pH of 7.

5.0 LEAKAGE SCREENING AND BURST TESTING

5.1 Introduction

To determine if a leak path had developed through the tube wall, each of the two TSP regions with confirmed crack-like eddy current indications were screened for leakage. If leakage had been identified, leak rate measurements would have been conducted.

Each TSP region was pressurized to the pressures identified for in situ leak testing in the Degradation Assessment (Reference 18) using room temperature water. An assessment was made if the sample was leaking based on visual observations and the loss of internal pressure. The leak screening was performed without internal bladders and without fixtures that simulate the constraints of TSP intersections.

The primary purpose of the burst testing was to determine if the degraded tube sections exceeded the NEI 97-06 requirements on burst strength (Reference 19), as implemented by EPRI Tube Integrity Assessment Guidelines (Reference 20). The most limiting requirement is that the tube must sustain three times normal operating pressure differential (3NOP) without burst. 3NOP is approximately 4446 psid for Beaver Valley Unit 2 at temperature, or 4950 psid for room temperature testing (Reference 18).

All four TSP regions and two freespan samples were pressurized to burst failure using room temperature water. Burst testing of the TSP regions were conducted with fixtures that simulate the constraints of TSP intersections under accident conditions. The freespan samples were tested without constraints.

5.2 Sample Preparation

A total of six samples were cut from the tube segments for leak screening and burst testing. Samples having a TSP region were cut, as best as possible, to center the TSP region along its length. The ends of each sample were deburred prior to testing. The samples are summarized in Table 5-1, as are referenced to their corresponding sectioning diagrams.

Sections were stored in individual containers, each labelled with the appropriate row, column and section number. Traceability was maintained in accordance with appropriate WCS work instructions (Reference 11).

The two TSP regions with field ECT indications (02H from R19C38-3B and 04H from R24C41-6B) were leak screened and subsequently burst tested. The two TSP regions without confirmed field ECT indications (02H from R24C41-3B and 03H from R24C41-5B) were burst tested without leak screening. Freespan sections were also burst tested, so as to determine the burst pressure of an unflawed section from each tube.

The diameters and wall thicknesses of each sample were measured after cutting. These are presented in Table 5-2. OD measurements were made at the elevation where the section was expected to burst; in the case of sections with TSP regions, this was the TSP region and in the case of the freespan sections, this was at the mid-length of the sample. Wall thickness

measurements were made at the bottom end of each section; measurements may include deposit thickness.

In preparation for leak screening and burst testing, a dummy piece was tested for each type of test to check for proper operation of the equipment and for any leakage in the test lines. All equipment was found to be working properly and all sources of leakage from the test lines were sealed. The results of the dummy samples are not included in this report.

Swagelok fittings were then affixed to the tube ends and each tube was pre-filled with deionized water. One end of each sample had a fitting that allowed pressurized room temperature water to pass into the sample from a 1/8 inch diameter supply line.

5.3 Leak Screening

5.3.1 Procedure

Leak screening was conducted in accordance with the appropriate WCS work instructions (Reference 21). These work instructions are in compliance with EPRI Guidelines (Reference 22).

Each sample was connected to pressurization equipment, which included a calibrated pressure transducer used to measure the internal pressure of the tube, a valve to isolate the pressure inside the tube and a data acquisition system for recording the pressure transducer reading versus time.

Axial flaw leak test pressures included a temperature adjustment factor of 1.10 and 50 psi was added for measurement uncertainty. The actual combined accuracy of the pressure transducer and digital measurement systems was well within the 50 psi adjustment. Target test pressures were rounded up to the nearest increment of 25 psi. Three target test pressures were used: normal operating pressure differential (1700 psig), an intermediate test pressure (2250 psig), and steam line break (SLB) condition (2875 psig).

Each sample was pressurized to the target pressure of 1700 psig, held for five (5.0) minutes, pressurized to the second target pressure of 2250 psig, held for five (5.0) minutes, then pressurized to the final target pressure of 2875 psig and held for five (5.0) minutes. The reported hold times do not include a one-minute hold to allow for the test system to stabilize after the pressure had been increased.

During each hold period, each sample was periodically observed for signs of leakage. Tissue paper was pressed against the sample to aid in this observation. Also, the loss of internal pressure was observed as a second criterion. A loss of 100 psi (maximum) was allowed during the hold period to account for system stabilization.

5.3.2 Results

Neither sample showed any sign of leakage by either the visual observation or the pressure loss criteria at any pressure. The results are summarized in Table 5-3.

As neither sample with a confirmed eddy current indication leaked during room temperature testing, it was deemed unnecessary to test the samples at an elevated temperature.

5.4 Burst Testing

5.4.1 Procedure

Room temperature burst tests were performed in accordance with the Reference 23 procedure and the Reference 22 EPRI Guidelines. The pressurized water for the burst test was supplied by a piston delivery system. Pressure was increased and supplied to the sample with a single, controlled stroke of the piston. A feedback loop was used to establish a relatively constant pressurization rate of 20-500 psi/second. The internal pressure of the specimen was recorded digitally through a data acquisition system and a redundant data acquisition system.

The Reference 22 guidelines and the Reference 23 procedure allow the use of an internal bladder and backing foil in order to achieve a successful burst test elevated pressure when there is a pre-identified leak path from the tube. Since none of the samples had a leak path and all eddy current signals were relatively small, an internal bladder or foil was judged to be unnecessary and not used.

The TSP regions were laterally restrained by a support system designed to simulate the conditions in the Beaver Valley Unit 2 steam generators under accident conditions. Figure 5-1 shows a sketch of the support system. An unpressurized extension was attached to the top end of each sample by a welded cap that both sealed the top end and added several feet to its length. The top end of the extension passed through a ¾ inch wide support plate simulation while the attached test sample passed through another ¾ inch wide support plate simulation. The tube-to-support clearance was obtained from the Reference 24 document. The support plate simulations were spaced a fixed 50.5 inches apart (see Table 1-1). The centerline of the TSP region on each section was positioned two (2.0) inches above the centerline of the support plate simulation to conservatively approximate the displacement encountered by the bowing of the tubesheet with tubes that are not locked into their supports during accident conditions. The specimen was pressurized through a Swagelok fitting that connected the bottom of the specimen with the pressurization equipment.

The freespan samples were not tested with the support system.

Once each sample was connected to the pressurization equipment, it was pressurized to burst, without hold points, at a rate of 20-500 psi/second. Section 2.2 of the EPRI Guidelines (Reference 22) provides the acceptance criteria for a burst test.

5.4.2 Results

Figure 5-2 through Figure 5-7 provides the burst pressurization data for all of the burst tests. Table 5-4 summarizes the burst test results. All burst pressures were significantly greater than the 3NOP criteria of 4950 psig and thus meet NEI 97-06 (Reference 19) and EPRI Guideline (Reference 20) criteria.

The 02H region of R19C38 and the 04H region of R24C41 both burst within the TSP region, both at 9678 psig. The other four samples burst in a freespan region at pressures equal to or above 10,733 psig. All bursts were axially-orientated.

5.4.3 Post-Burst Observations

Table 5-4 presents a summary of the post-test measurements made on the burst test samples.

Figure 5-8 through Figure 5-13 present photos of the burst openings. Tearing was confirmed at all burst tips, by microscope, for all six samples, thus (in accordance with Reference 22 criteria) each burst test was considered to be a valid burst test. The 02H region of R19C38 and the 04H region of R24C41 (Figure 5-8 and Figure 5-12, respectively) show secondary cracks outside of the burst opening; the freespan bursts of the other four samples showed no evidence of any cracks.

Each burst test sample was viewed under a stereomicroscope around its entire circumference in the vicinity of the burst. No corrosion or cracks were observed in the vicinity of any freespan burst.

Each burst test sample with a TSP location was also viewed under a stereomicroscope around its entire circumference in the vicinity of the TSP region. Cracks were observed in all four TSP regions of various depths and numbers. Cellular cracking was not observed. One TSP region had marginally-discernable OD corrosion that was difficult to distinguish as a region of short axial cracks or intergranular attack (IGA). Cracking was not found outside of a TSP region.

Each TSP region was viewed under a stereomicroscope (up to 20X magnification) to identify the location of cracks, corrosion or other features. These were mapped out to show location and extent, such as that shown in Figure 5-14. The features were photographed to provide qualitative documentation of the feature. In this section, each photo is oriented with the axial direction as horizontal and the bottom side of the view to the left side of the photo.

The 02H TSP region of tube R19C38 burst in the TSP region. The center of the burst was skewed about 0.2 inches above the TSP centerline and the burst opening extended above and below the TSP region. The burst occurred at the 350° orientation. There were several regions of short (<0.15 inch) axial cracks around the circumference, most of which were located near the burst opening. These are shown in the Figure 5-14 diagram. Some of

these short cracks can be seen near the burst opening as shown in Figure 5-8; others are shown in Figure 5-15, Figure 5-16 and Figure 5-17.

The 02H TSP region of tube R24C41 did not have a burst. There was a region of marginally-discernable (shallow) corrosion that was partially obscured by surface deposits, and was either a patch of short axial cracks or IGA. It also had another region with shallow corrosion that was discernable as axial cracks. These are shown in the Figure 5-18 diagram and in the Figure 5-19 photo.

The 03H TSP region of tube R24C41 did not have a burst. There were two regions with shallow cracks. These are shown in the Figure 5-20 diagram. The photo in Figure 5-21 shows the shallow axial cracks located near the 180° orientation, as indicated by the two arrows. Figure 5-22 shows the shallow cracks at the top of the TSP region near the 0° orientation. These cracks are all less than 50 mils long and are primarily axial. The axial crack nearest the bottom of Figure 5-22 appears to have a circumferential element, but this is a shadow cast by raised surface deposits and is not a crack.

The 04H TSP region of tube R24C41 burst in the TSP region. The center of the burst was aligned with the TSP centerline and the burst opening extended above and below the TSP region. The burst occurred at the 90° orientation. There were several regions of small axial cracks around the circumference, most of which were located near the centerline of the TSP region. There was another region of larger axial cracks, located between 315° and 360°, all within the center third (0.25-inch long) portion of the TSP length. These are shown in the Figure 5-23 diagram. Figure 5-24 and Figure 5-25 show the region of the larger cracks. These cracks are significantly oriented in the axial direction. Figure 5-12 shows some cracking adjacent to the burst opening; Figure 5-26 shows a closer view of these cracks.

Table 5-1: Leak and Burst Test Samples

Tube	Segment	Region	Confirmed ECT Indication	Sectioning Diagram	Section Tested	Leak Screen	Burst Test
R19C38	3	TSP (02H)	x	Figure 6-3	R19C38-3B	x	x
	4	Freespan		Figure 6-7	R19C38-4B		x
R24C41	3	TSP (02H)		Figure 6-13	R24C41-3B		x
	5	TSP (03H)		Figure 6-18	R24C41-5B		x
	6	TSP (04H)	x	Figure 6-21	R24C41-6B	x	x
	7	Freespan		Figure 6-24	R24C41-7B		x

Table 5-2: Pre-Leak/Burst Test Wall Thickness Measurements

Tube	R19C38	R19C38	R24C41	R24C41	R24C41	R24C41
Segment	3B	4B	3B	5B	6B	7B
Region	02H TSP	freespan	03H TSP	04H TSP	05H TSP	freespan
Length (in)	12.0	12.0	12.0	12.0	12.0	12.0
OD Measurement Location (in)	BES+6.0	BES+6.0	BES+6.0	BES+4.5	BES+6.0	BES+6.0
OD (0°-180°) (in)	0.876	0.876	0.873	0.879	0.880	0.873
OD (90°-270°) (in)	0.876	0.876	0.869	0.880	0.876	0.874
Wall Thickness 0° (in)	0.056	0.056	0.054	0.056	0.057	0.052
Wall Thickness 90° (in)	0.060	0.058	0.055	0.056	0.057	0.056
Wall Thickness 180° (in)	0.057	0.053	0.055	0.057	0.056	0.055
Wall Thickness 270° (in)	0.054	0.055	0.057	0.055	0.057	0.057

Note – OD and wall thickness measurements may also include deposits
BES = Bottom End of Section

Table 5-3: Leak Screening Results

Sample	Region	Target Pressure (psig)	Start Pressure (psig)	End Pressure (psig)	Leakage Observed
R19C38-3B	02H	1700	1799	1789	no
		2250	2253	2243	no
		2875	2905	2892	no
R24C41-6B	04H	1700	1743	1719	no
		2250	2335	2315	no
		2875	3070	3040	no

Table 5-4: Burst Results and Post-Burst Measurements

Tube	R19C38	R19C38	R24C41	R24C41	R24C41	R24C41
Section	3B	4B	3B	5B	6B	7B
Region	02H	Freespan	02H	03H	04H	Freespan
Burst Pressure (psig)	9,678	10,983	10,741	10,733	9,678	10,770
Burst Orientation	axial	axial	axial	axial	axial	axial
Avg. Pressurization Rate (psi/sec)	100	99	98	99	99	97
Location of Burst	02H	freespan	freespan	freespan	04H	freespan
Center of Burst, inches above bottom	6.20	4.91	8.20	7.73	6.00	5.29
Azimuthal Location of Burst	350°	310°	315°	220°	90°	240°
Length of Burst Opening (in)	1.20	1.91	1.42	1.83	1.28	1.82
Width of Burst Opening (in)	0.33	0.38	0.32	0.36	0.33	0.41
Maximum Diameter (in)	1.180	1.249	1.309	1.265	1.102	1.285
Diameter, 90° from Maximum (in)	1.066	1.103	1.154	1.129	1.076	1.137

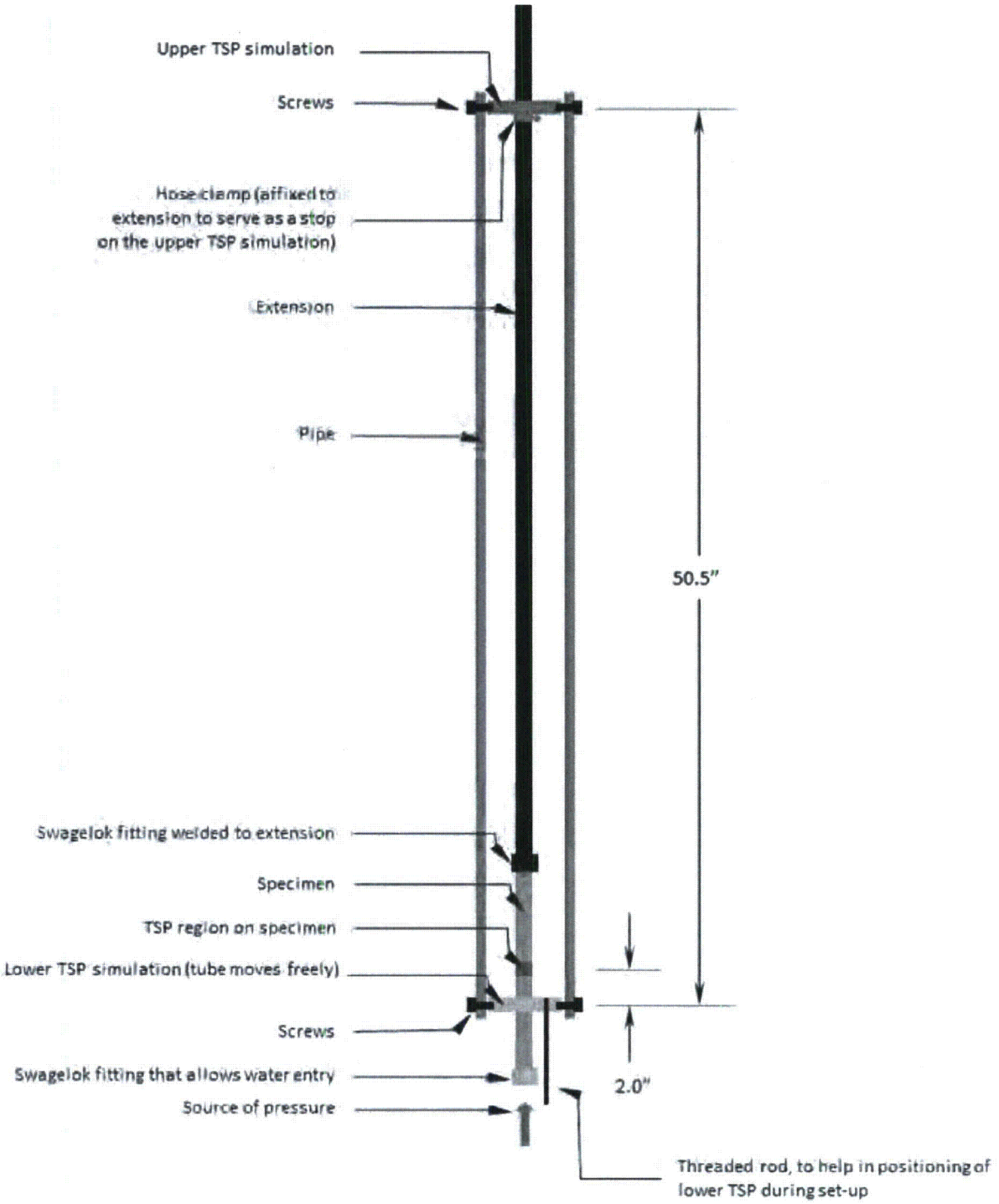

Figure 5-1: Burst Test Support Simulation

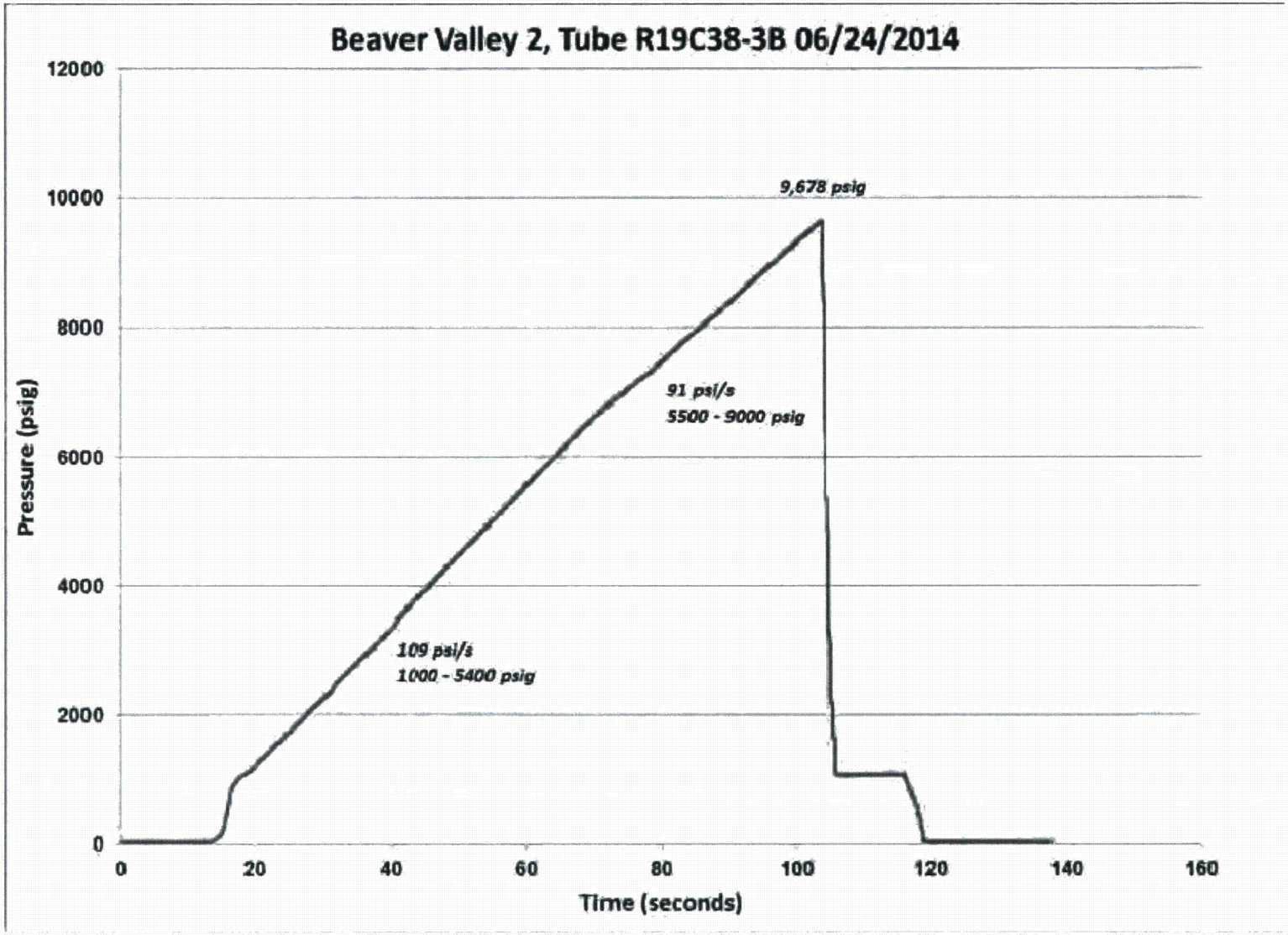

Figure 5-2: Burst Pressurization of R19C38-3B (02H)

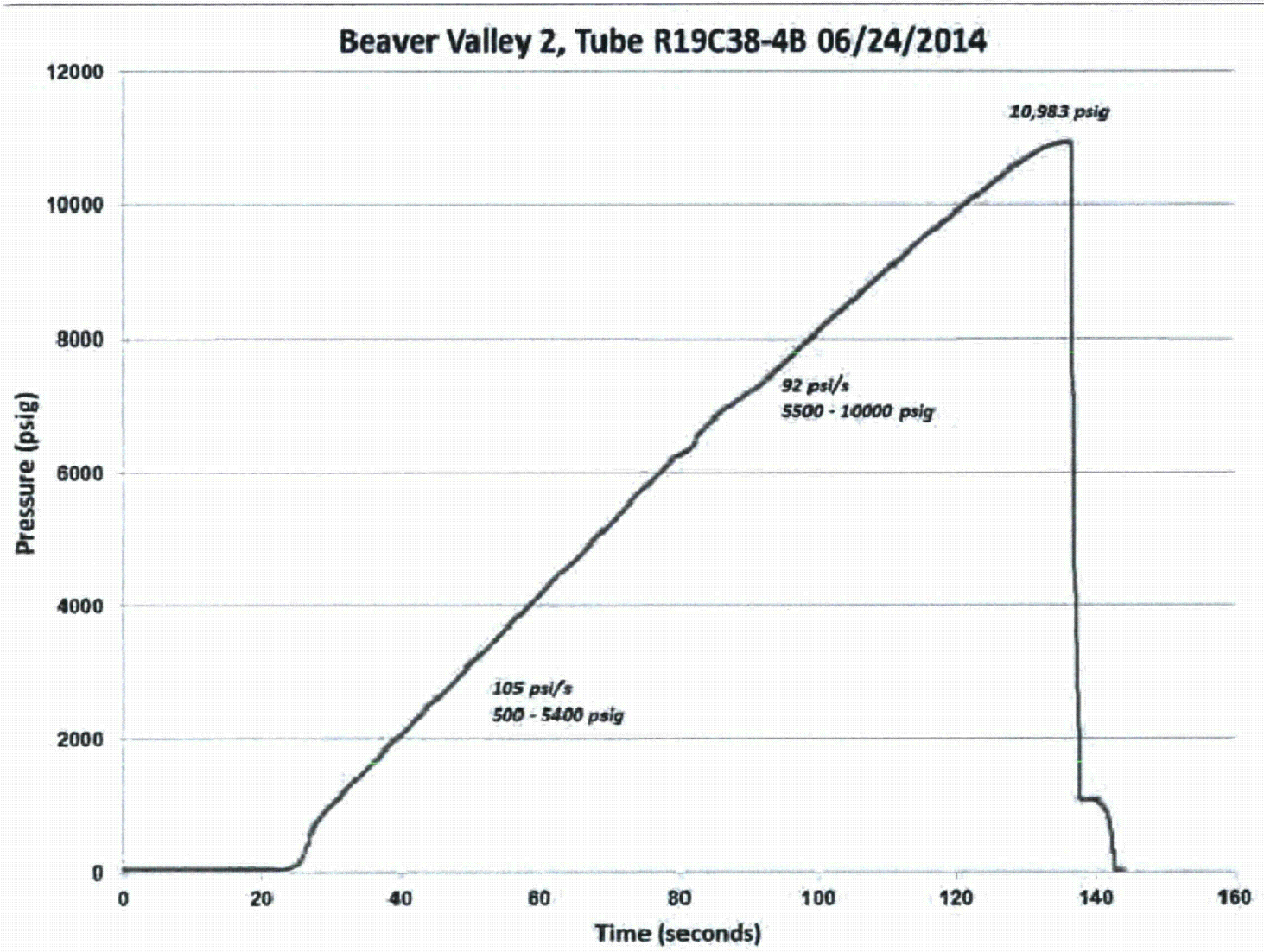

Figure 5-3: Burst Pressurization of R19C38-4B (Freespan)

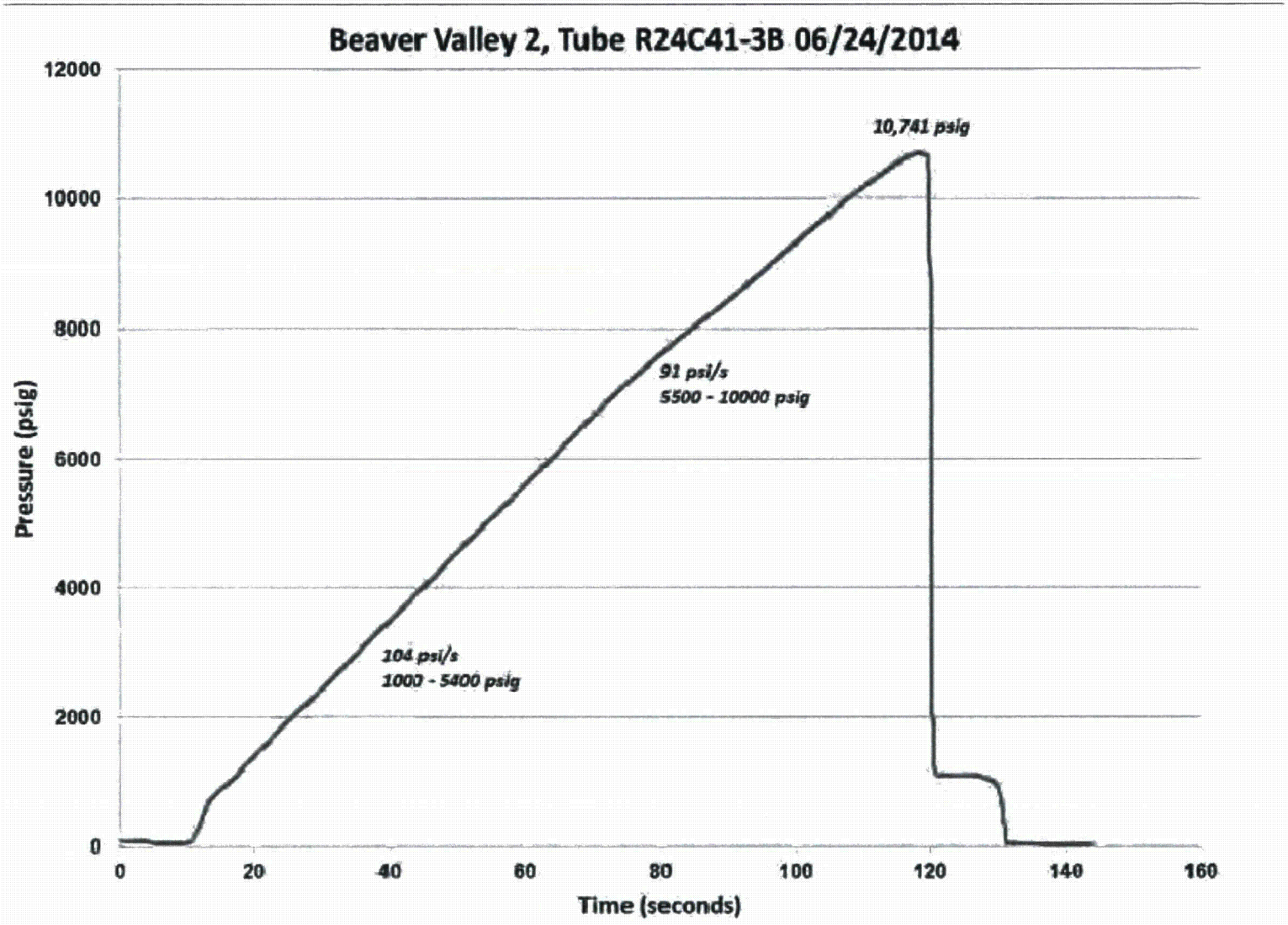

Figure 5-4: Burst Pressurization of R24C41-3B (02H)

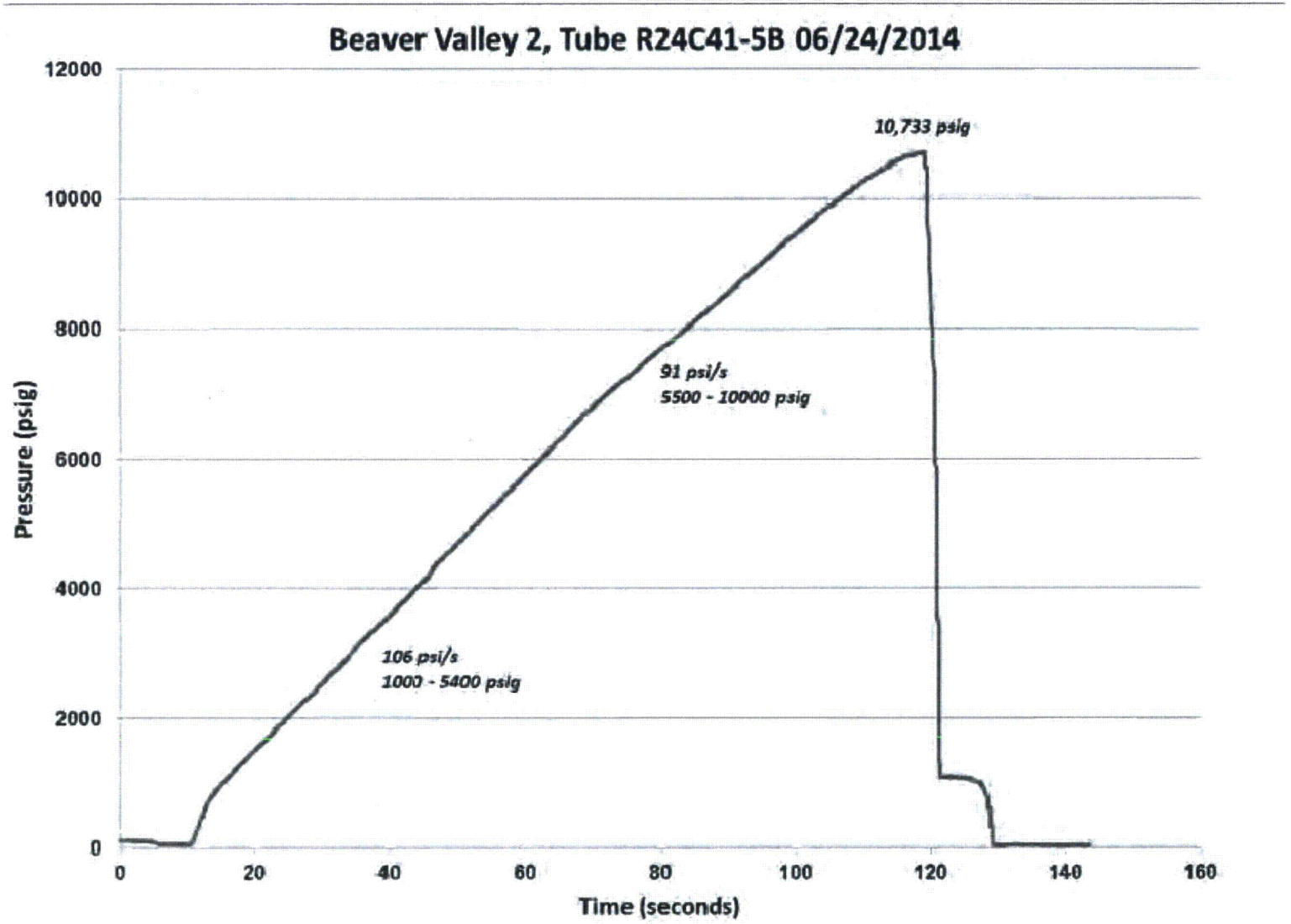

Figure 5-5: Burst Pressurization of R24C41-5B (03H)

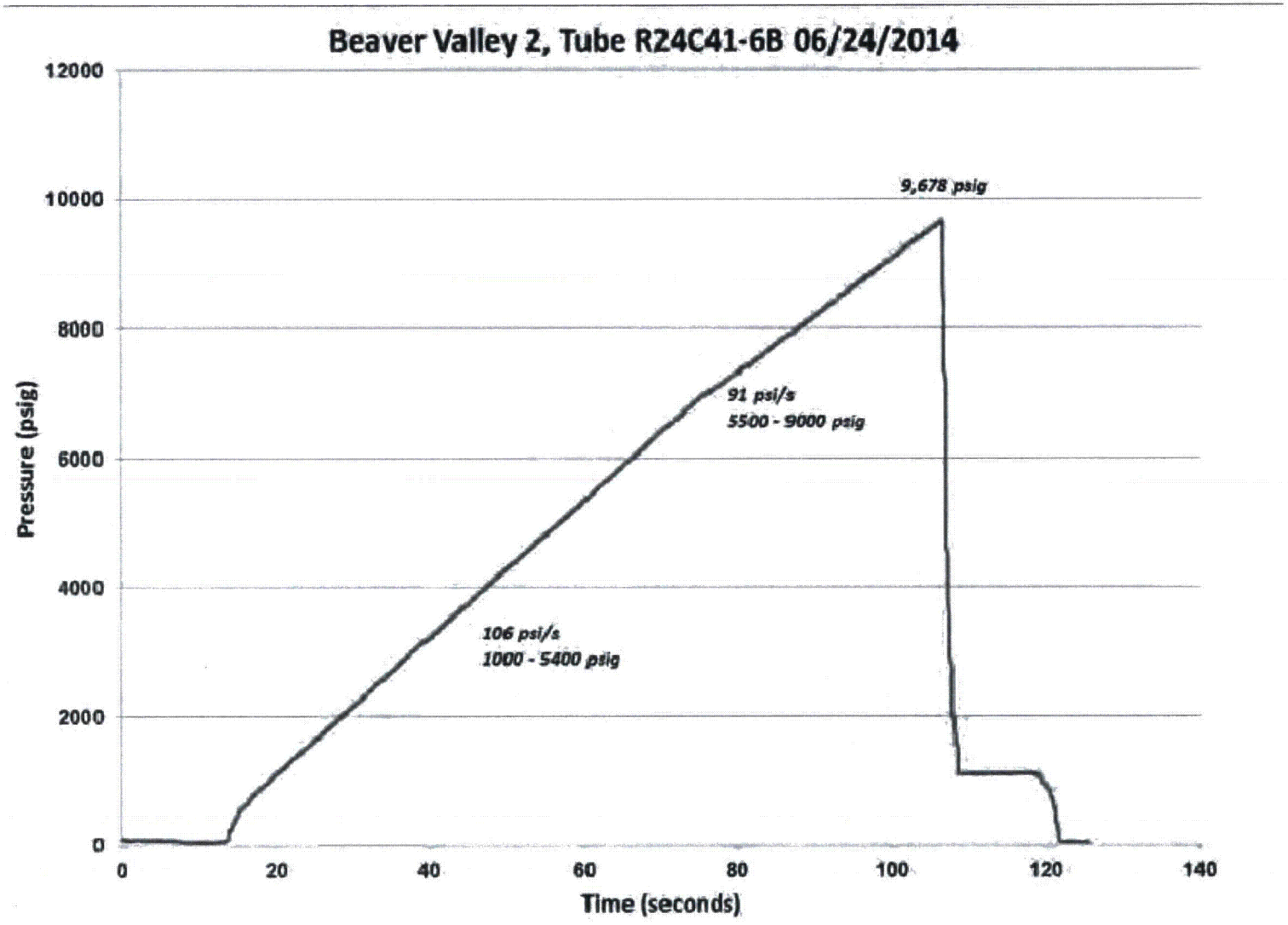

Figure 5-6: Burst Pressurization of R24C41-6B (04H)

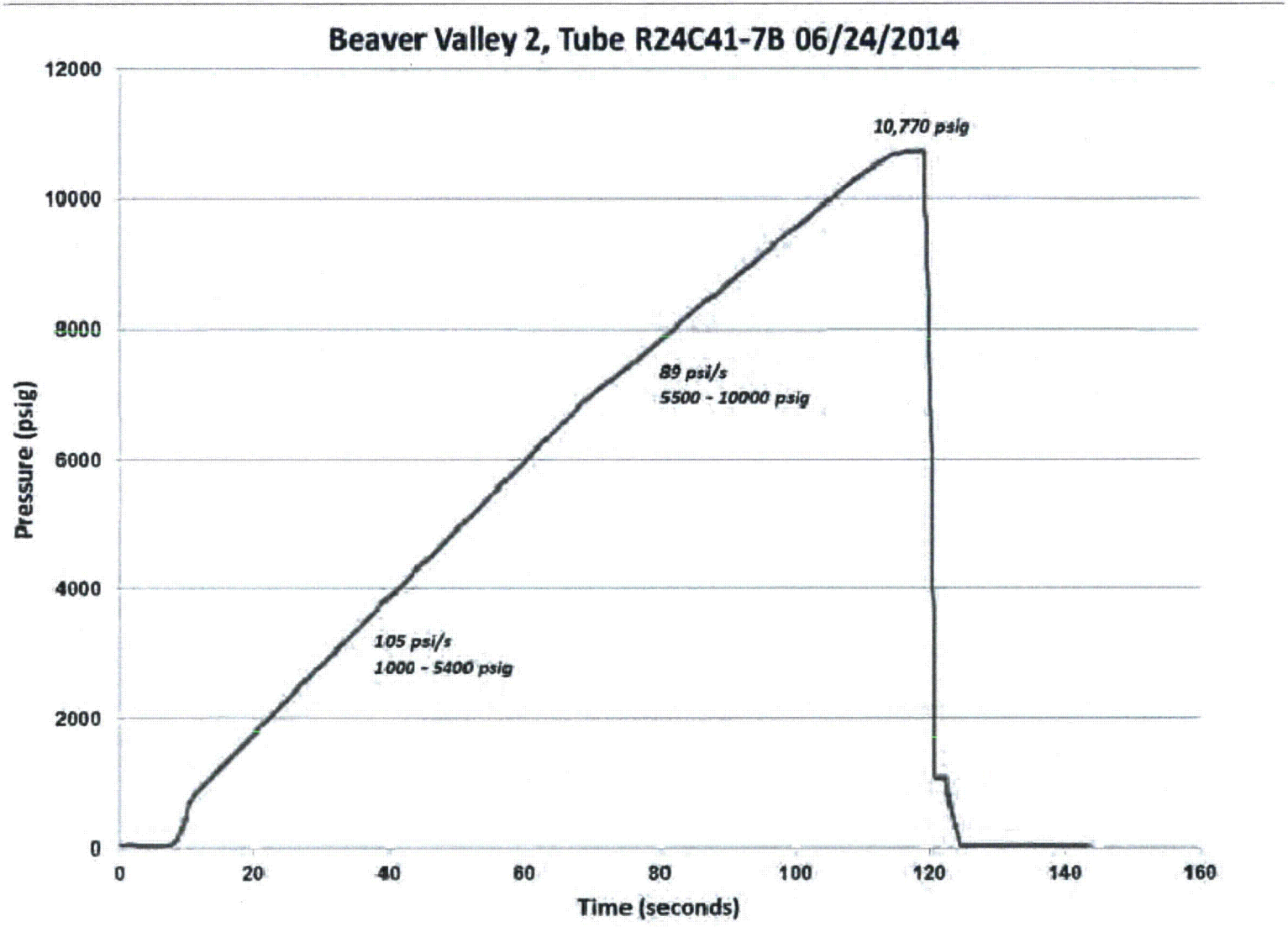

Figure 5-7: Burst Pressurization of R24C41-7B (Freespan)

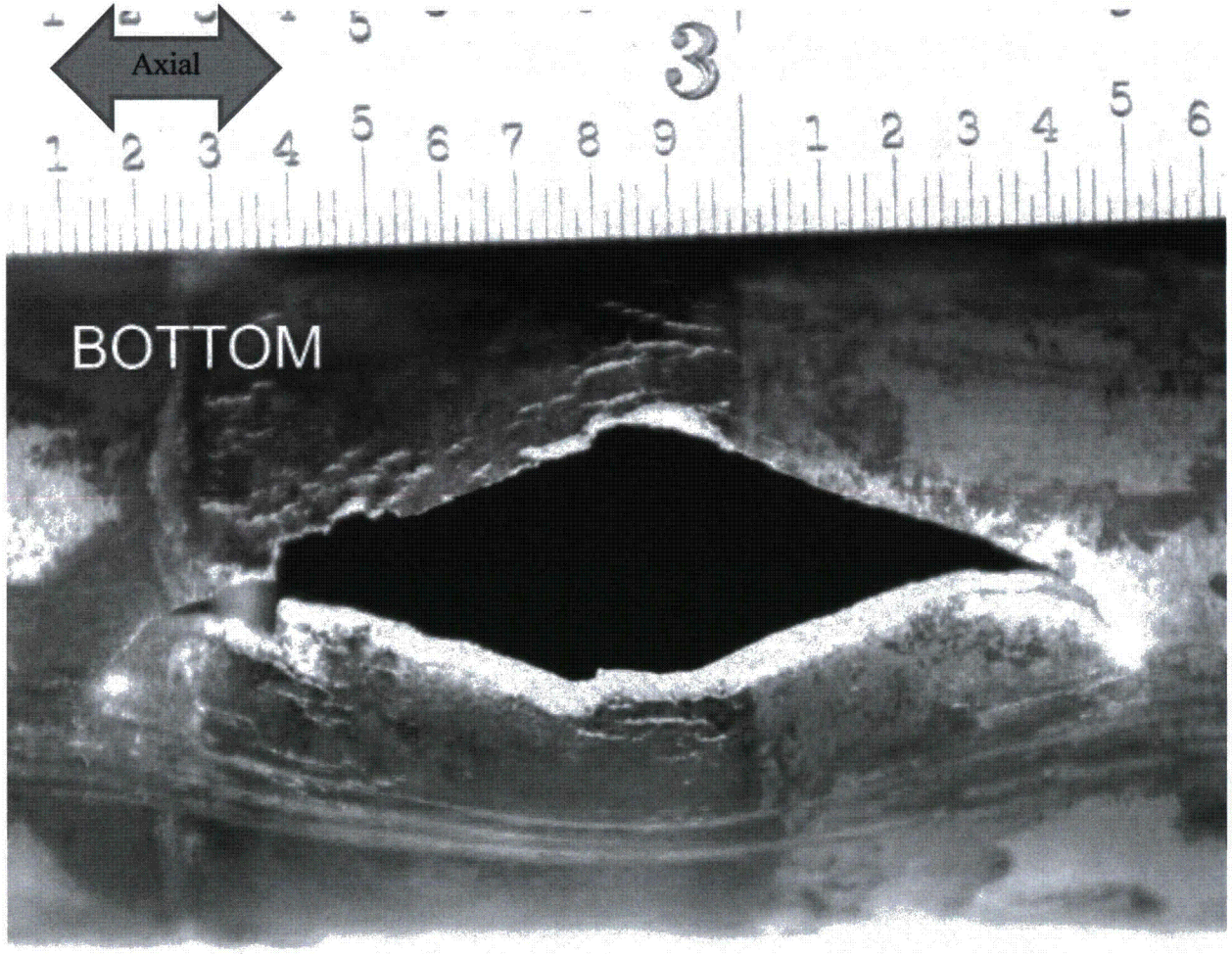

Figure 5-8: Burst Opening at R19C38-3B (02H)

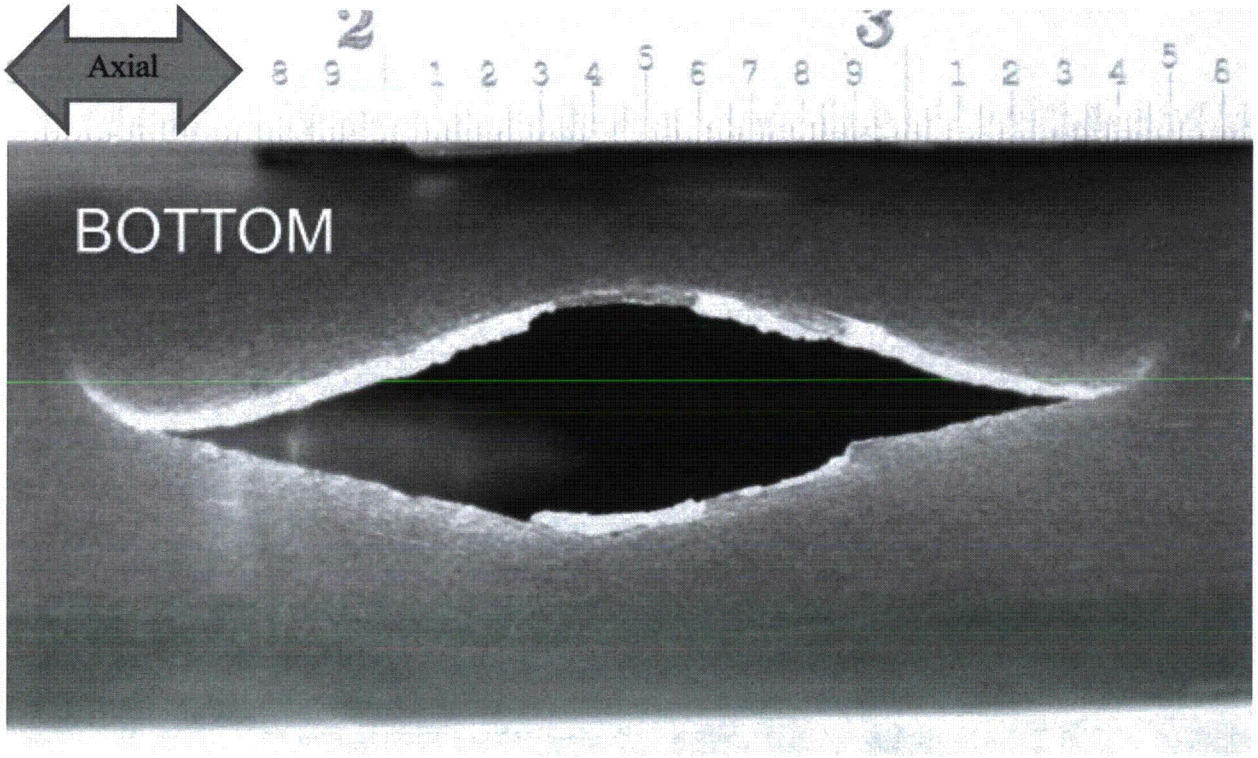

Figure 5-9: Burst Opening at R19C38-4B (Freespan)

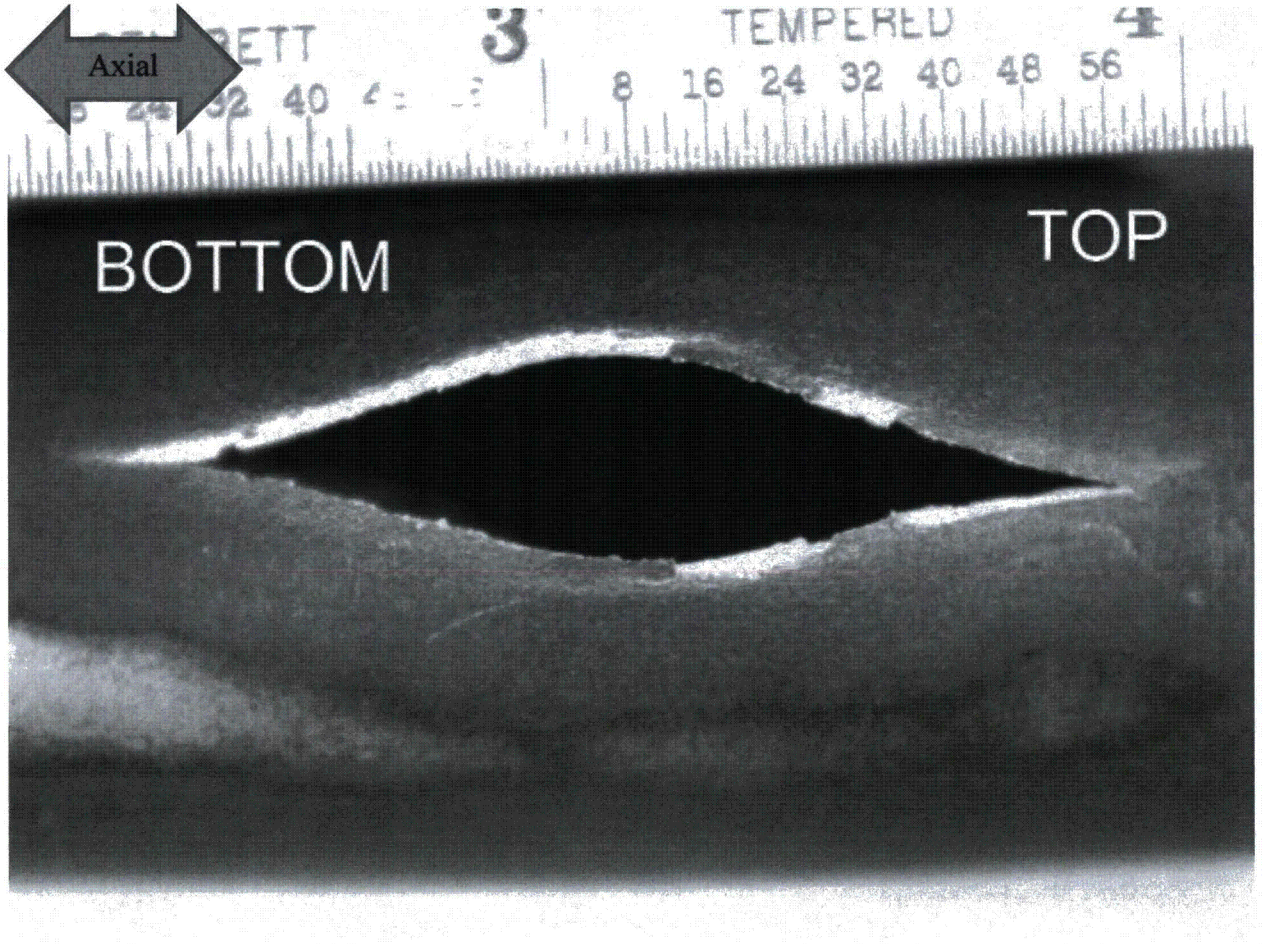

Figure 5-10: Burst Opening at R24C41-3B (Burst in Freespan, Outside of 02H)

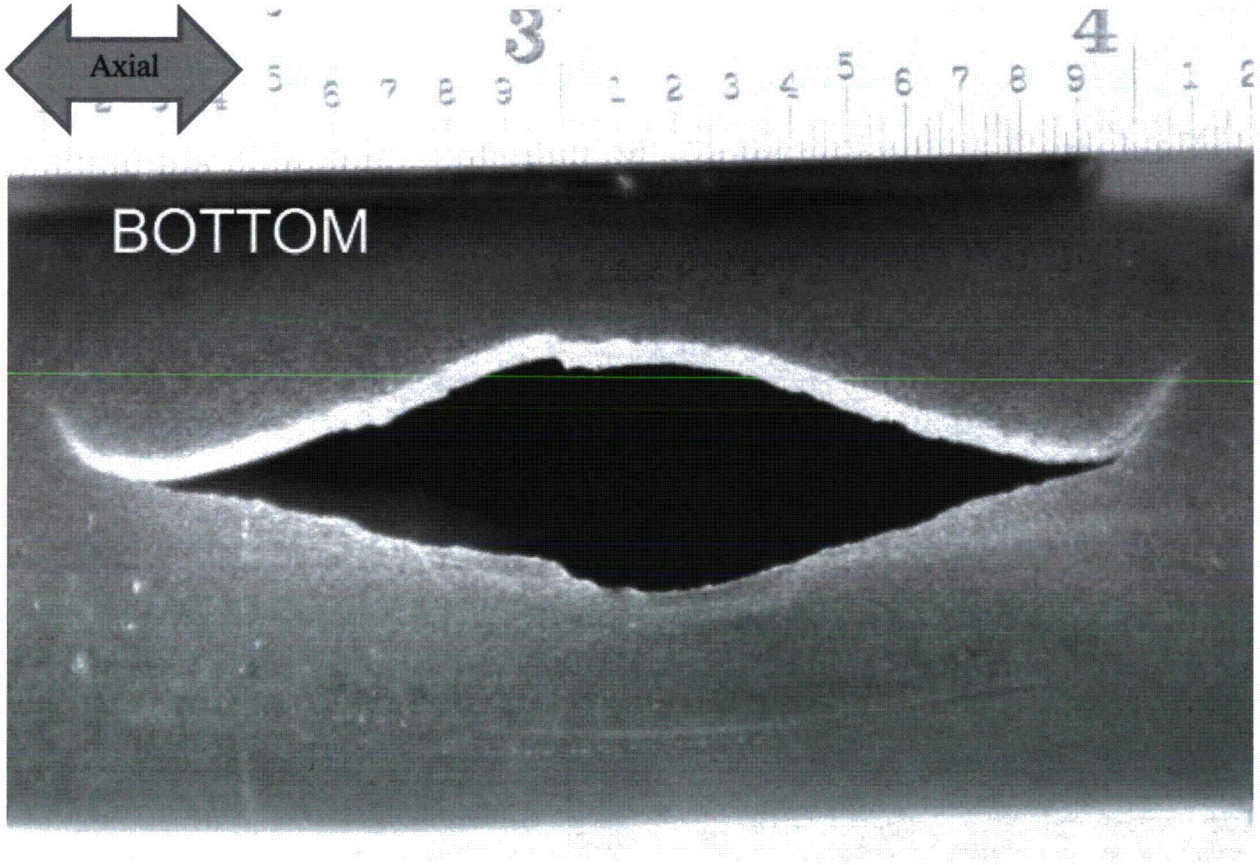

Figure 5-11: Burst Opening at R24C41-5B (Burst in Freespan, Outside of 03H)

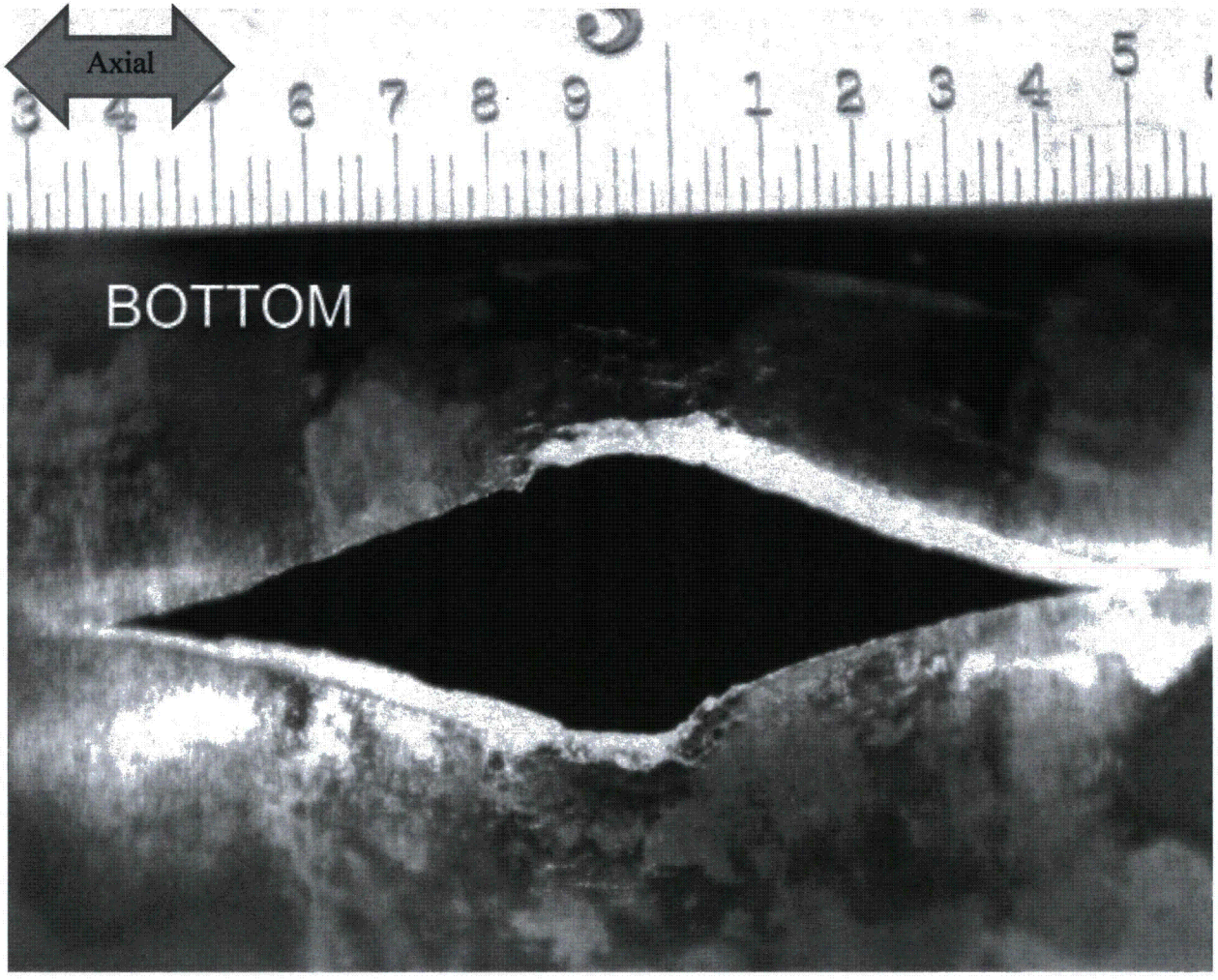

Figure 5-12: Burst Opening at R24C41-6B (04H)

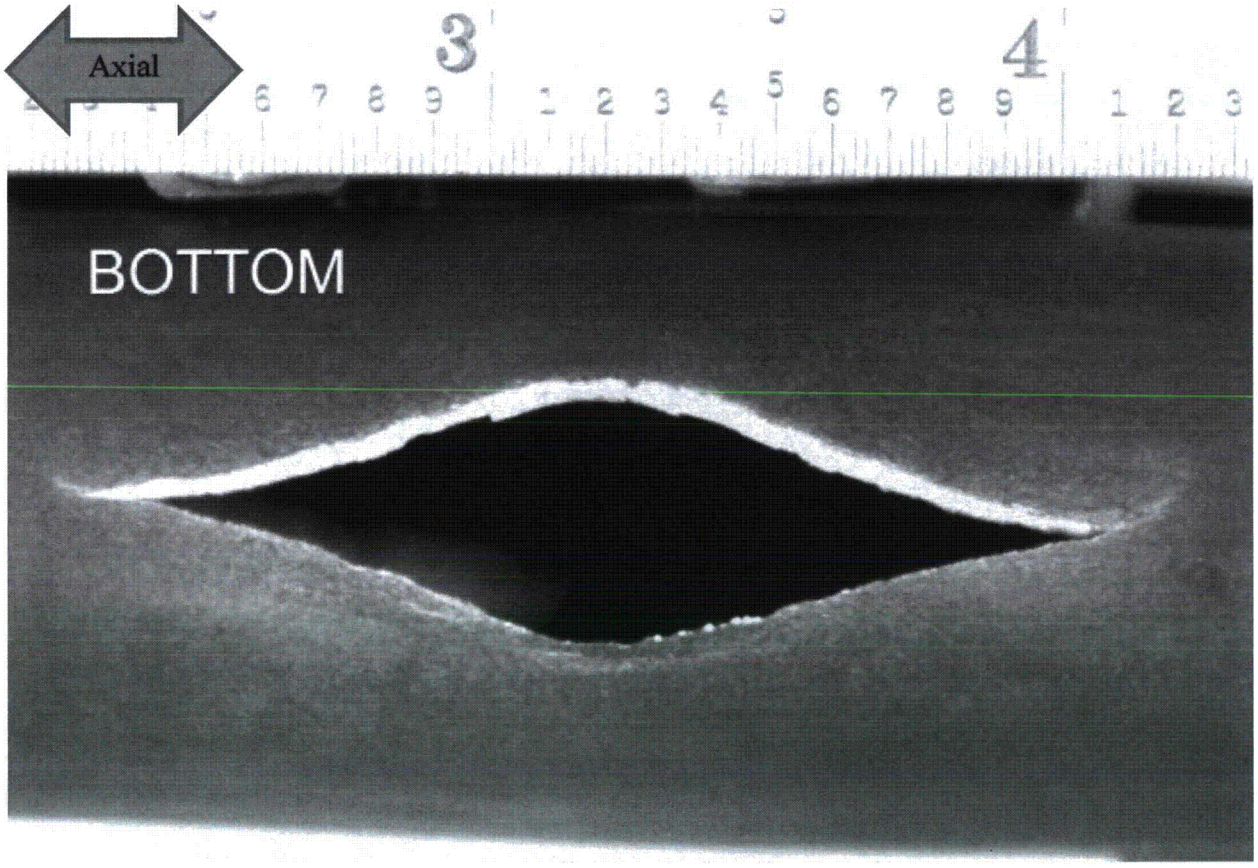

Figure 5-13: Burst Opening at R24C41-7B (Freespan)

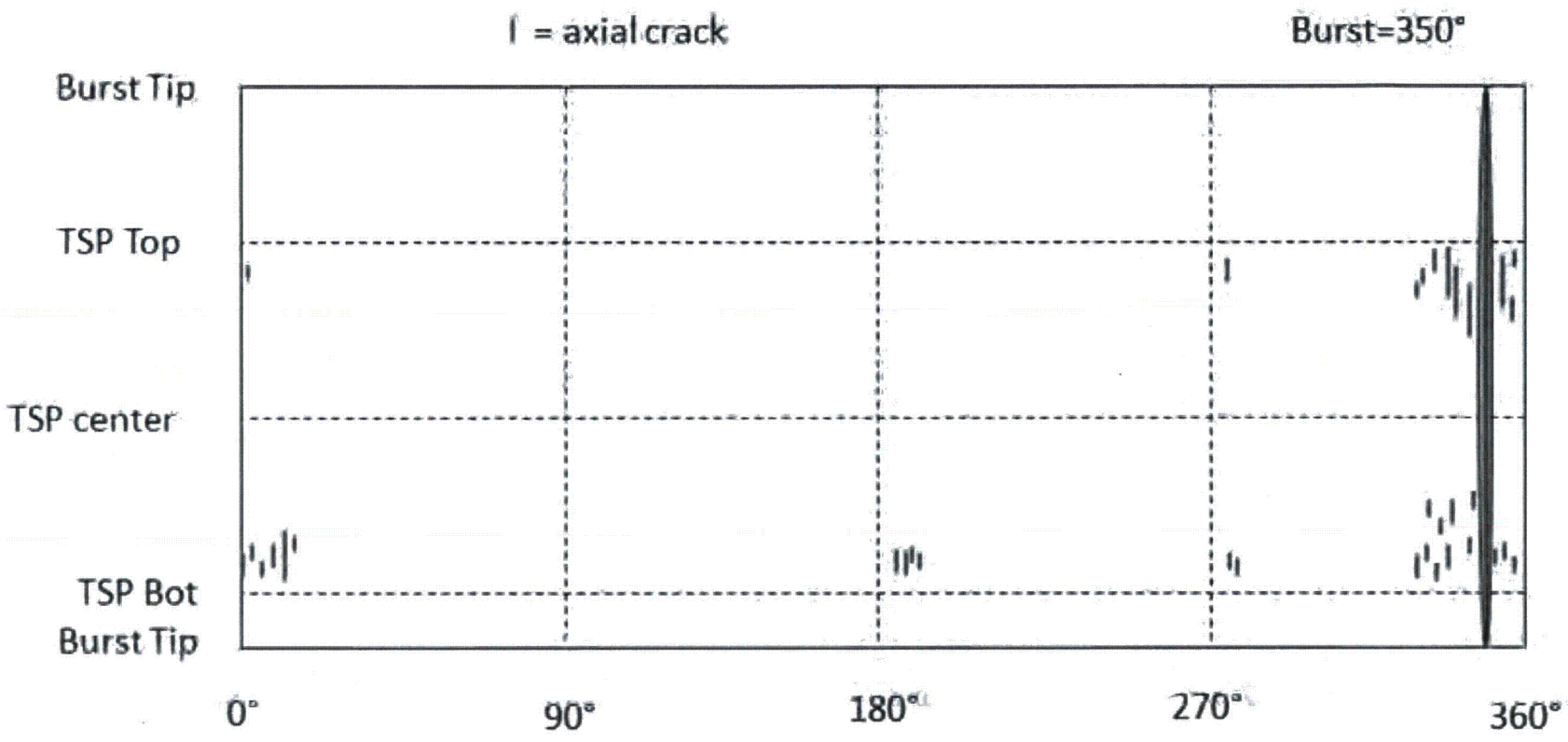

Figure 5-14: Post-Burst Observations on R19C38-3B (02H Region)

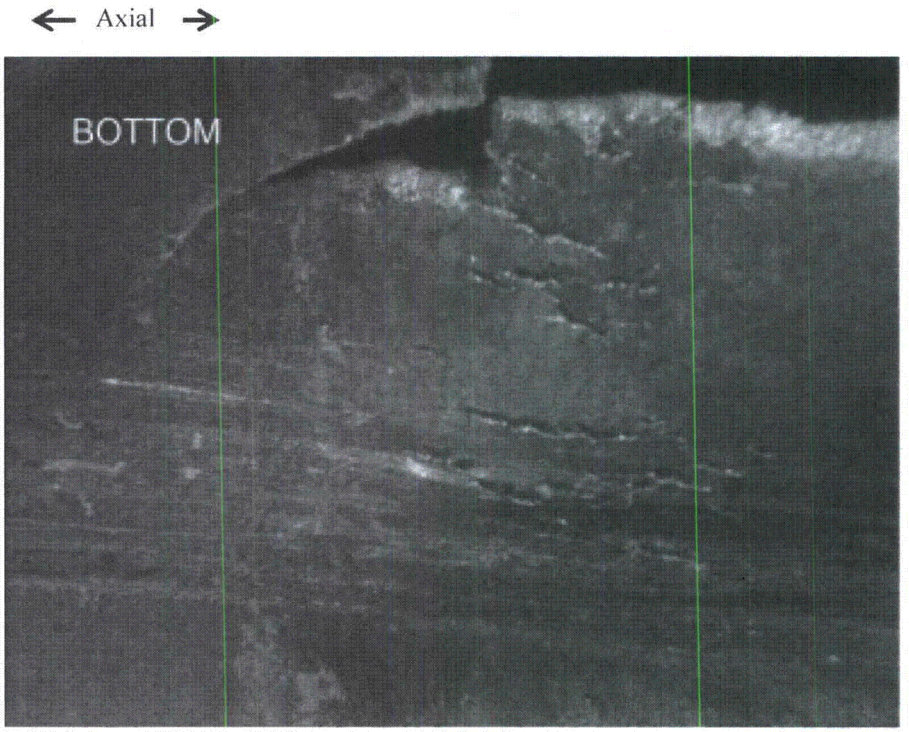

Figure 5-15: Short Cracks near the Bottom of the 02H TSP of R19C38 (0° Orientation)

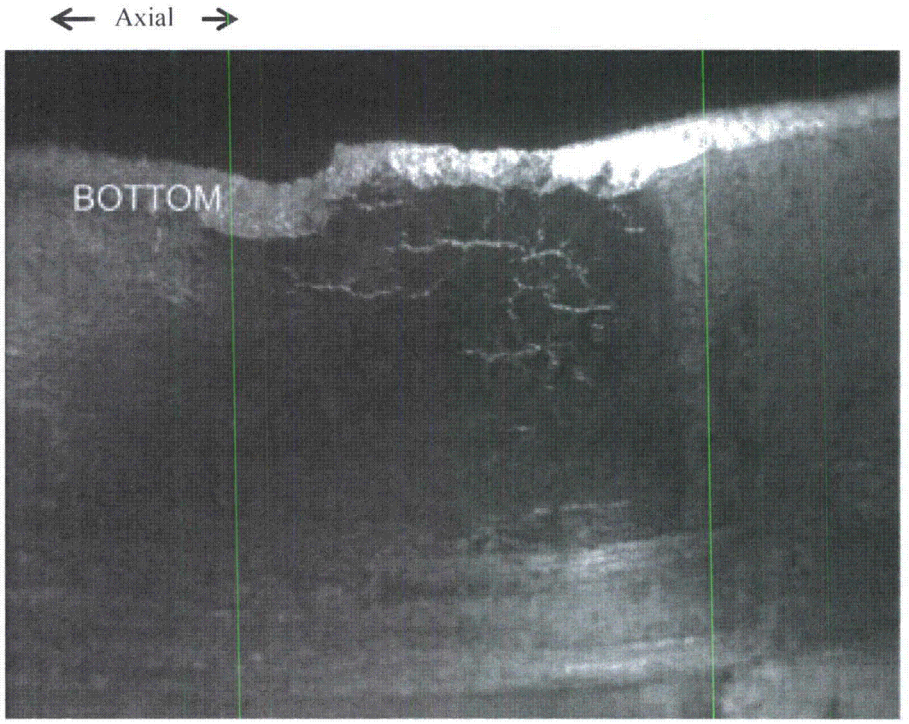

Figure 5-16: Short Cracks near the Top of the 02H TSP of R19C38 (0° Orientation)

Figure 5-17: Short Cracks near the Bottom of the 02H TSP of R19C38 (200° Orientation)

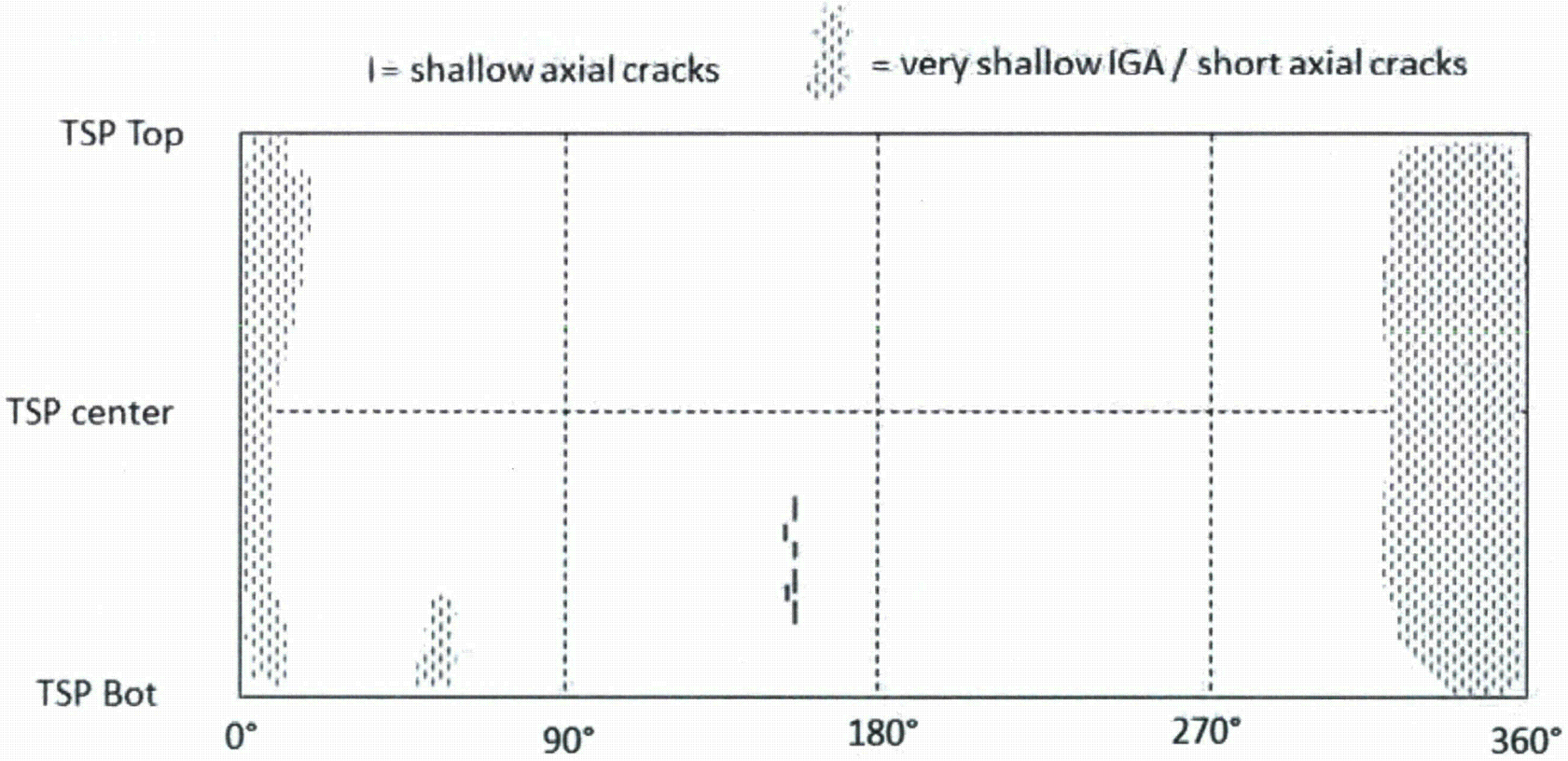

Figure 5-18: Post-Burst Observations on R24C41-3B (02H Region)

Figure 5-19: Shallow Corrosion Partially Obscured by Surface Deposits, Near the 0° Orientation of R24C41 02H

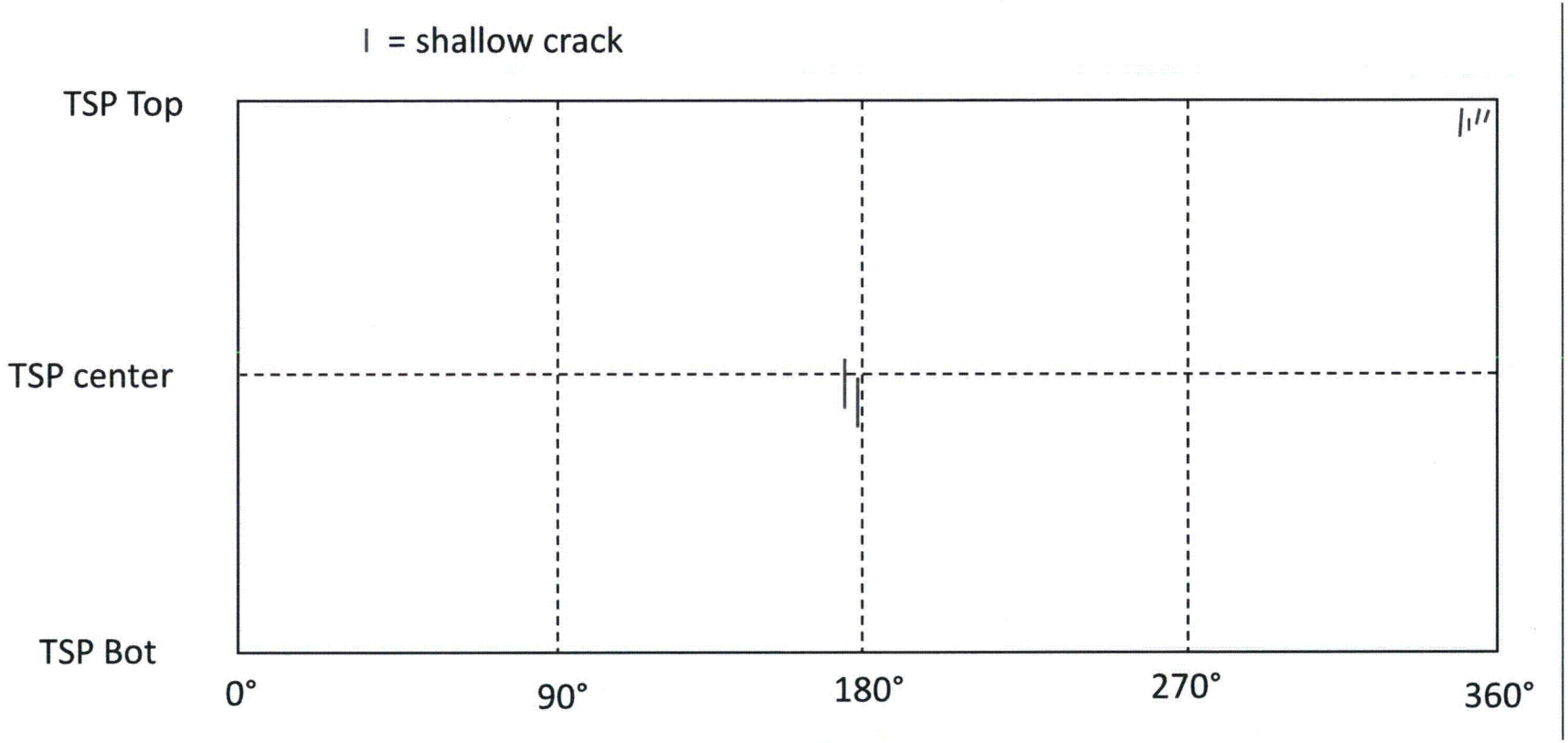

Figure 5-20: Post-Burst Observations on R24C41-5B (03H Region)

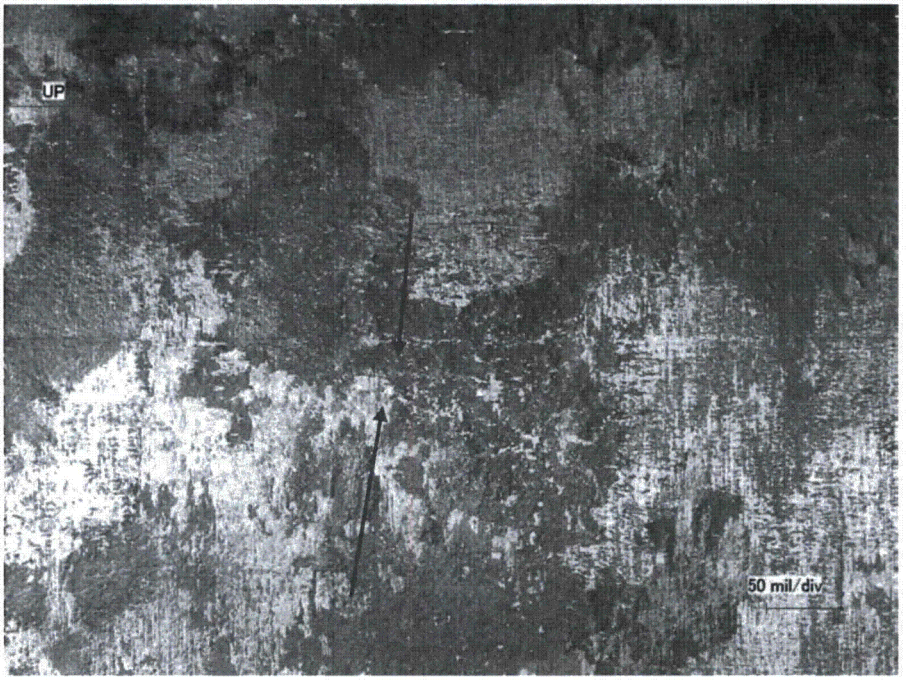

Figure 5-21: Shallow Axial Cracks (Marked with Arrows) Near Center of R24C41 03H TSP Region (180° Orientation)

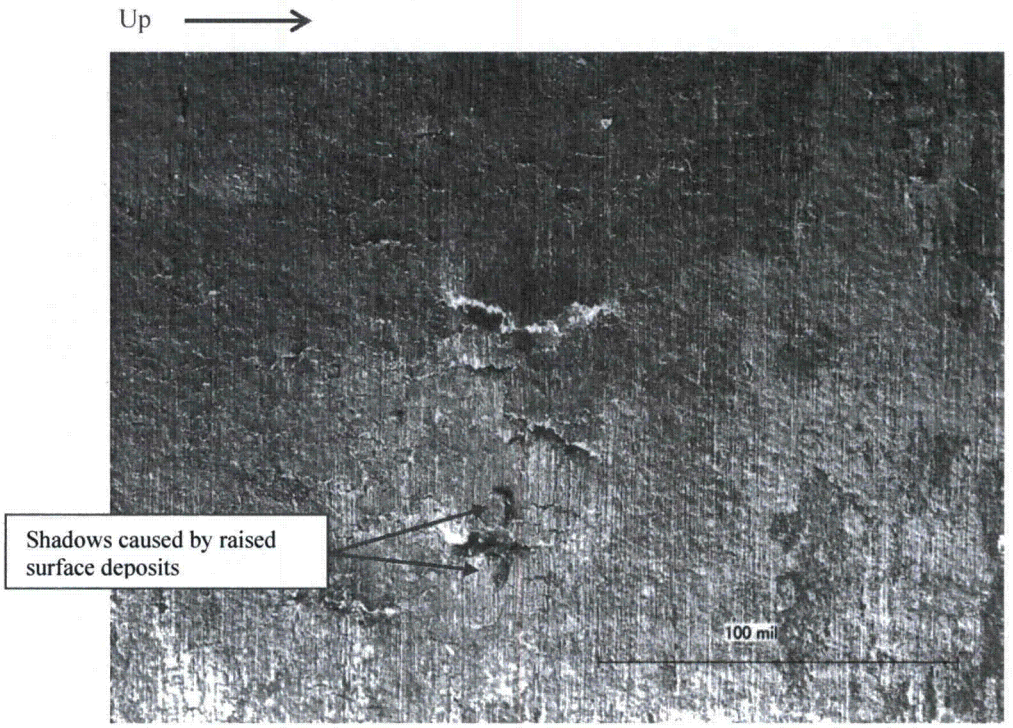

Figure 5-22: Shallow Cracks at Top of R24C41 03H TSP Region (0° Orientation)

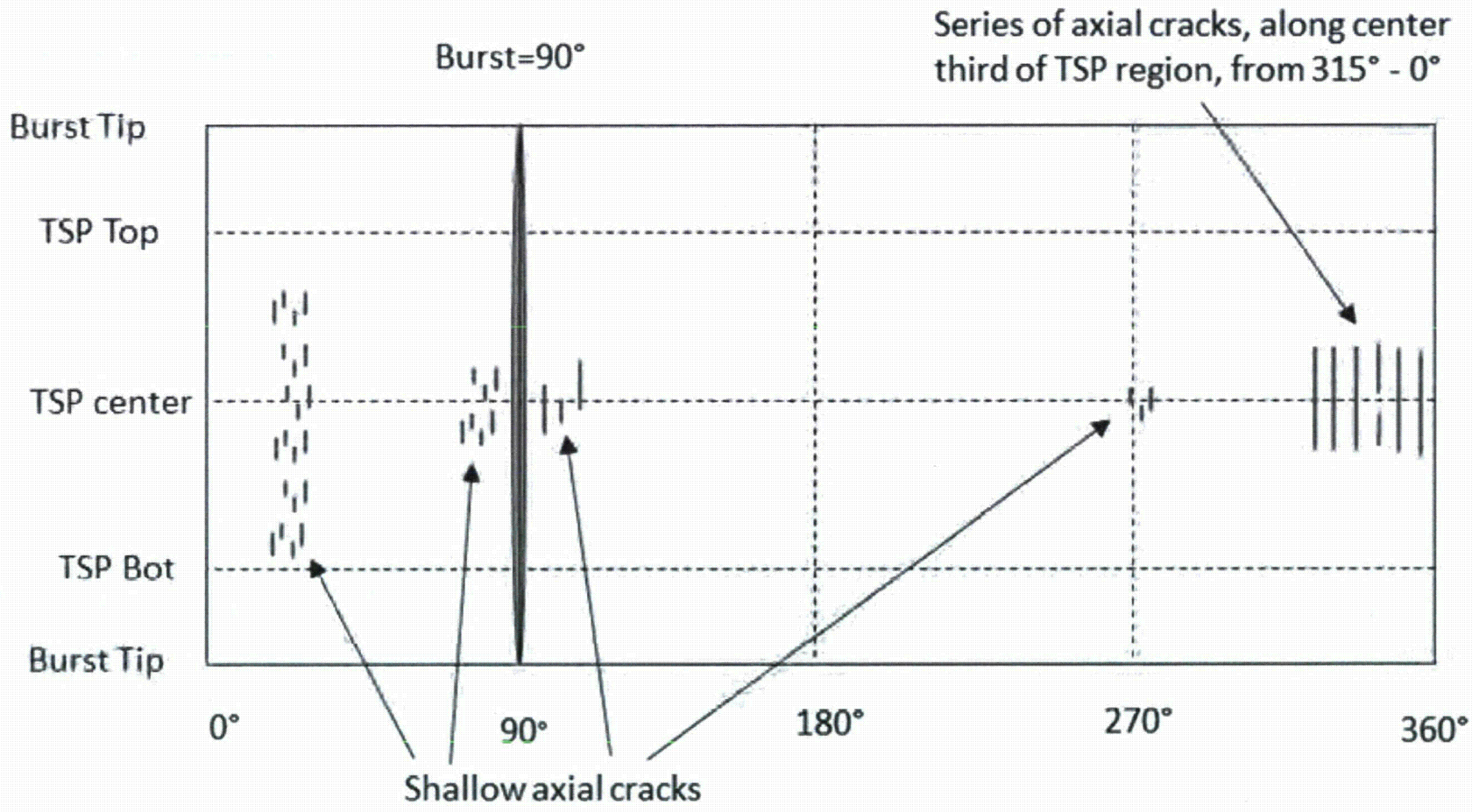

Figure 5-23: Post-Burst Observations on R24C41-6B (04H Region)

Figure 5-24: Larger Axial Cracks Near the Centerline of R24C41 04H TSP Region, Between 335°-350°

Figure 5-25: Larger Axial Cracks Near the Centerline of R24C41 04H TSP Region, Between 305°-340°

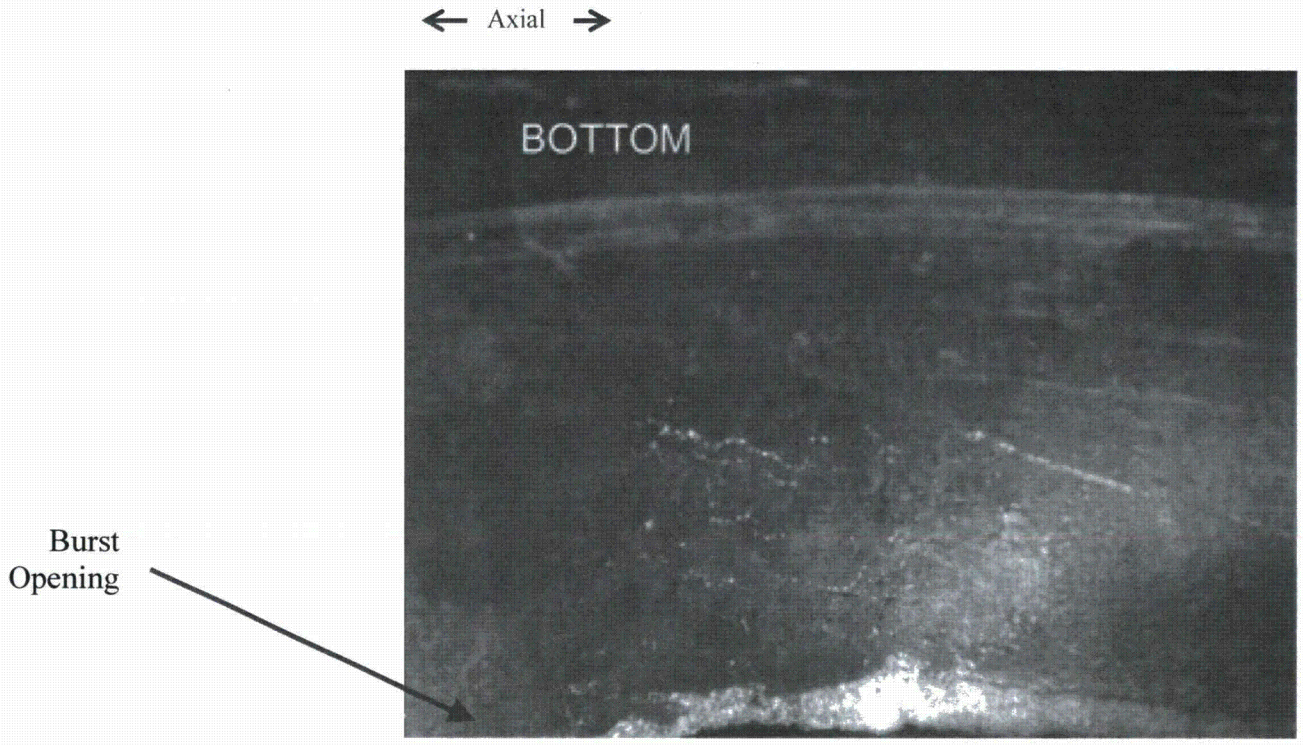

Figure 5-26: Example of Shallow Cracks Located Adjacent to the Burst Opening Of R24C41-6B (04H) at the 90° Orientation

6.0 SECTIONING

Figure 6-1 through Figure 6-27 show where selected pieces from both pulled tubes were obtained. TSP and FDB regions are shown as darker blue regions. Burst locations are indicated as a red line on the tube, and by text to the left of the applicable red line. In certain diagrams, the circled "A" and "B", and the adjacent dotted line, represent the cuts that were made within the section. These cuts were made in order of the "A" cut first and the "B" cut second (where applicable).

The table below (Table 6-1) provides an index for the cutting diagrams:

Table 6-1: Sectioning Diagrams

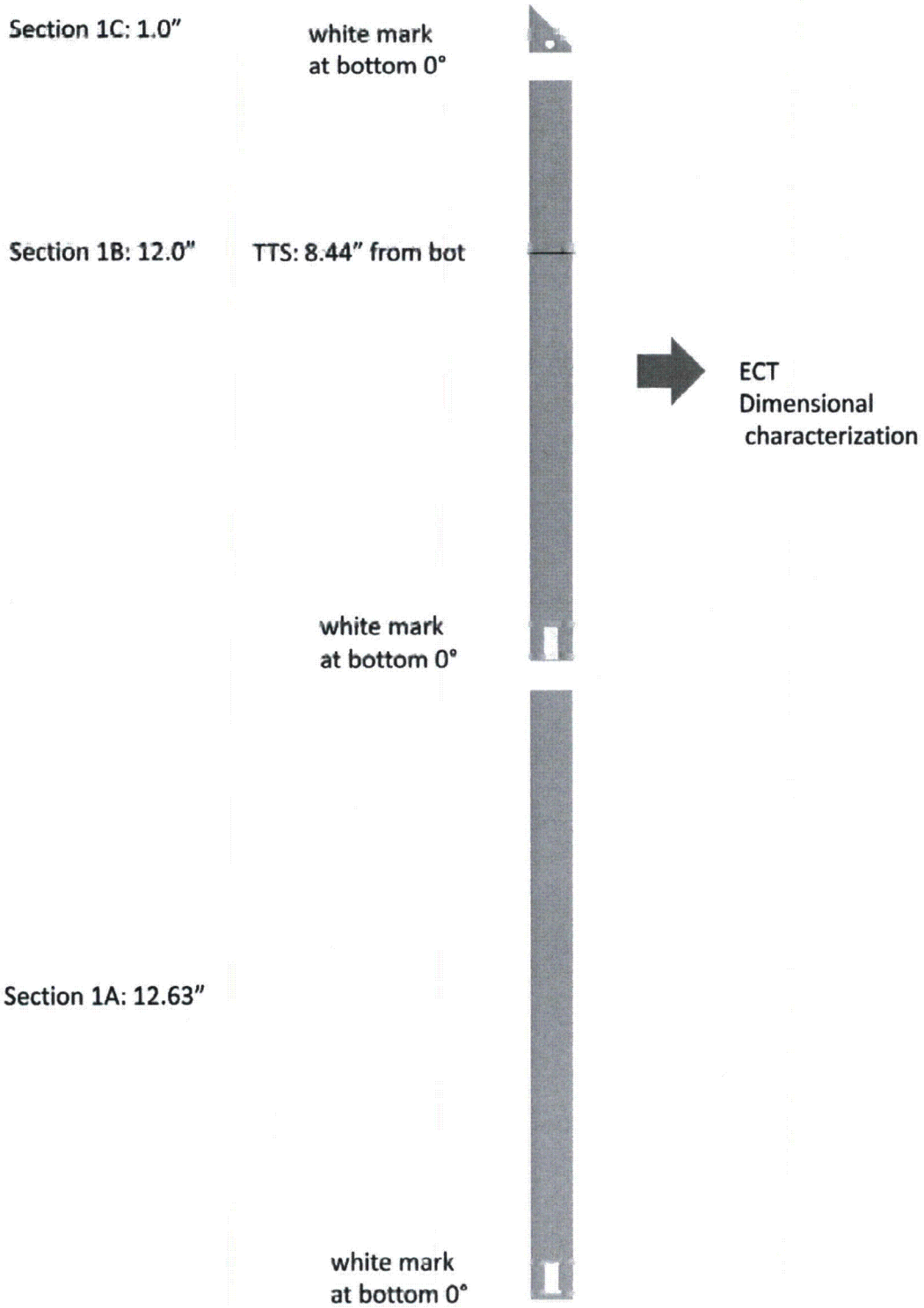

Figure 6-1: Sectioning Diagram for R19C38 Segment 1

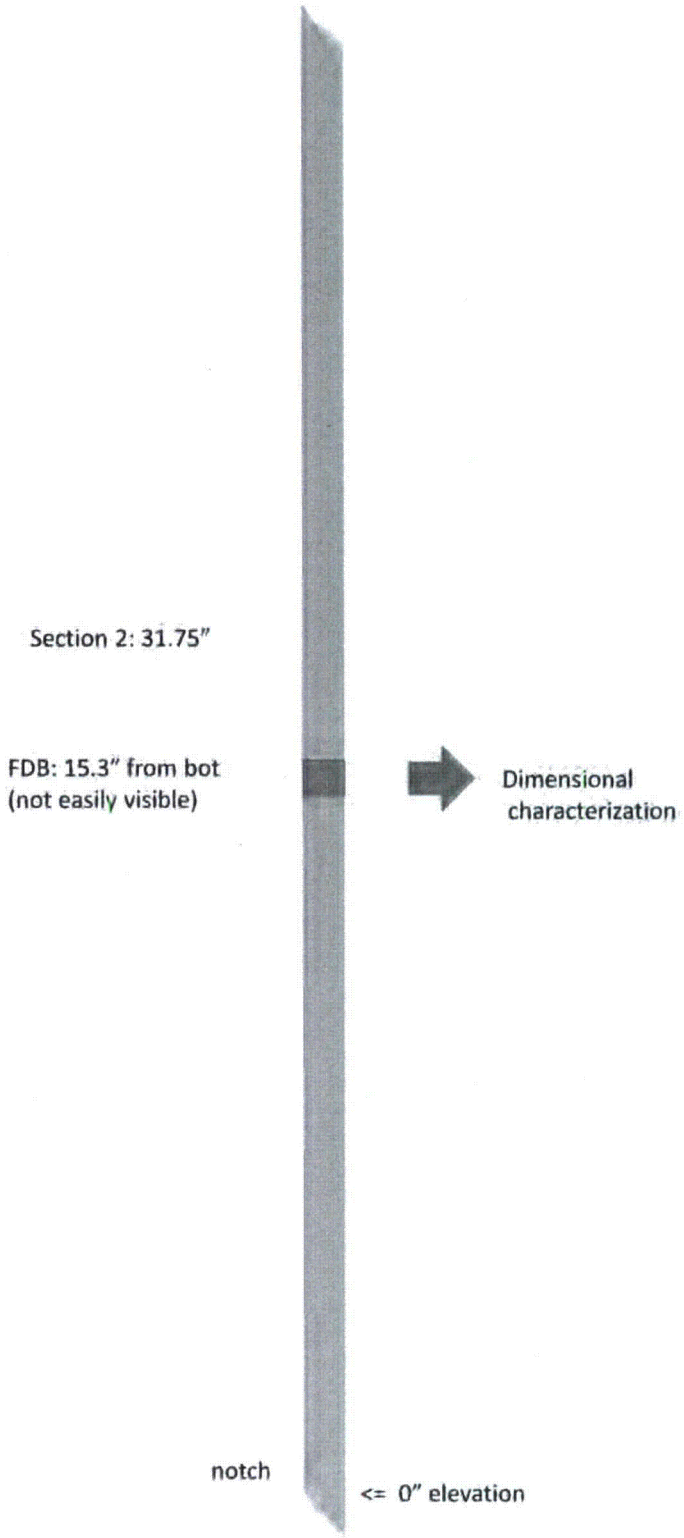

Figure 6-2: Sectioning Diagram for R19C38 Segment 2

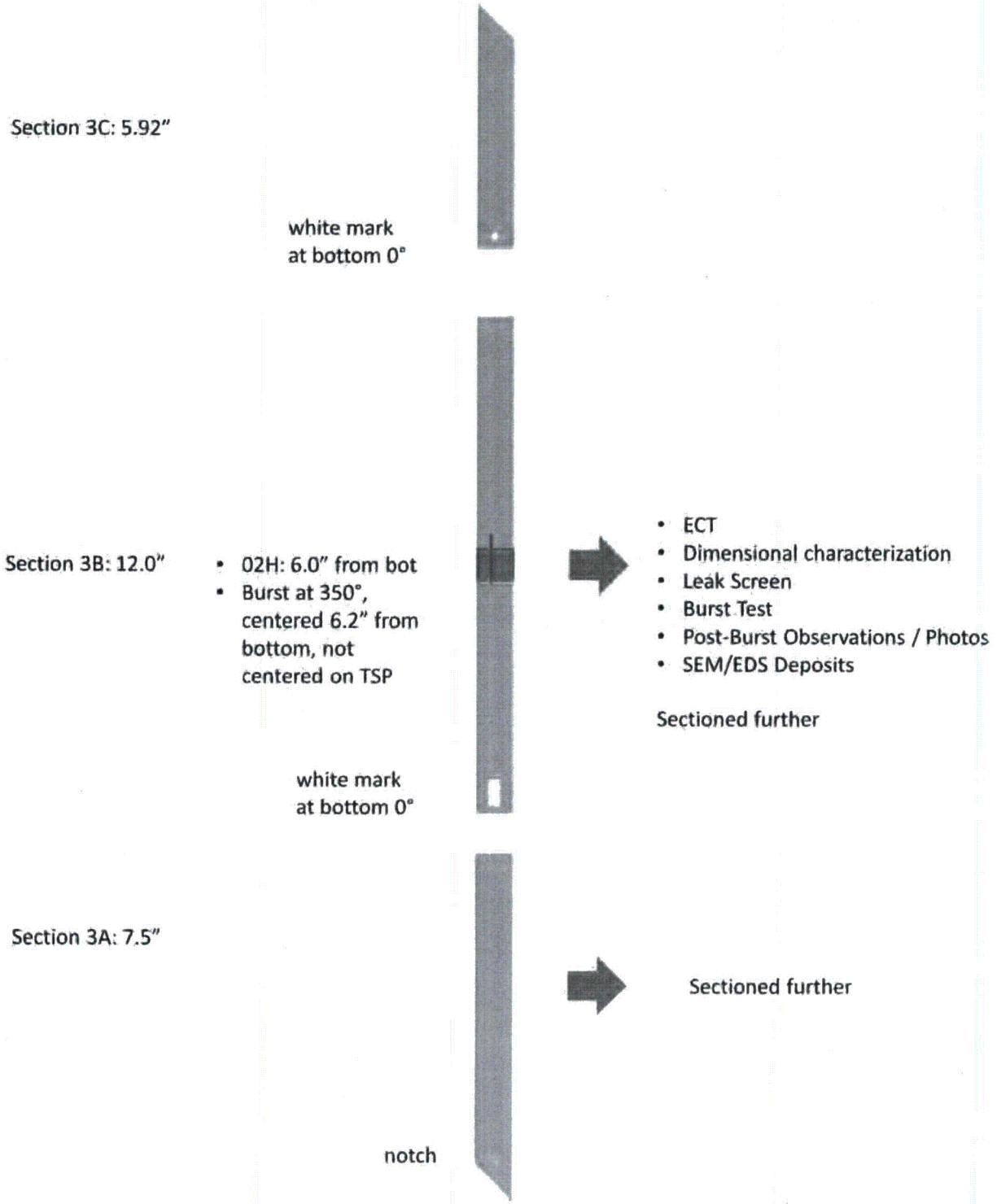

Figure 6-3: Sectioning Diagram for R19C38 Segment 3

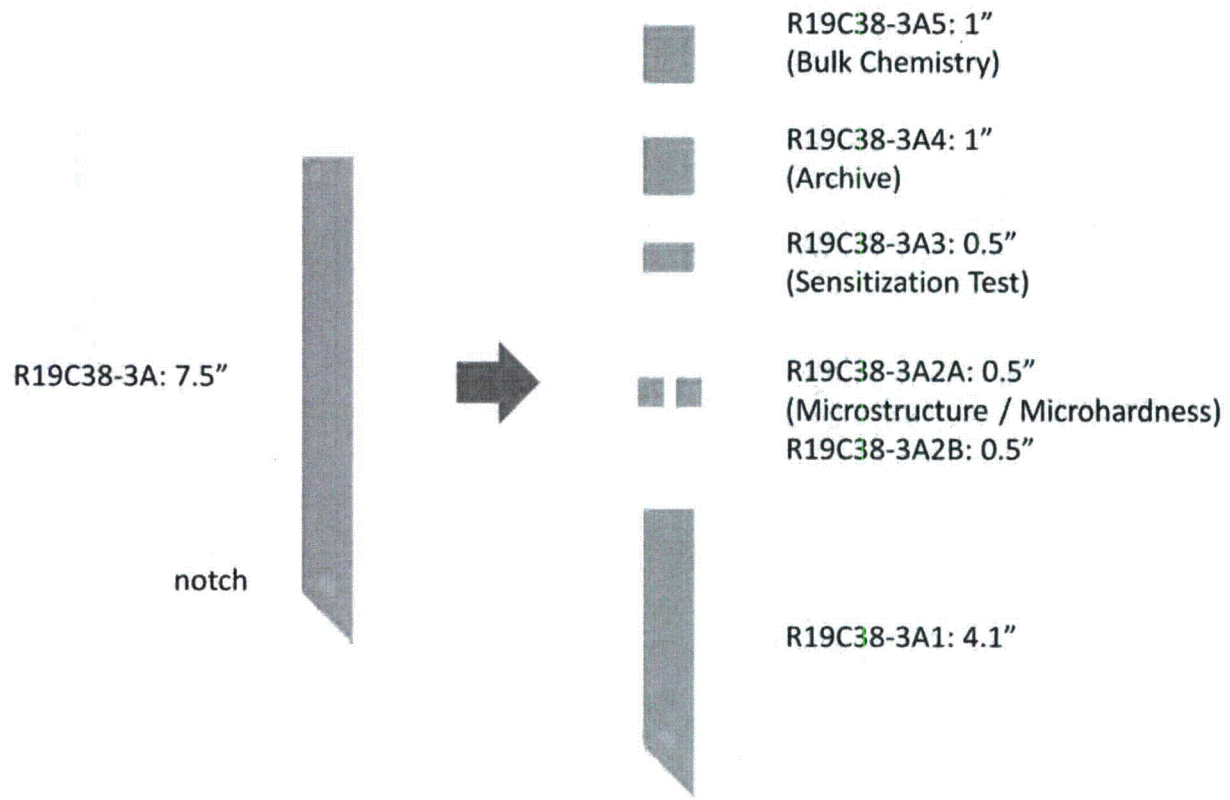

Figure 6-4: Sectioning Diagram for R19C38 Section 3A

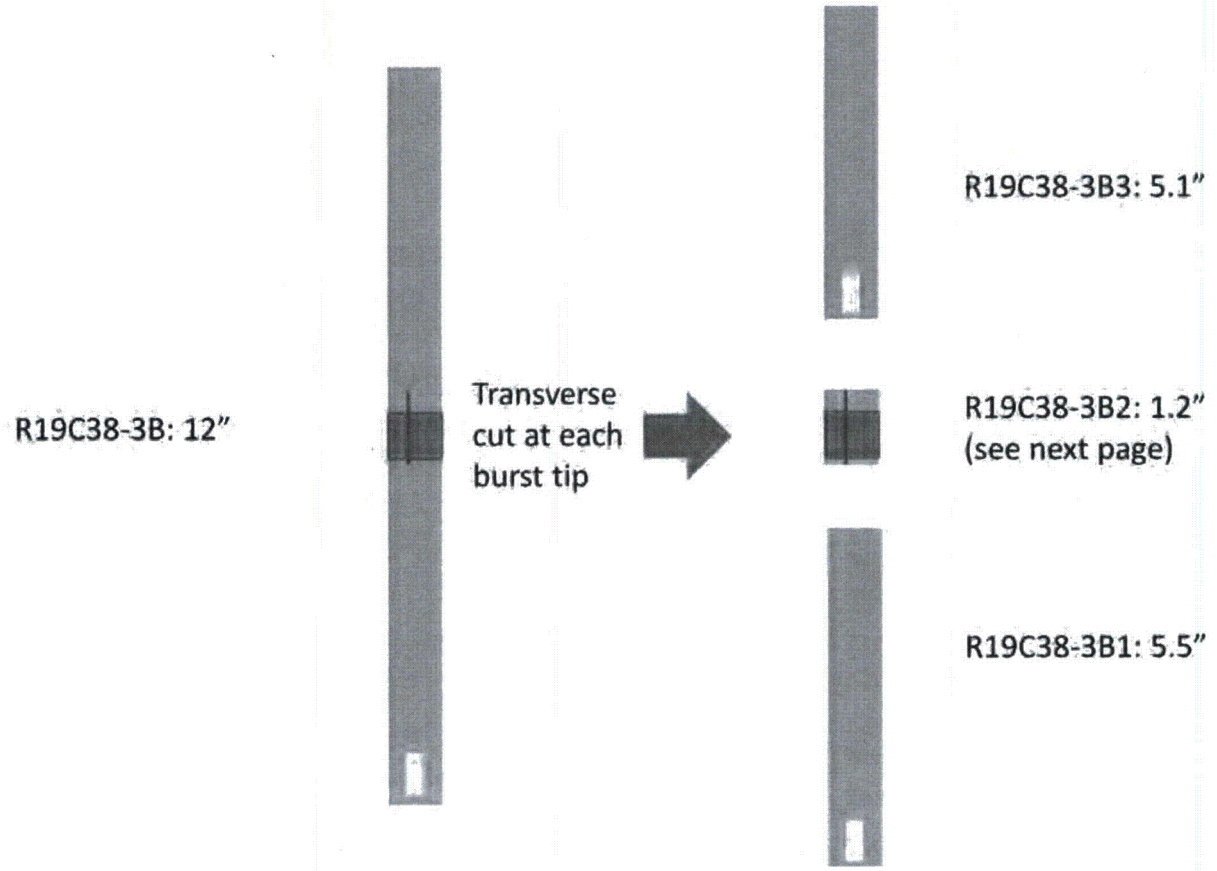

Figure 6-5: Sectioning Diagram for R19C38 Section 3B

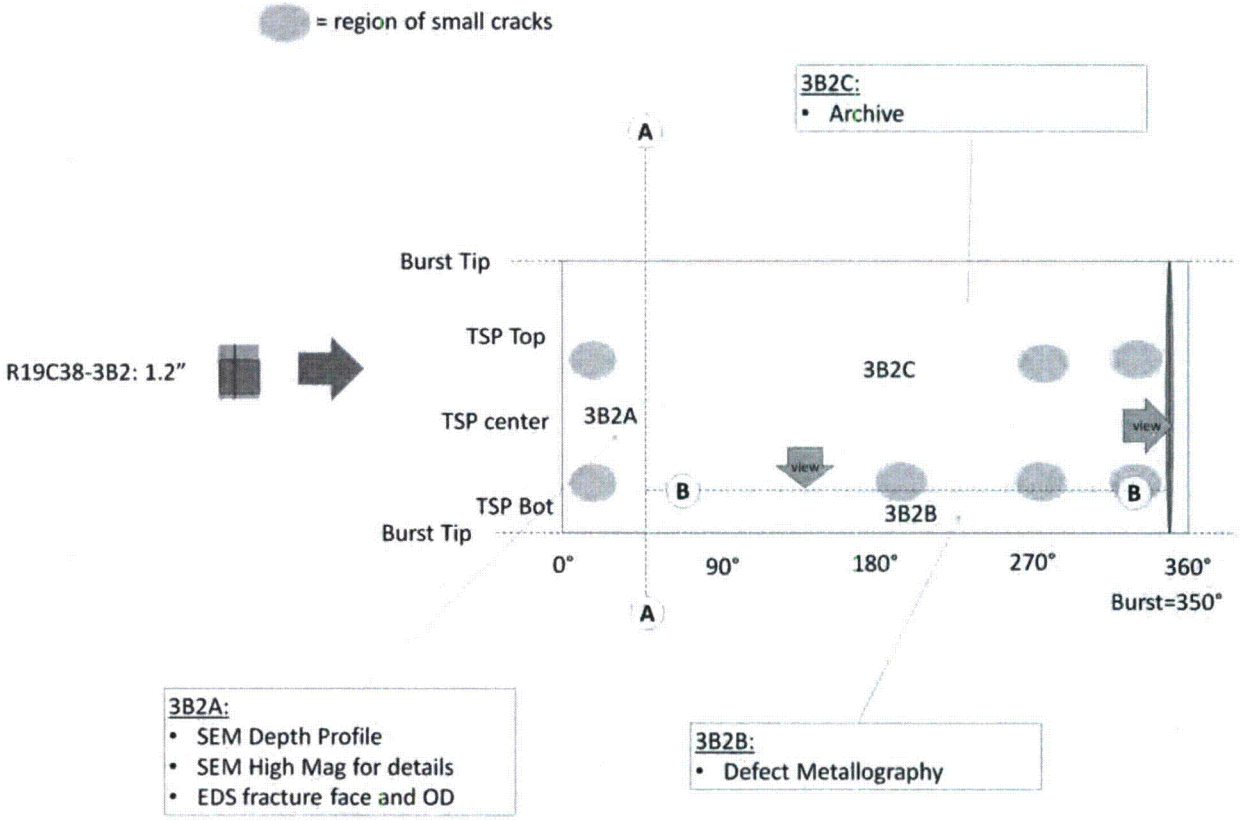

Figure 6-6: Sectioning Diagram for R19C38 Section 3B2

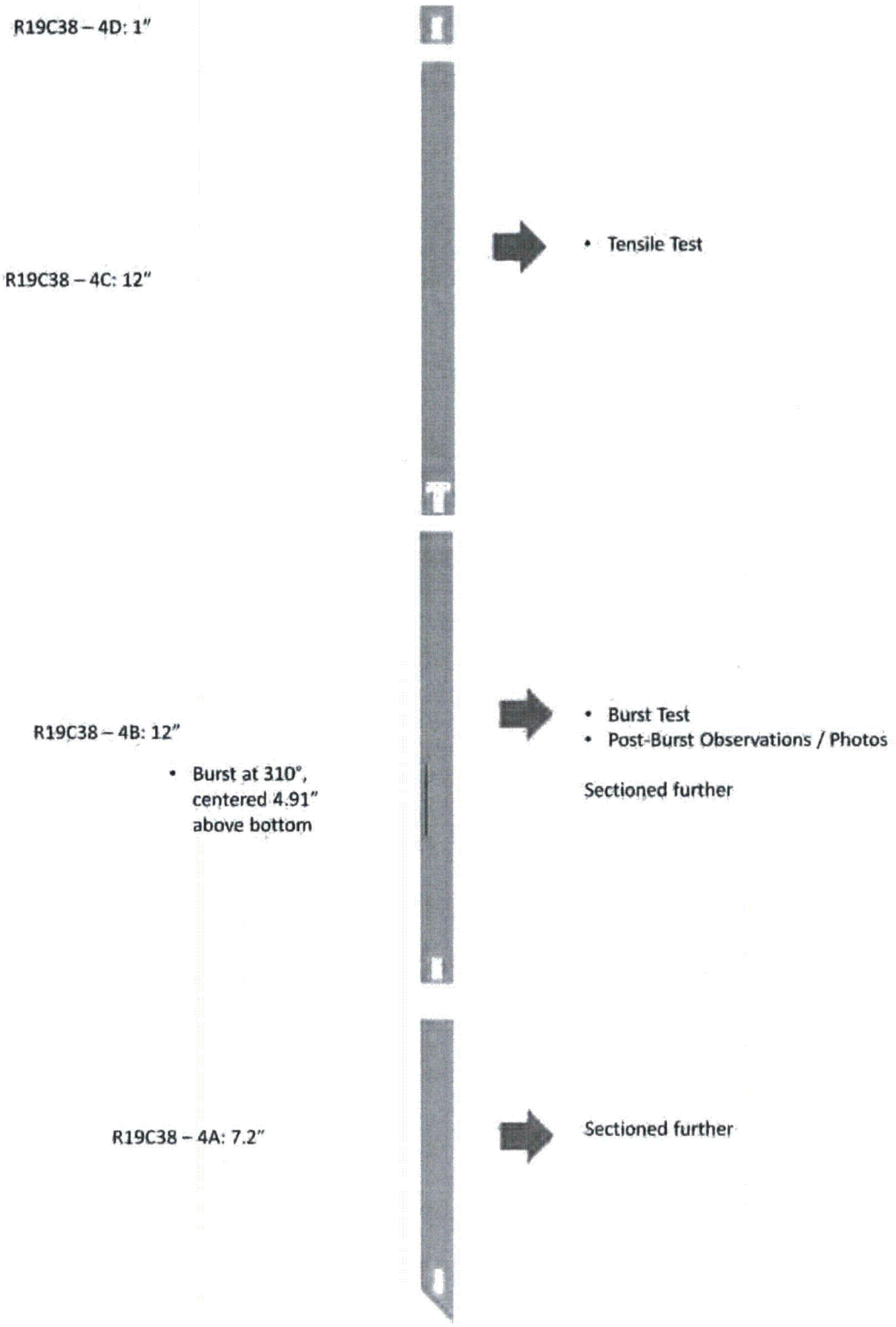

Figure 6-7: Sectioning Diagram for R19C38 Segment 4

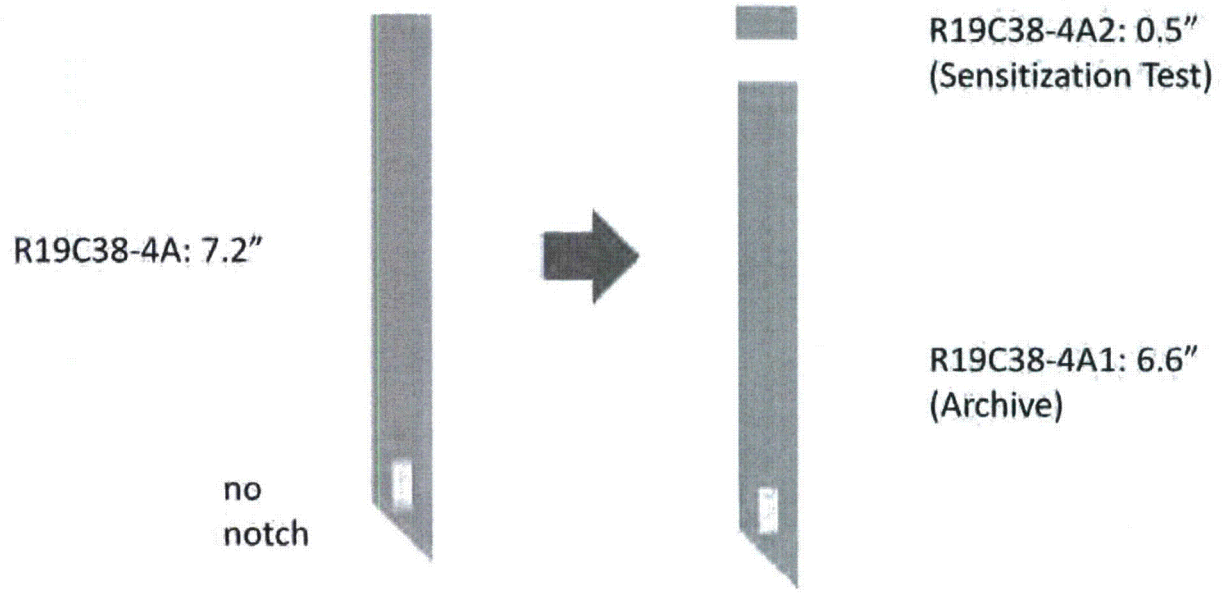

Figure 6-8: Sectioning Diagram for R19C38 Section 4A

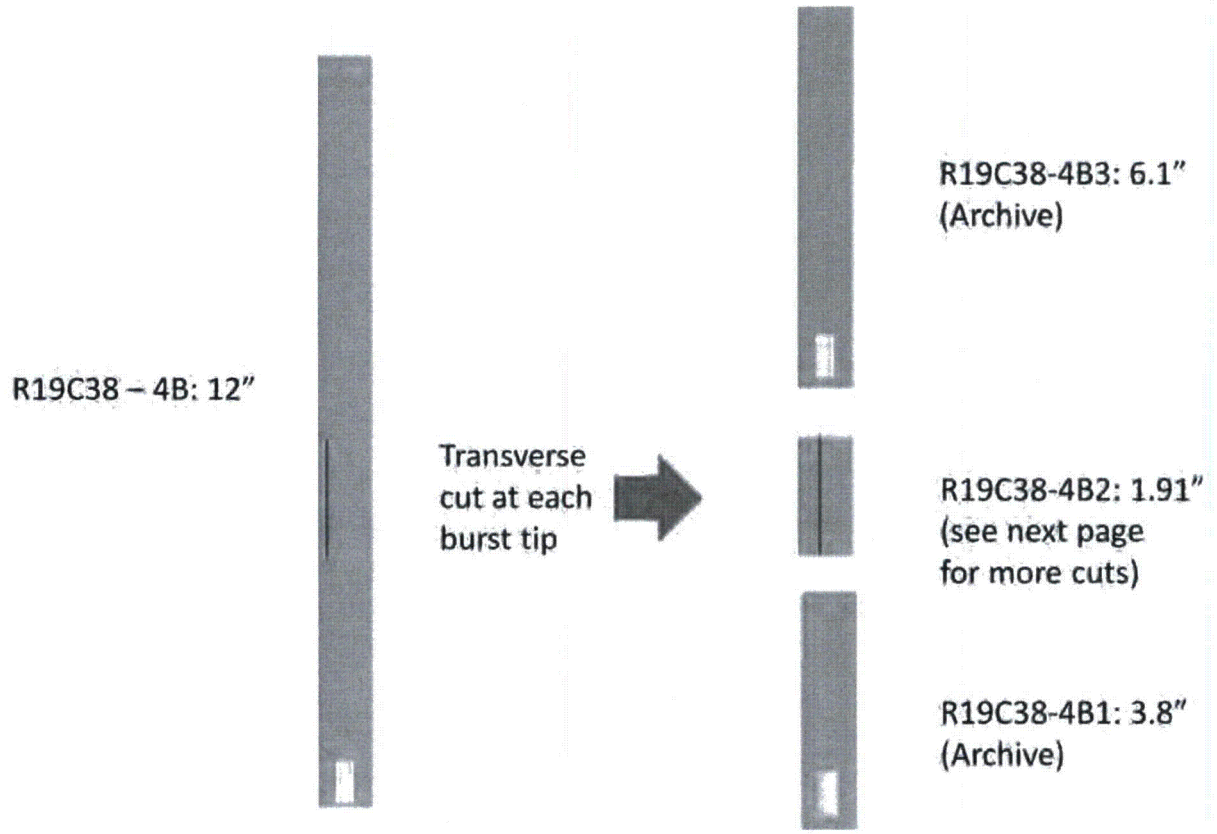

Figure 6-9: Sectioning Diagram for R19C38 Section 4B

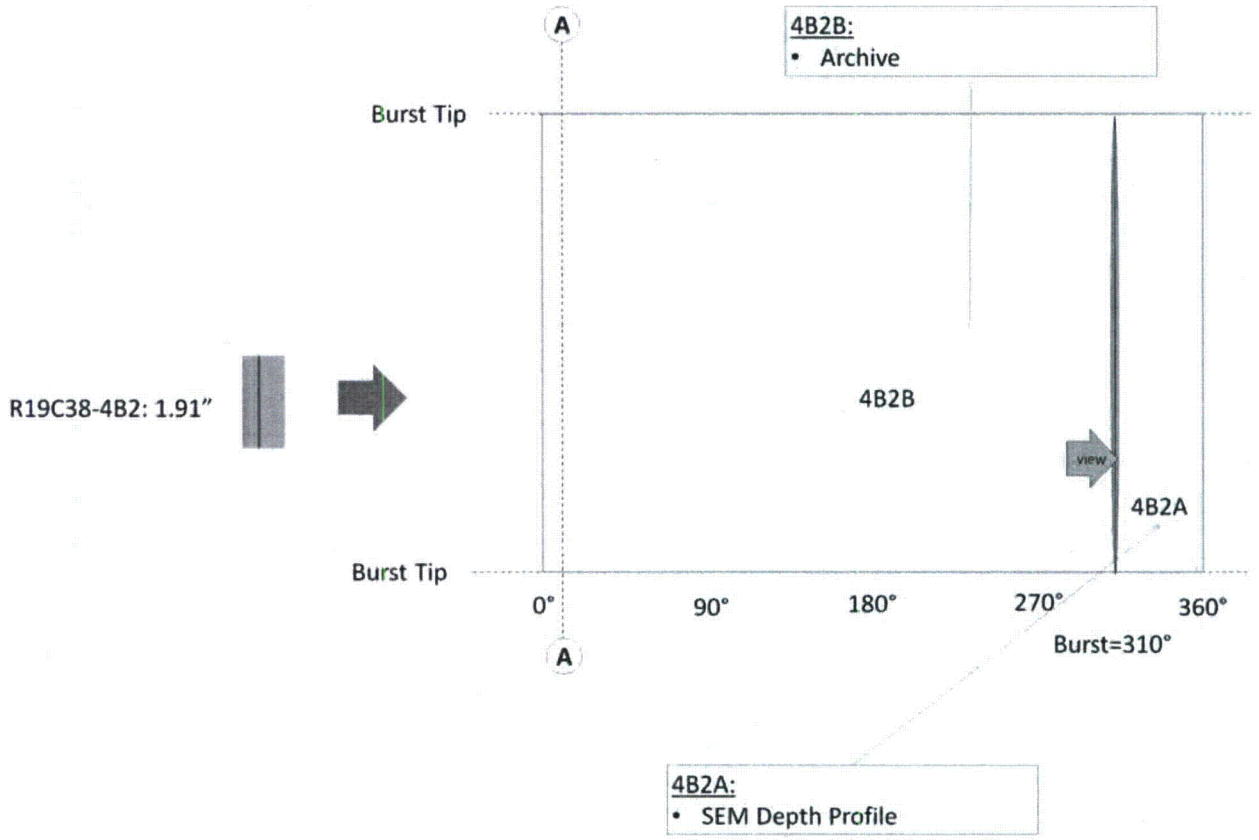

Figure 6-10: Sectioning Diagram for R19C38 Section 4B2

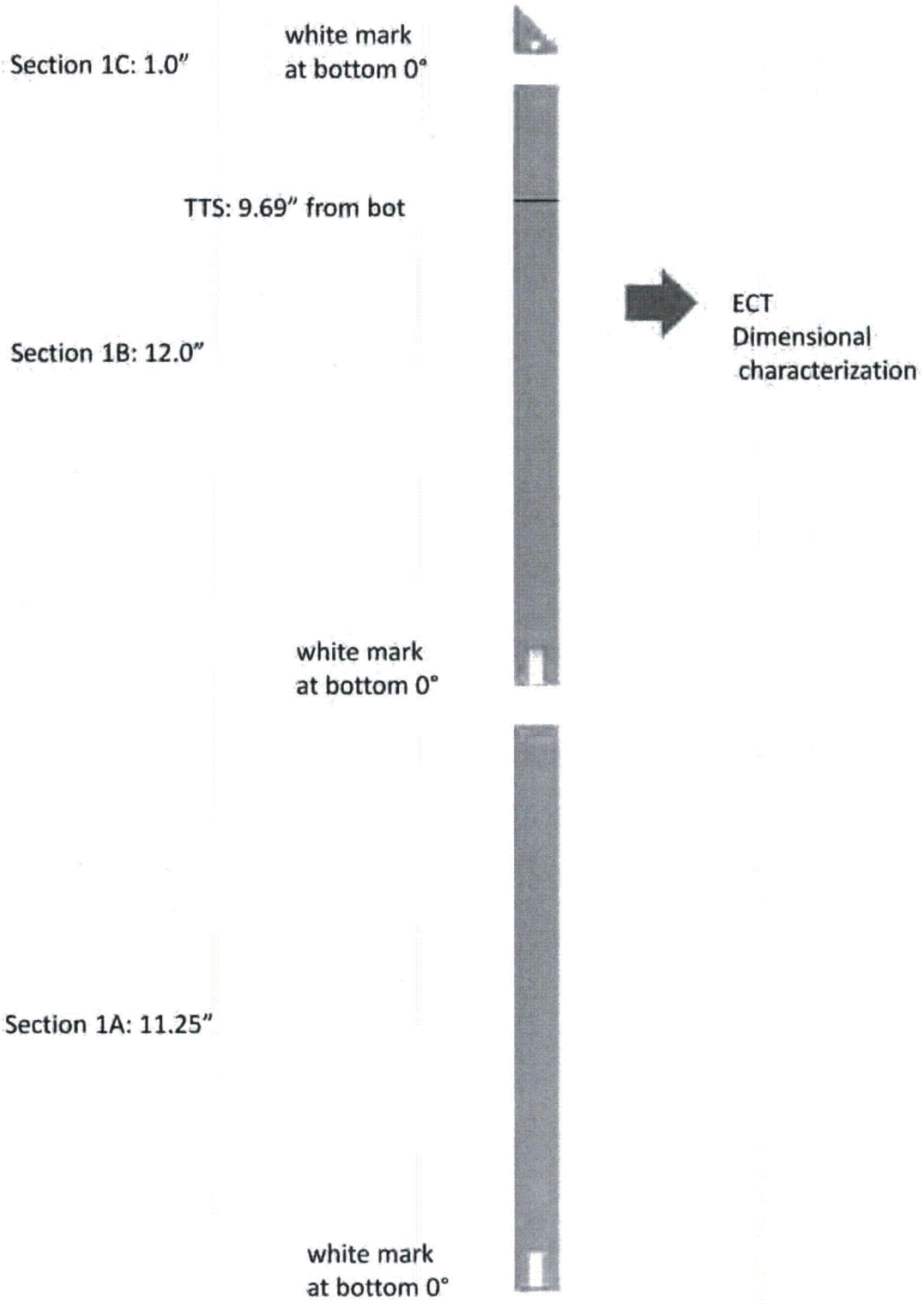

Figure 6-11: Sectioning Diagram for R24C41 Segment 1

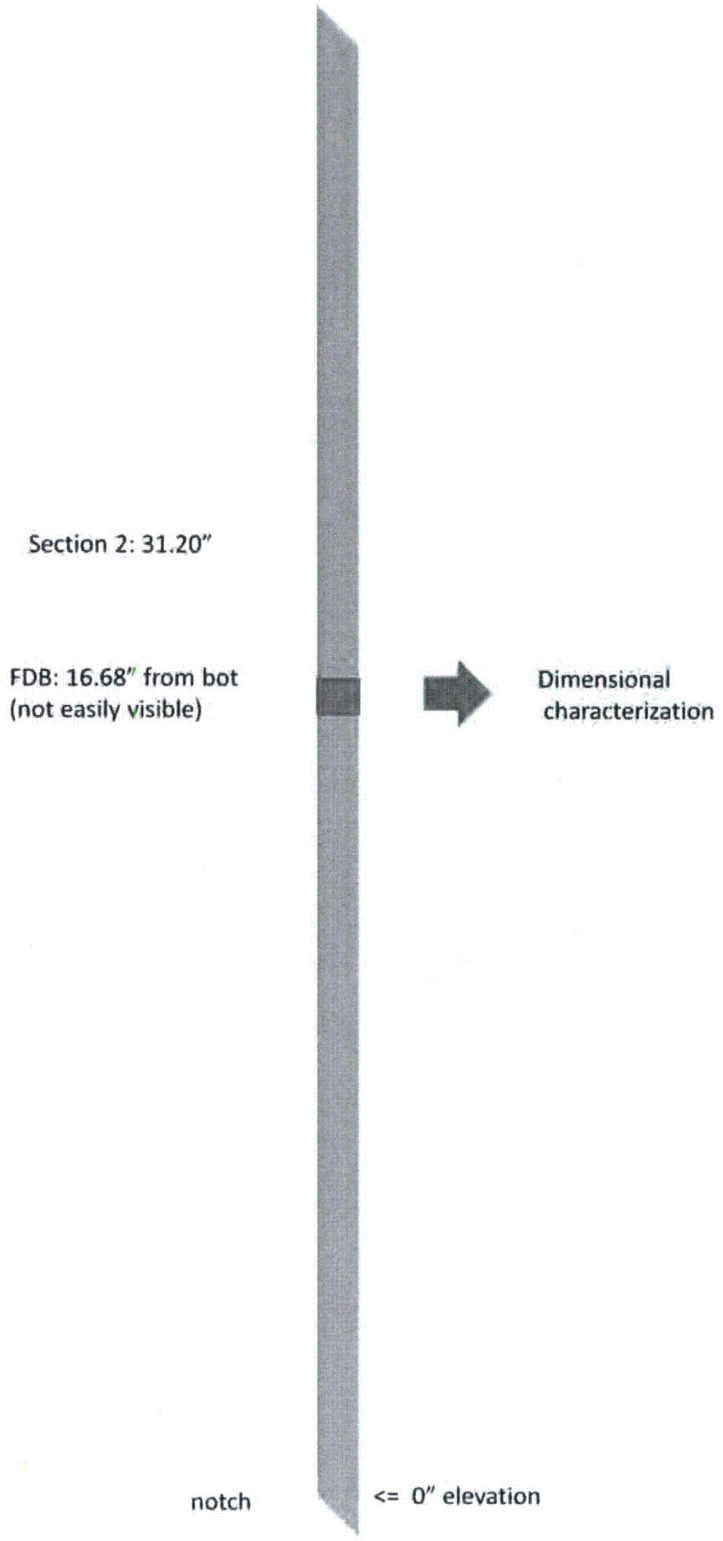

Figure 6-12: Sectioning Diagram for R24C41 Segment 2

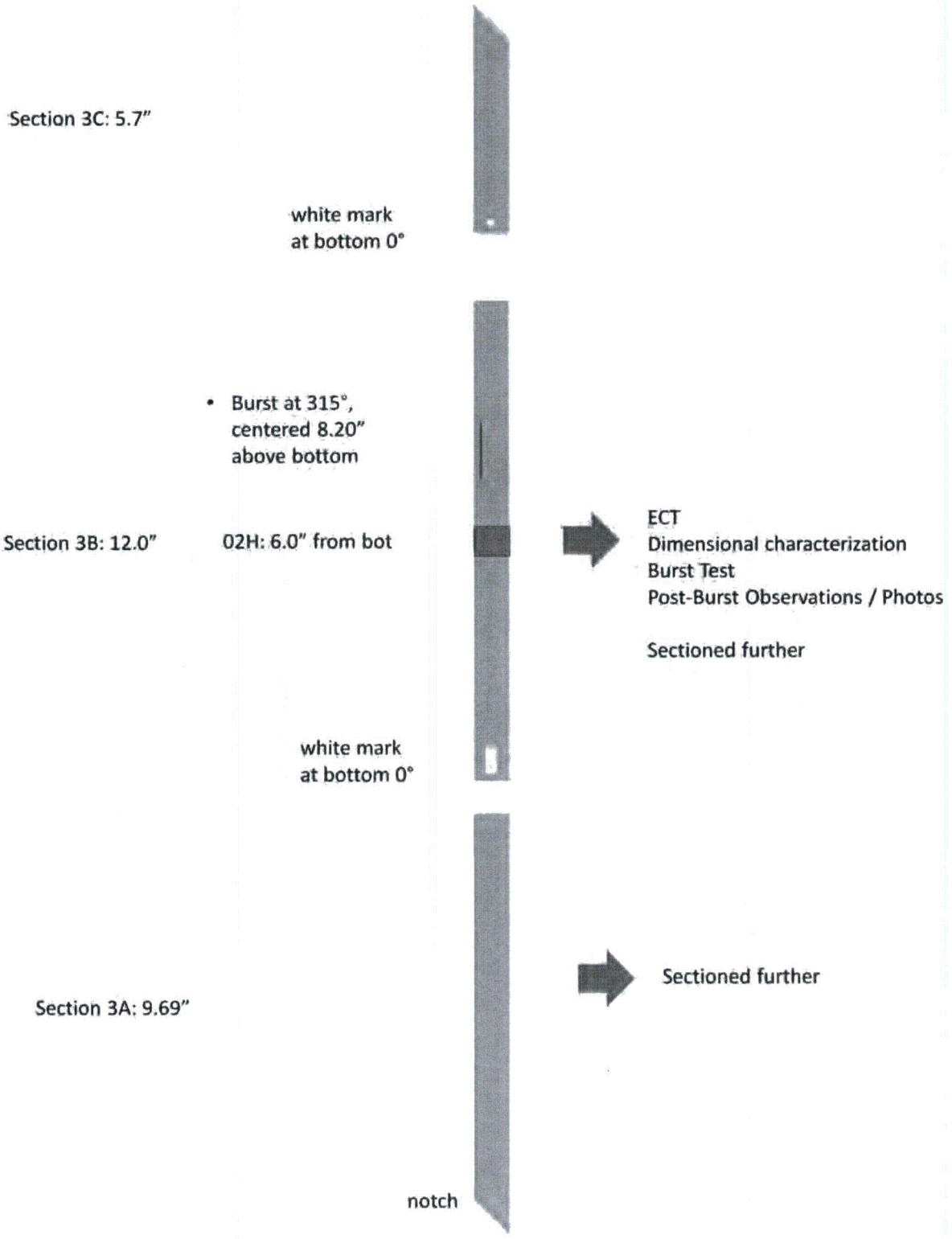

Figure 6-13: Sectioning Diagram for R24C41 Segment 3

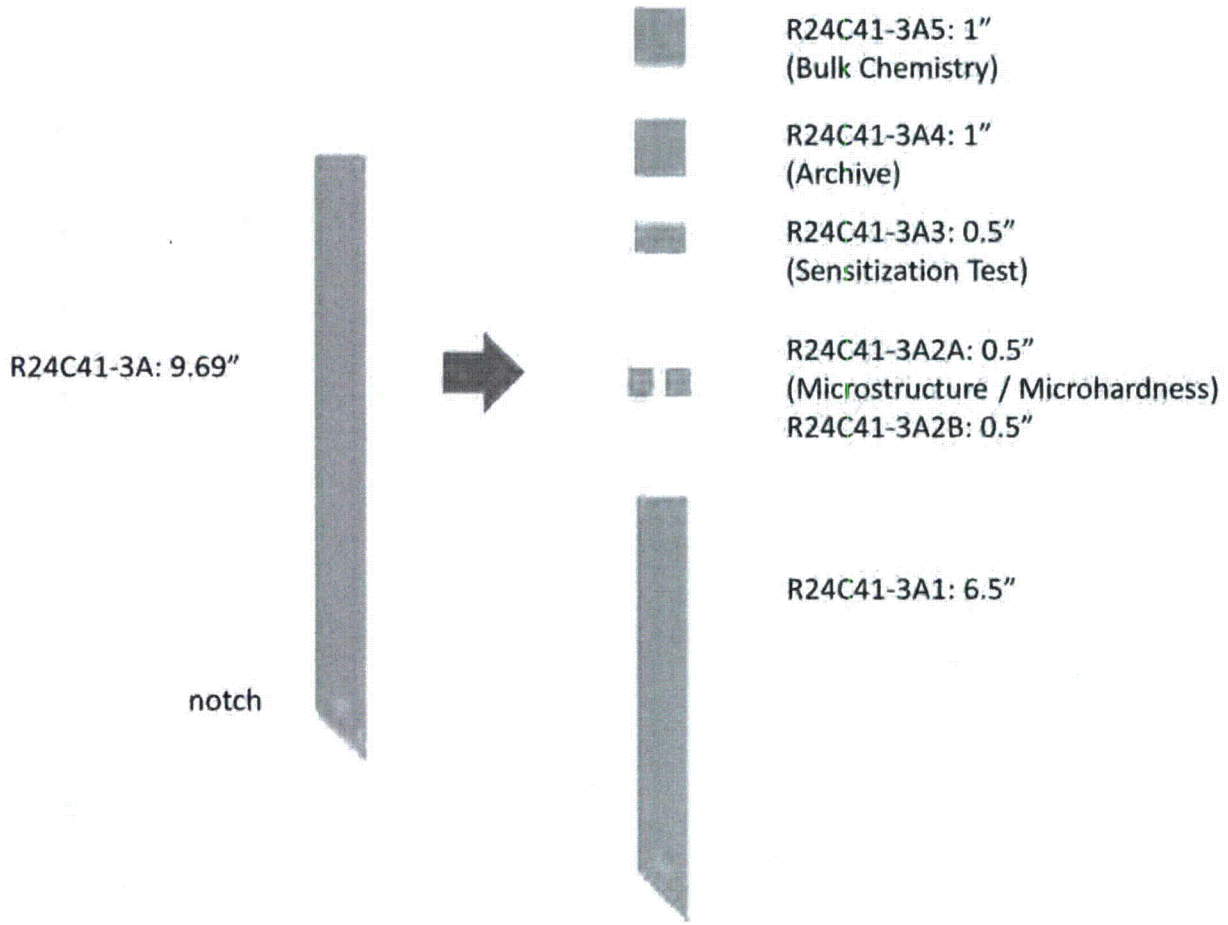

Figure 6-14: Sectioning Diagram for R24C41 Section 3A

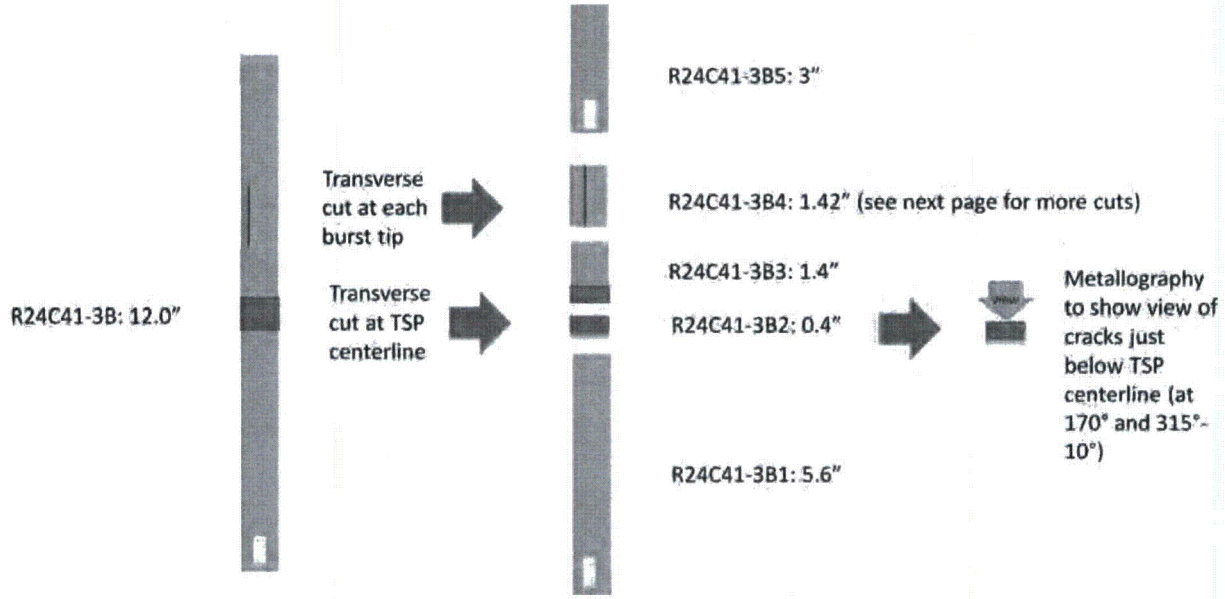

Figure 6-15: Sectioning Diagram for R24C41 Section 3B

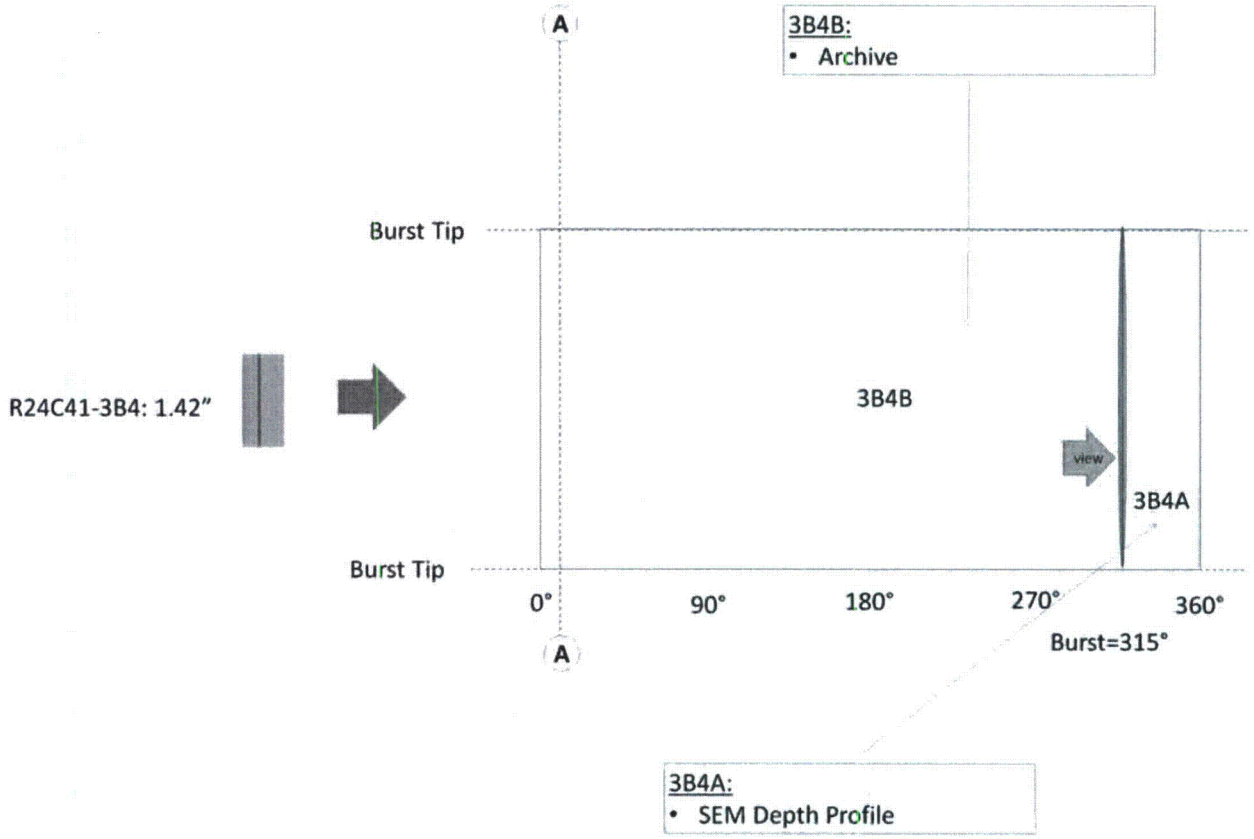

Figure 6-16: Sectioning Diagram for R24C41 Section 3B4

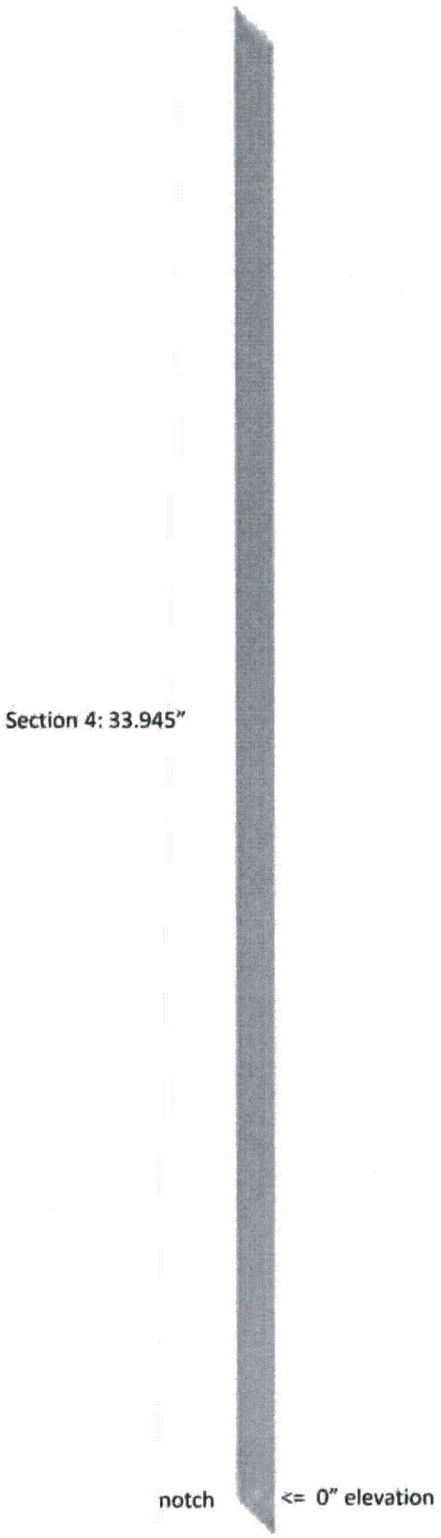

Figure 6-17: Sectioning Diagram for R24C41 Segment 4

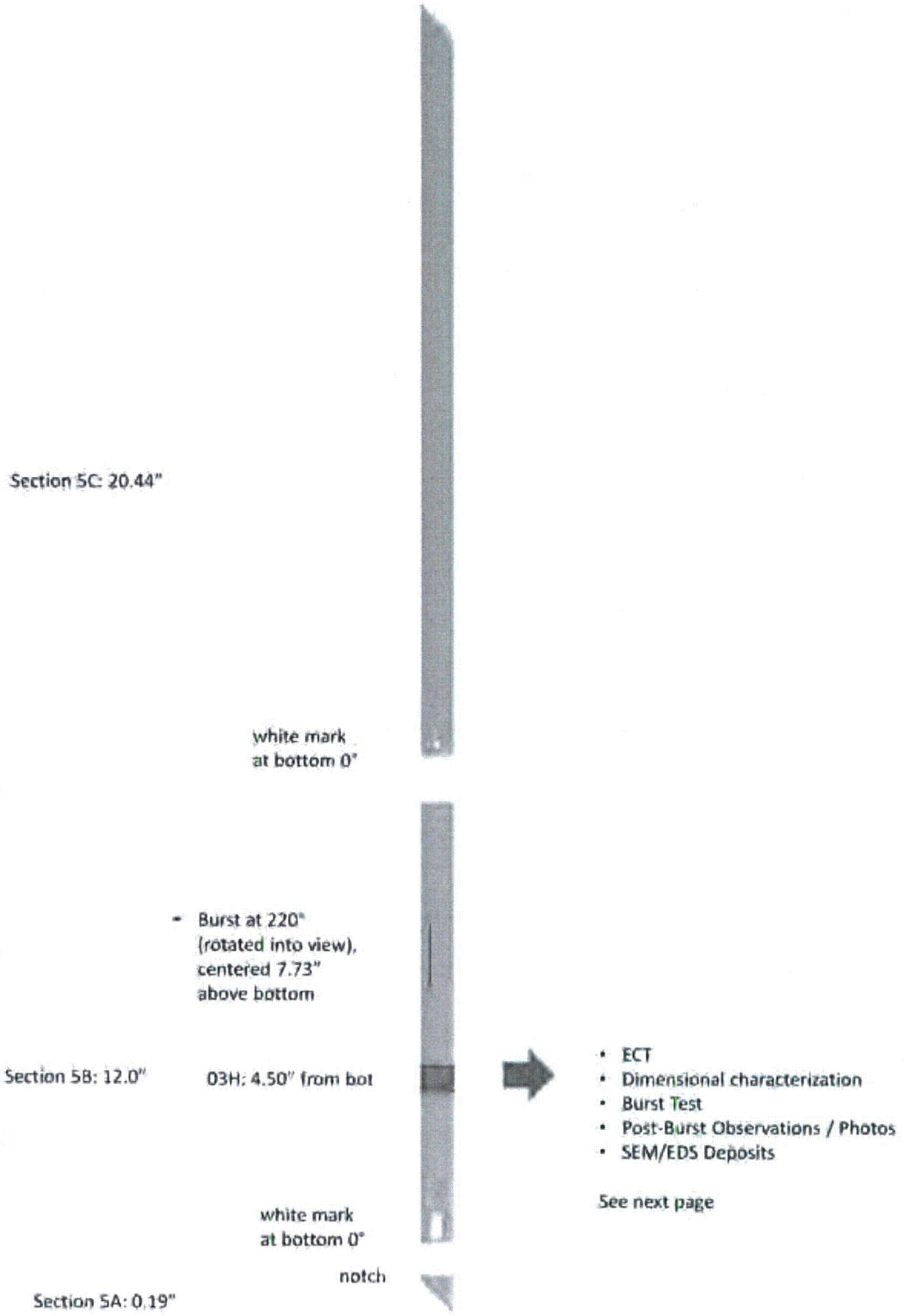

Figure 6-18: Sectioning Diagram for R24C41 Segment 5

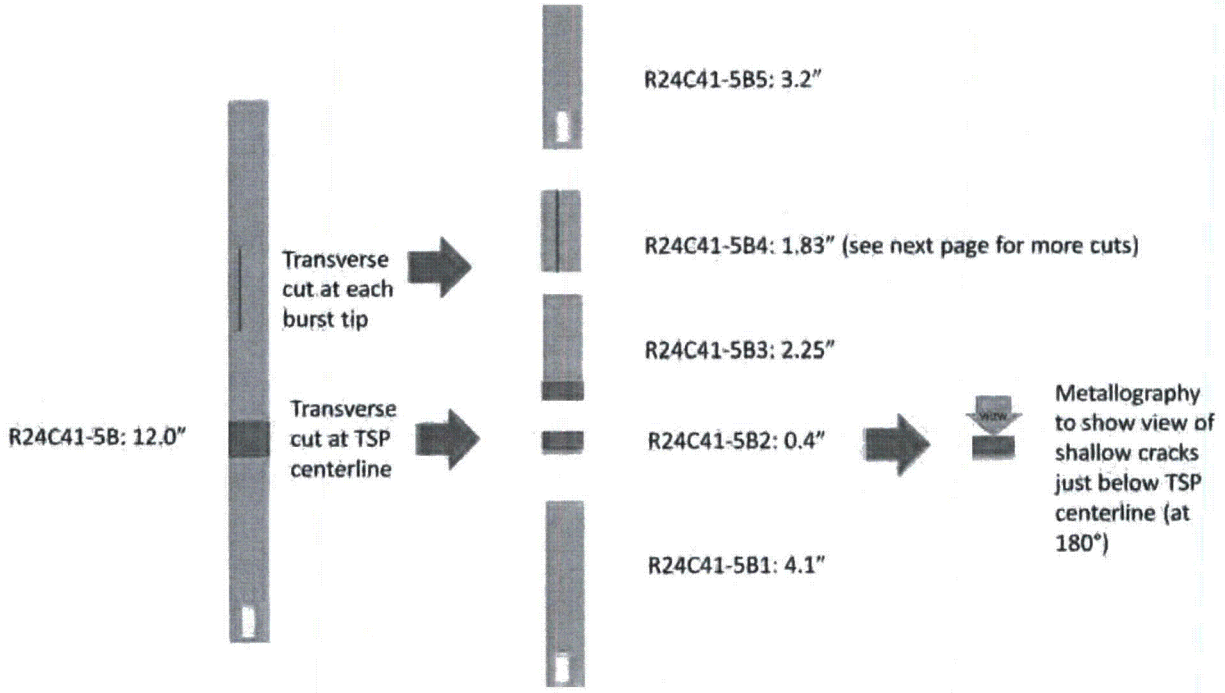

Figure 6-19: Sectioning Diagram for R24C41 Section 5B

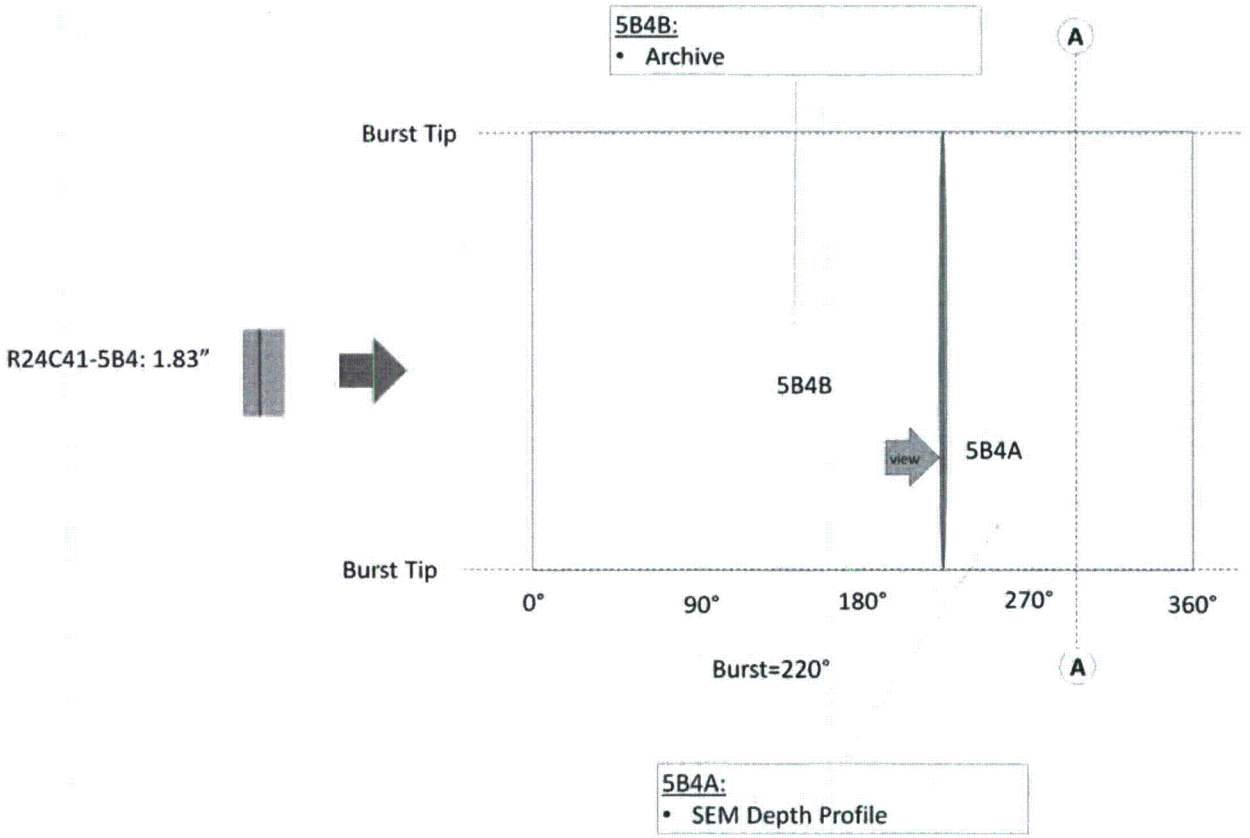

Figure 6-20: Sectioning Diagram for R24C41 Section 5B4

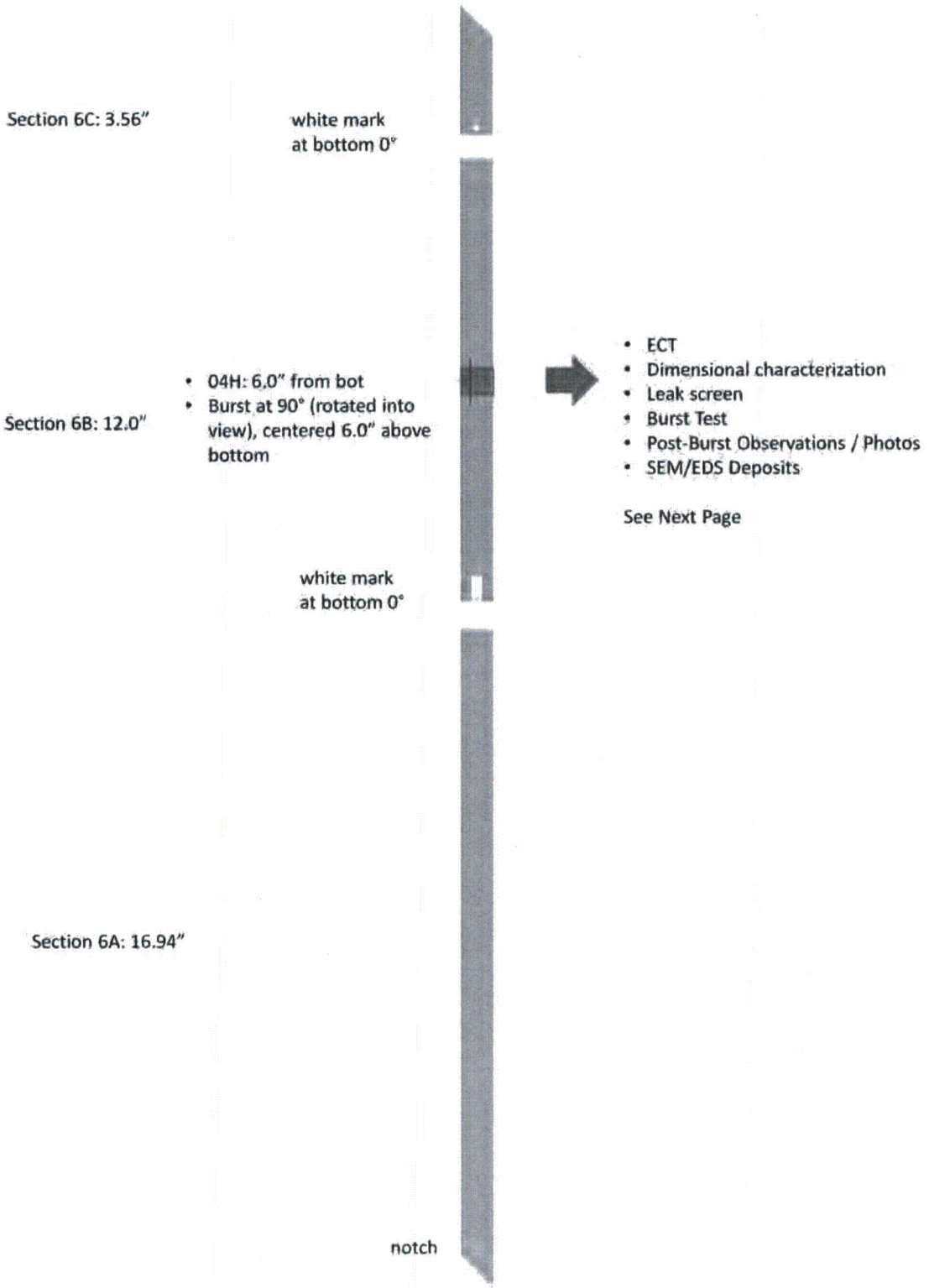

Figure 6-21: Sectioning Diagram for R24C41 Segment 6

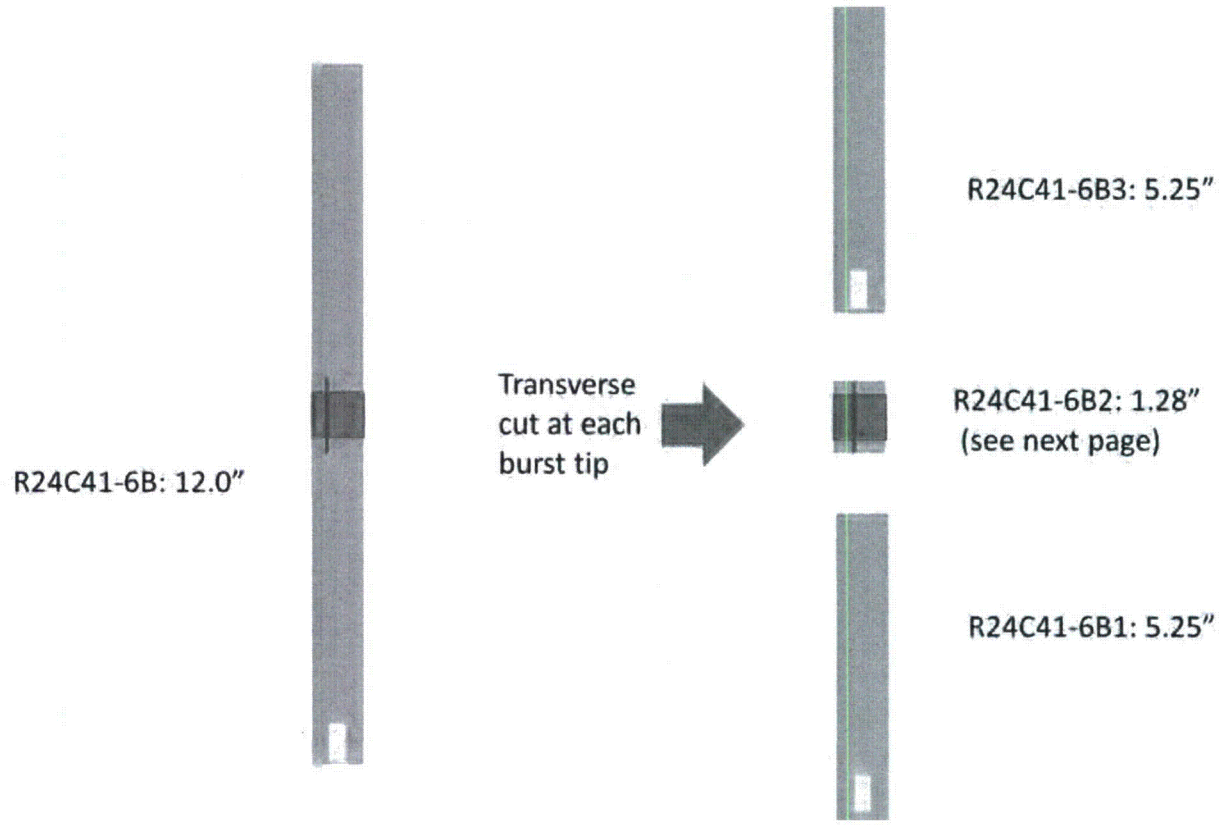

Figure 6-22: Sectioning Diagram for R24C41 Section 6B

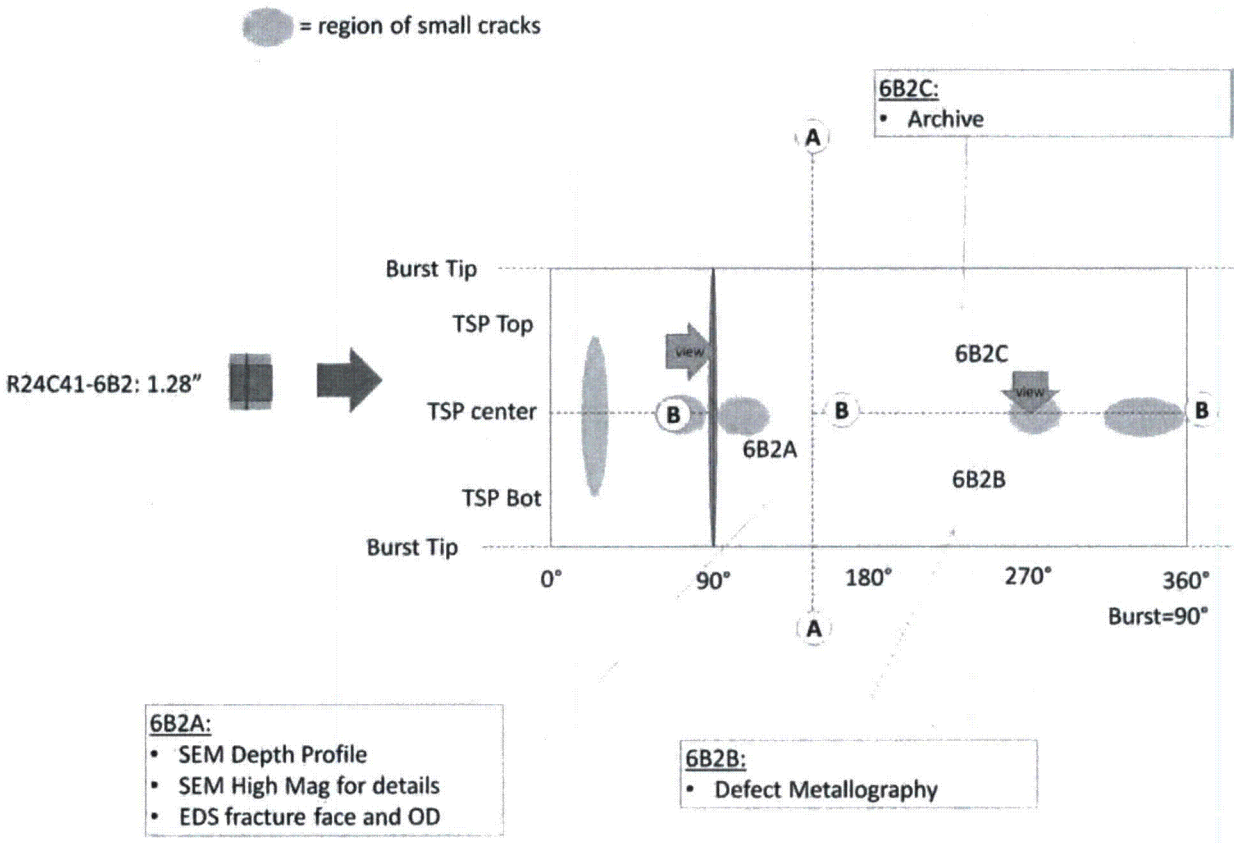

Figure 6-23: Sectioning Diagram for R24C41 Section 6B2

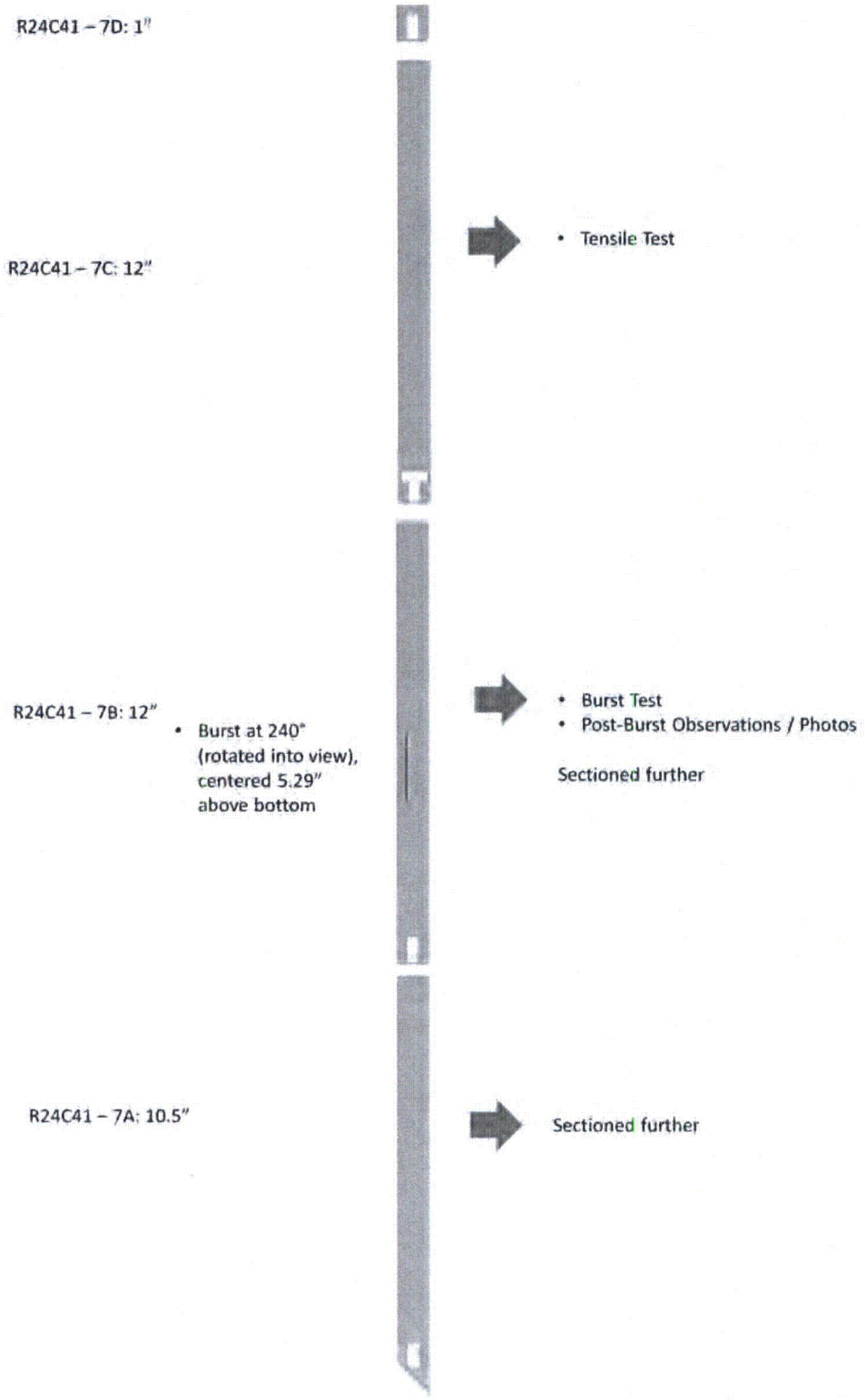

Figure 6-24: Sectioning Diagram for R24C41 Segment 7

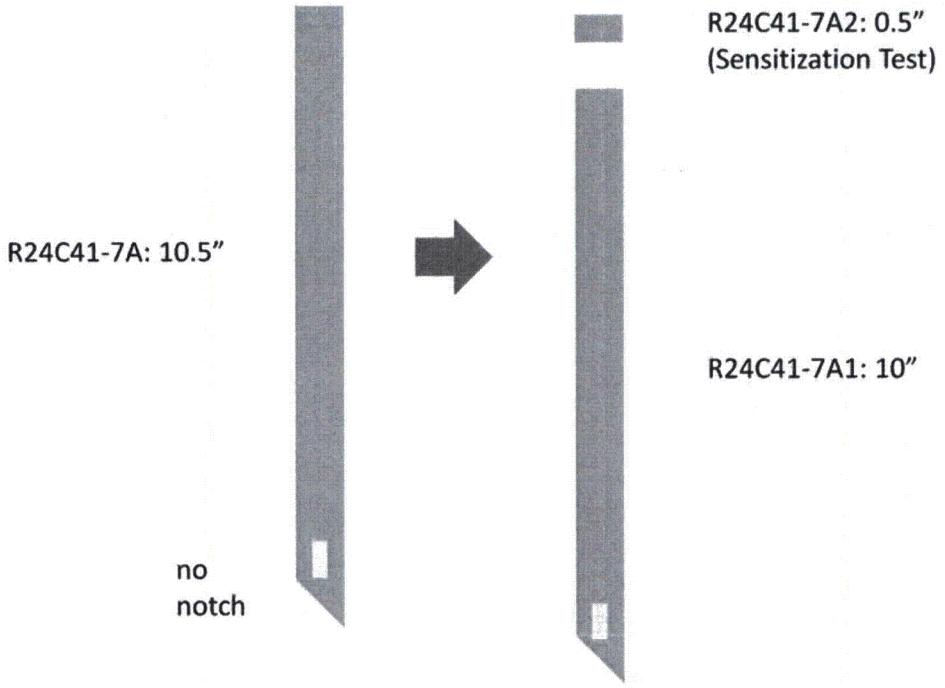

Figure 6-25: Sectioning Diagram for R24C41 Section 7A

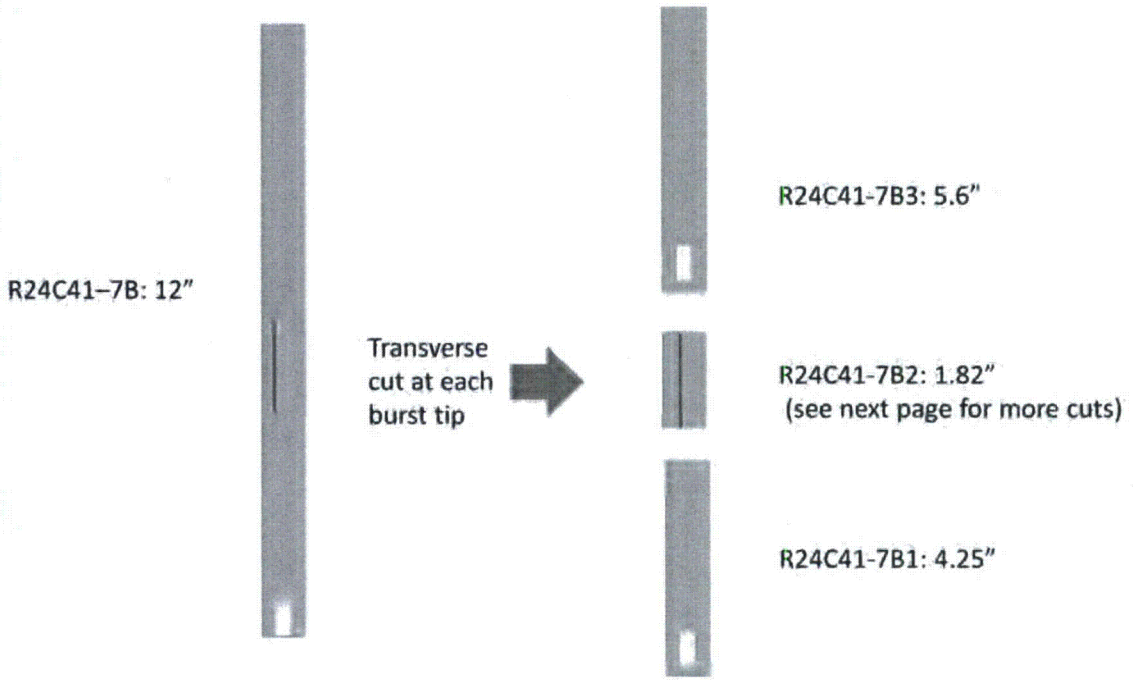

Figure 6-26: Sectioning Diagram for R24C41 Section 7B

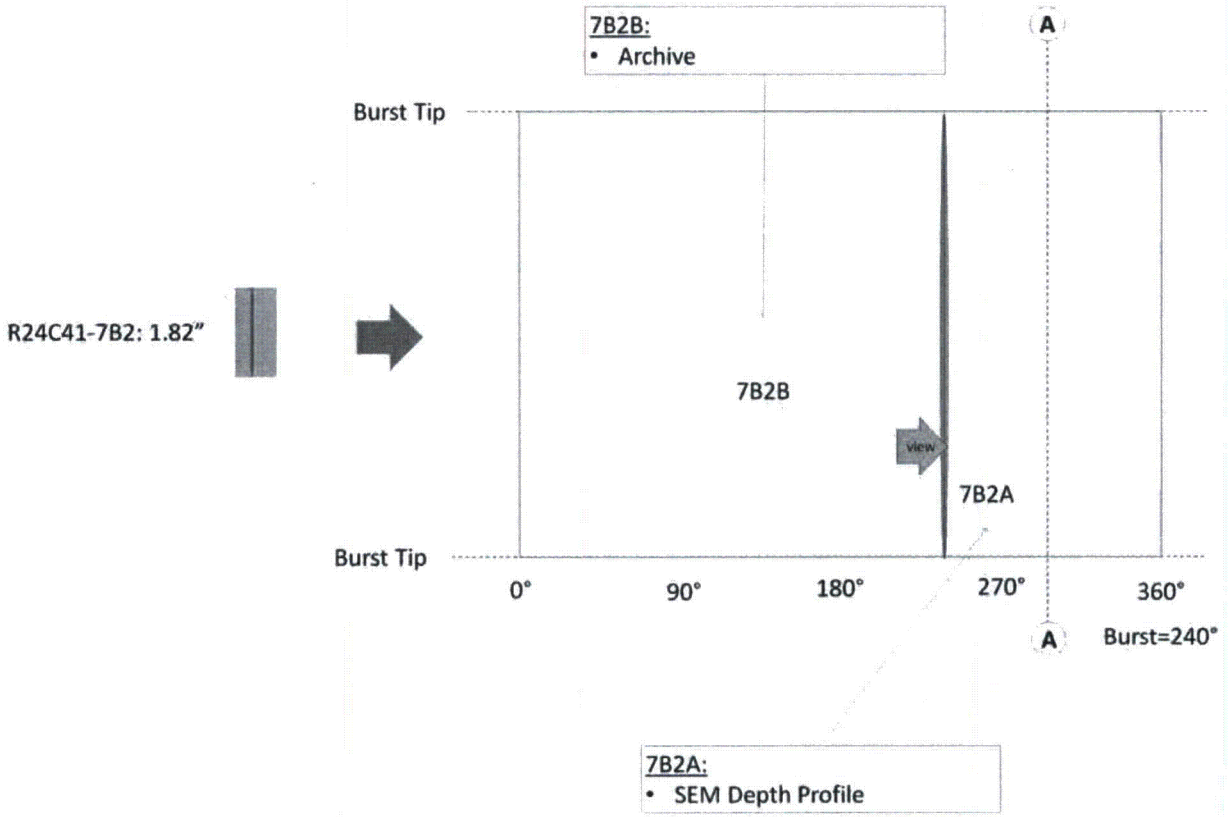

Figure 6-27: Sectioning Diagram for R24C41 Section 7B2

7.0 SEM FRACTOGRAPHY

7.1 Sample Preparation

A ½-inch wide sample was cut from the right side of each burst opening, as was depicted in the diagrams of Section 6.0. The cuts were made so as to include both tips of the burst opening. Each sample examined by Scanning Electron Microscopy (SEM) was blown with a jet of dry oil-free air to minimize non-conductive particulates from the fracture surfaces that would otherwise collect an electrical charge (and thus hinder the view) during the SEM examination.

7.2 Procedure

Observations made during the SEM examination were documented with micrographs. A TESCAN LYRA Scanning Electron Microscope was used for the fractography examination. Operation of the SEM followed the manufacturer's instruction. ASTM has not published procedures for fractography examinations. However, surfaces examined by SEM in accordance with accepted scientific principles and EPRI guidelines can be compared with fractographs presented in various fractography textbooks, such as "Metals Handbook, Volume 12, Fractography," 9th Edition, American Society of Metals, 1985.

SEM fractographs were taken of the entire fracture surface of each burst opening. These fractographs were then aligned end to end to complete a photomontage of each crack surface. The photomontage was obtained using the back-scattered electron SEM detector. The depth of the corrosion was measured at selected intervals, providing a set of depth vs. axial location measurements. The depths were converted to percent throughwall (%TW) values by dividing the depth measurement by the nominal wall thickness of 50 mils.

Fractographs were taken of selected locations at higher magnifications to characterize the crack morphology. Crack characterization was performed using the secondary electron SEM detector.

Uncorroded ligaments within the length of the crack were sized in terms of depth, area and axial location. Ligaments were characterized as "in-plane" (the face of the ligament running parallel with the crack face) or "out-of-plane" (running perpendicular to the crack face), depending on which direction most of the ligament area was oriented.

7.3 Fractography Depth Profiles

The four burst openings that occurred in regions of freespan tubing were confirmed to have no sign of intergranular corrosion on the burst surfaces. The remaining two burst openings that occurred on the TSP regions in section R19C38-3B (02H) and R24C41-6B (04H) both displayed intergranular corrosion morphologies within each TSP region. Degradation (a crack-like or volumetric feature not associated with the tube pulling operation) was not observed outside of any TSP region.

Each burst opening was cut from its tube so as to include both the upper burst tip and the lower burst tip in the same sample. Figure 7-1 and Figure 7-2 show low magnification views of the burst opening fractography photomontages for R19C38-3B (02H) and R24C41-6B (04H),

respectively. Because of the length of each image, the photomontage was split in two with some overlap. The top of the burst opening is shown in the upper end of the left photomontage and the bottom of the burst opening is shown in the lower end of the right photomontage.

Appendix A presents the crack depth and ligament size data. The depth profiles of the cracks in these two burst openings are shown in Figure 7-3 and Figure 7-4, respectively. Crack depth measurements were taken along the axial direction of the burst opening, starting at the lowest elevation of the burst opening (bottom of the sample, located at the bottom tip of the burst opening) and proceeding up the tube, in the axial direction, to the upper tip of the burst opening. Figure 7-1 shows how one crack depth measurement was obtained at the indicated distance from the bottom of the sample. Table 7-1 summarizes the ligament sizing results.

Table 7-2 provides a summary of the depth profiles for the burst openings. R19C38-3B (02H) had the deepest corrosion, at 49.9%TW. The burst opening of R24C41-6B (04H) had a maximum depth of corrosion of 48.6%TW.

7.4 Crack Surface Characterization

Figure 7-5 presents an example of the crack surface of the R19C38-3B burst opening. The surfaces having the rock candy appearance is intergranular cracking – this degradation of the tube wall occurred during in-service operation. The dimpled surface is ductile tearing - the part of the tube wall that mechanically failed during the burst test. Figure 7-6 presents another region of the fracture surface with intergranular cracking. The entire R19C38-3B burst opening was composed of ductile tearing and intergranular cracking of varying depth.

Figure 7-7 shows the OD surface of R19C38 02H near the burst opening. In this view, the axial direction is horizontal. This fractographic montage shows several secondary axial cracks with some minor branching and a small patch of intergranular attack (IGA). All of the secondary cracks are intergranular. This surface is typical of axial OD initiated stress corrosion cracking (ODSCC).

Figure 7-8 shows an area on the crack surface of the R24C41-6B burst opening. The figure shows both intergranular cracking (the rock candy topography) and ductile tearing. The figure shows a higher magnification view of the intergranular fracture surface. The entire R24C41-6B burst opening was composed of ductile tearing and intergranular cracking of varying depth.

Figure 7-9 shows the OD surface of R24C41 04H near the burst opening. In this view, the axial direction is horizontal. This fractographic montage shows several secondary axial cracks and some patches of shallow intergranular attack (IGA). This surface is typical of axial ODSCC.

The corrosion morphology observed on all surfaces was intergranular; there was no evidence of transgranular stress corrosion cracking.

Table 7-1: Ligament Sizing Results

Tube TSP Sample	Axial Position Above Bottom End of Sample (mils)	Crack Depth (%TW)	Ligament Orientation Compared to Crack Face	Ligament Uncorroded Area ($mils^2$)	Ligament Depth (%TW)
R19C38 02H Sample 3B2A	90.84	23.1	Out-of-Plane	123.65	13
	129.04	20.6	In-Plane	37.44	14
	163.08	26.0	In-Plane	68.80	19
	192.07	28.1	Out-of-Plane	275.32	24
	221.40	22.2	Out-of-Plane	14.42	15
	404.38	11.7	Out-of-Plane	26.56	10
	507.67	39.2	Out-of-Plane	128.28	19
	637.29	39.1	Out-of-Plane	32.72	11
	686.43	44.6	Out-of-Plane	29.27	18
R24C41 04H Sample 6B2A	507.67	20.2	Out-of-Plane	40.33	14
	669.91	37.8	Out-of-Plane	18.14	19
	732.92	13.1	Out-of-Plane	16.31	13

Table 7-2: Summary of Burst Opening Depth Profiles

Section	Region of Burst	Crack Length (in)	Maximum Depth (%TW)
R19C38-3B	02H	0.702	49.9
R19C38-4B	Freespan	0	0
R24C41-3B	Freespan	0	0
R24C41-5B	Freespan	0	0
R24C41-6B	04H	0.270	48.6
R24C41-7B	Freespan	0	0

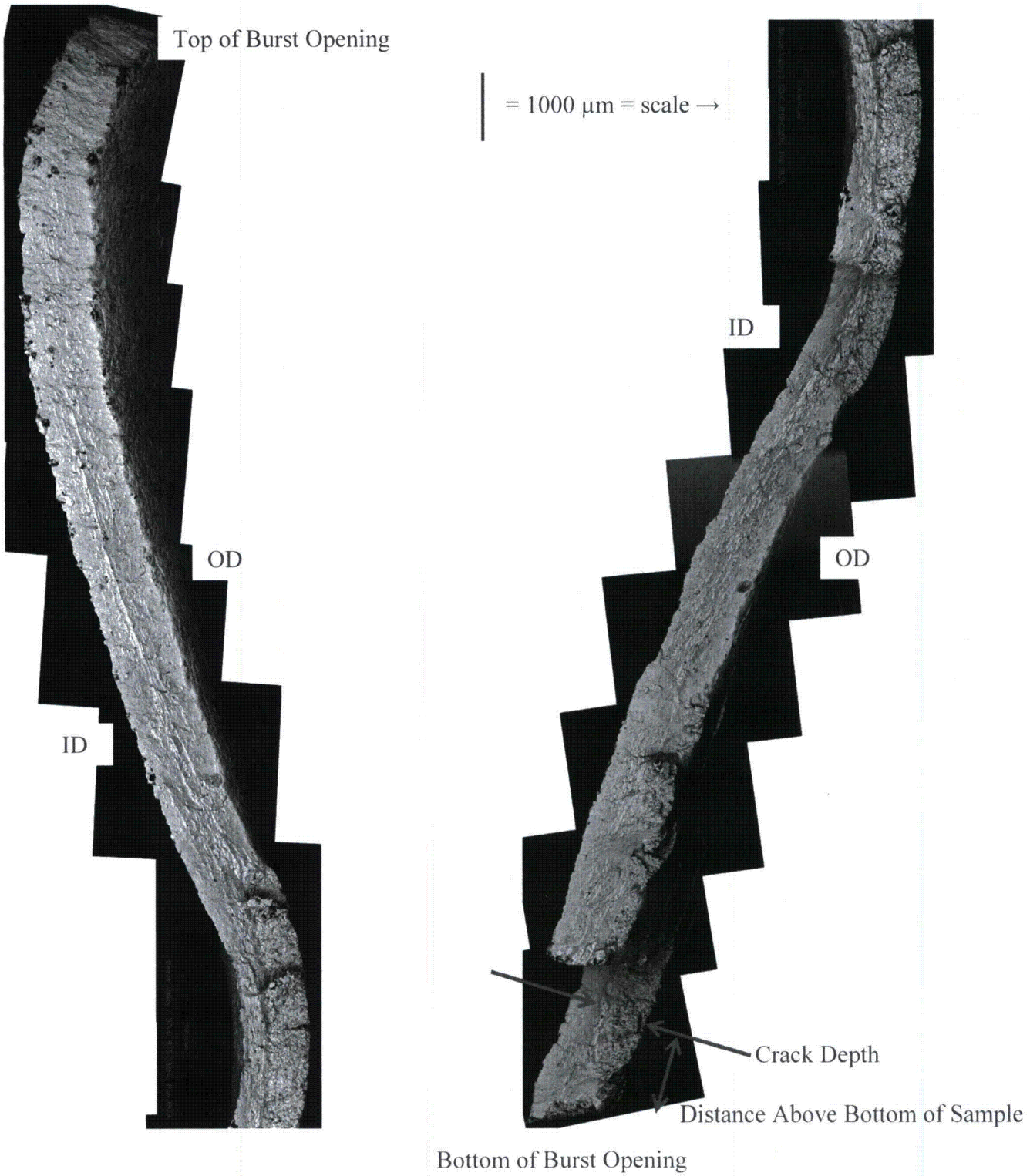

Figure 7-1: SEM Photomontage of R19C38-3B (02H) Burst Opening

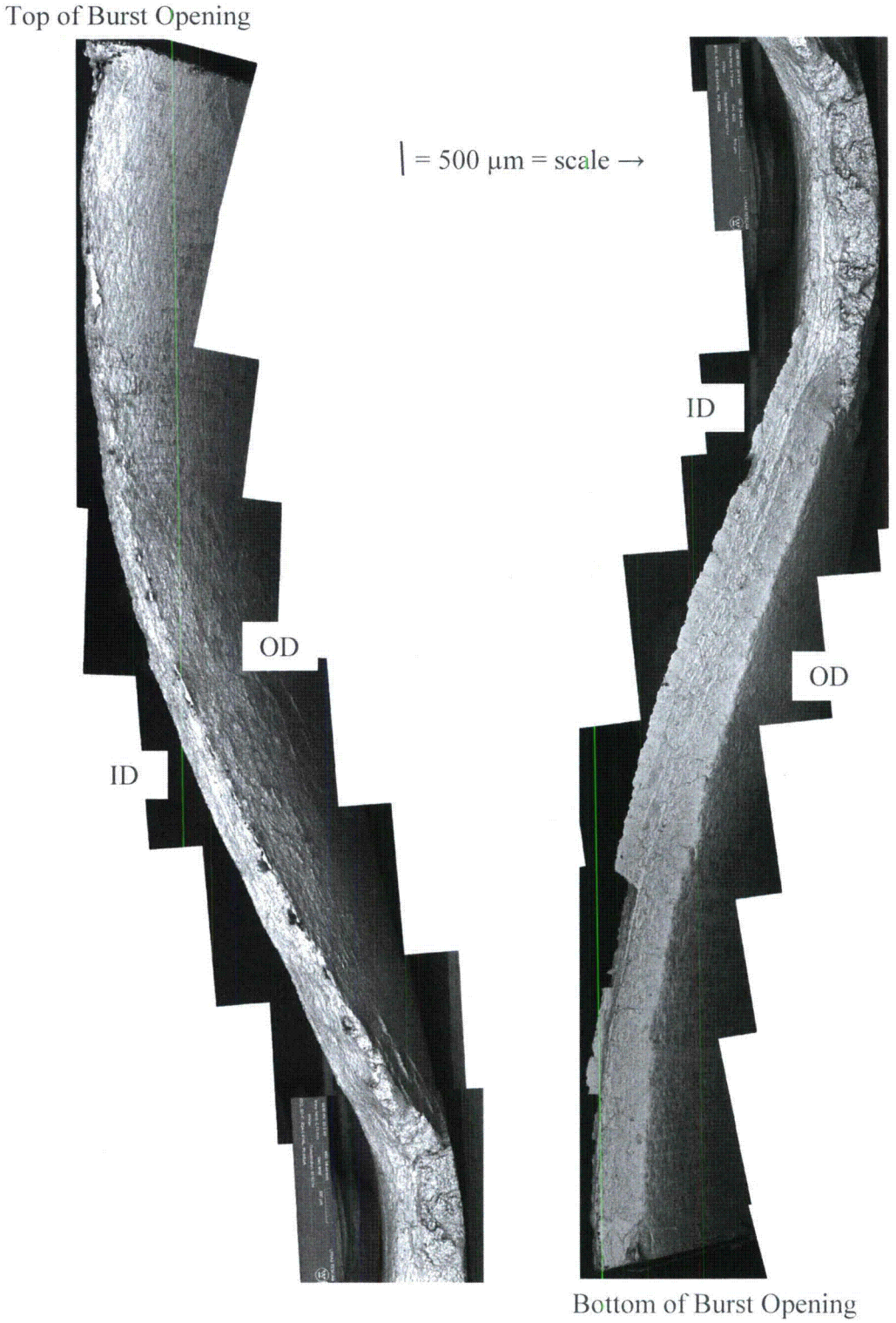

Figure 7-2: SEM Photomontage of R24C41-6B (04H) Burst Opening

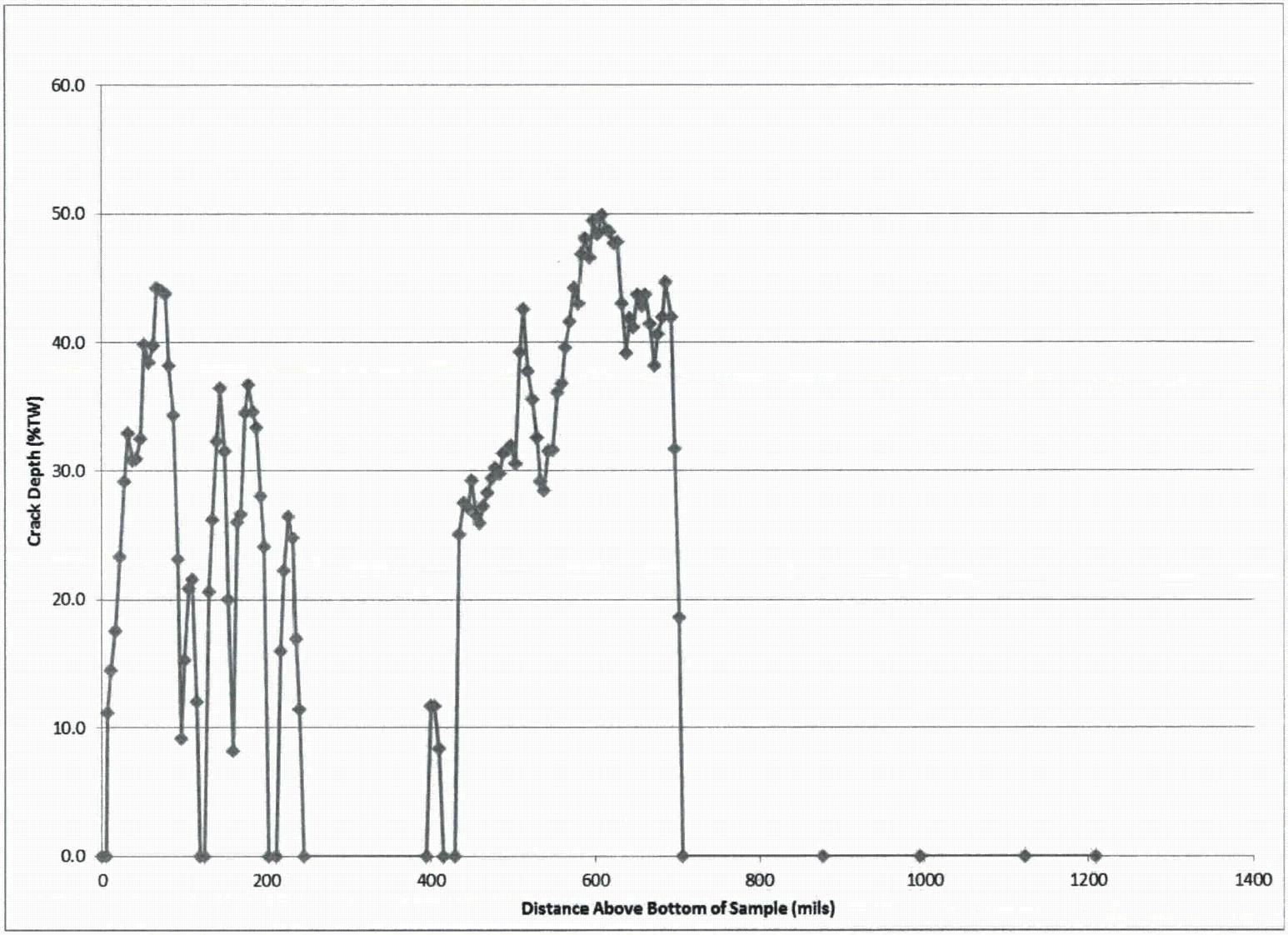

Figure 7-3: R19C38-3B (02H) Burst Opening Depth Profile

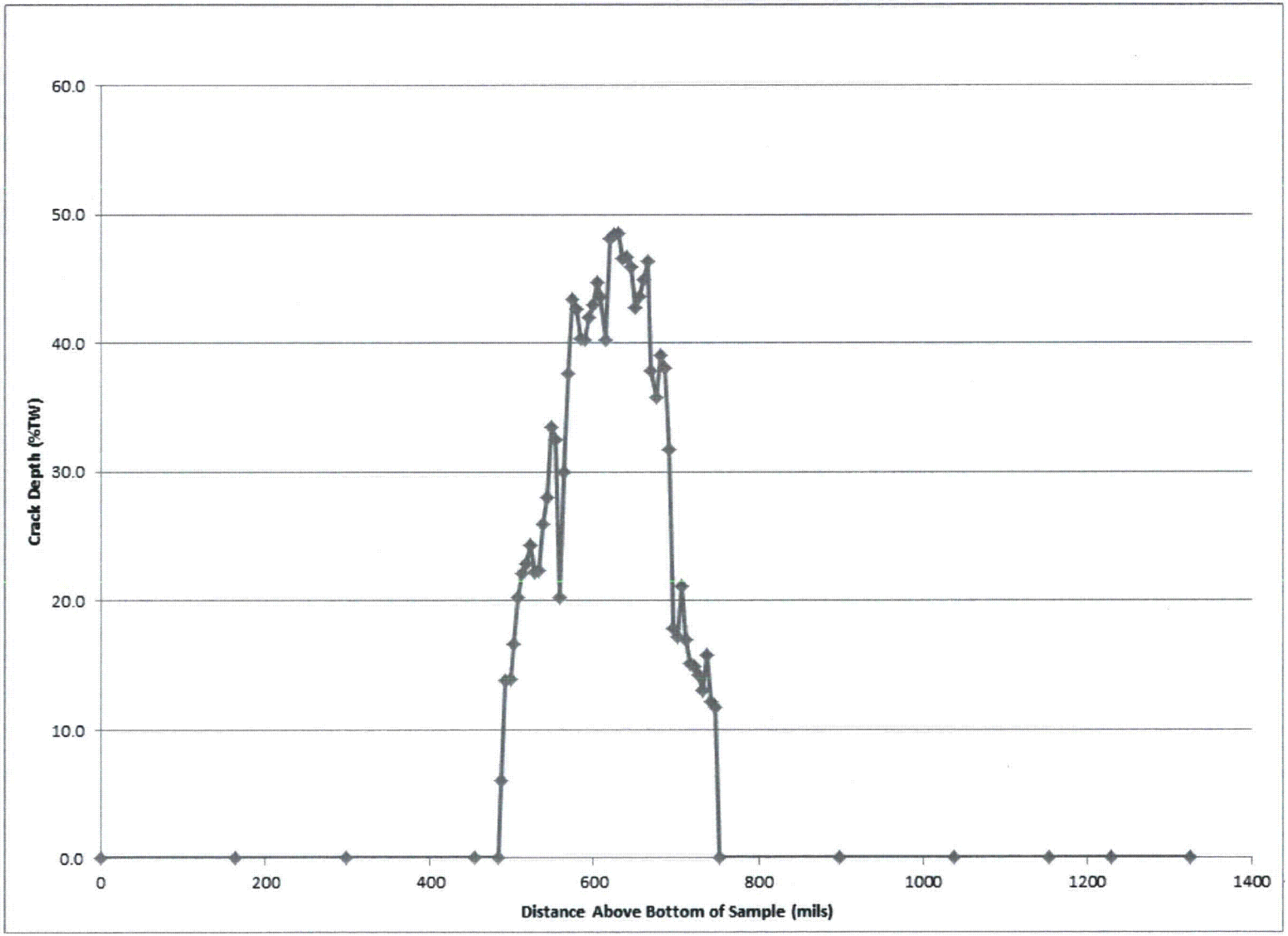

Figure 7-4: R24C41-6B (04H) Burst Opening Depth Profile

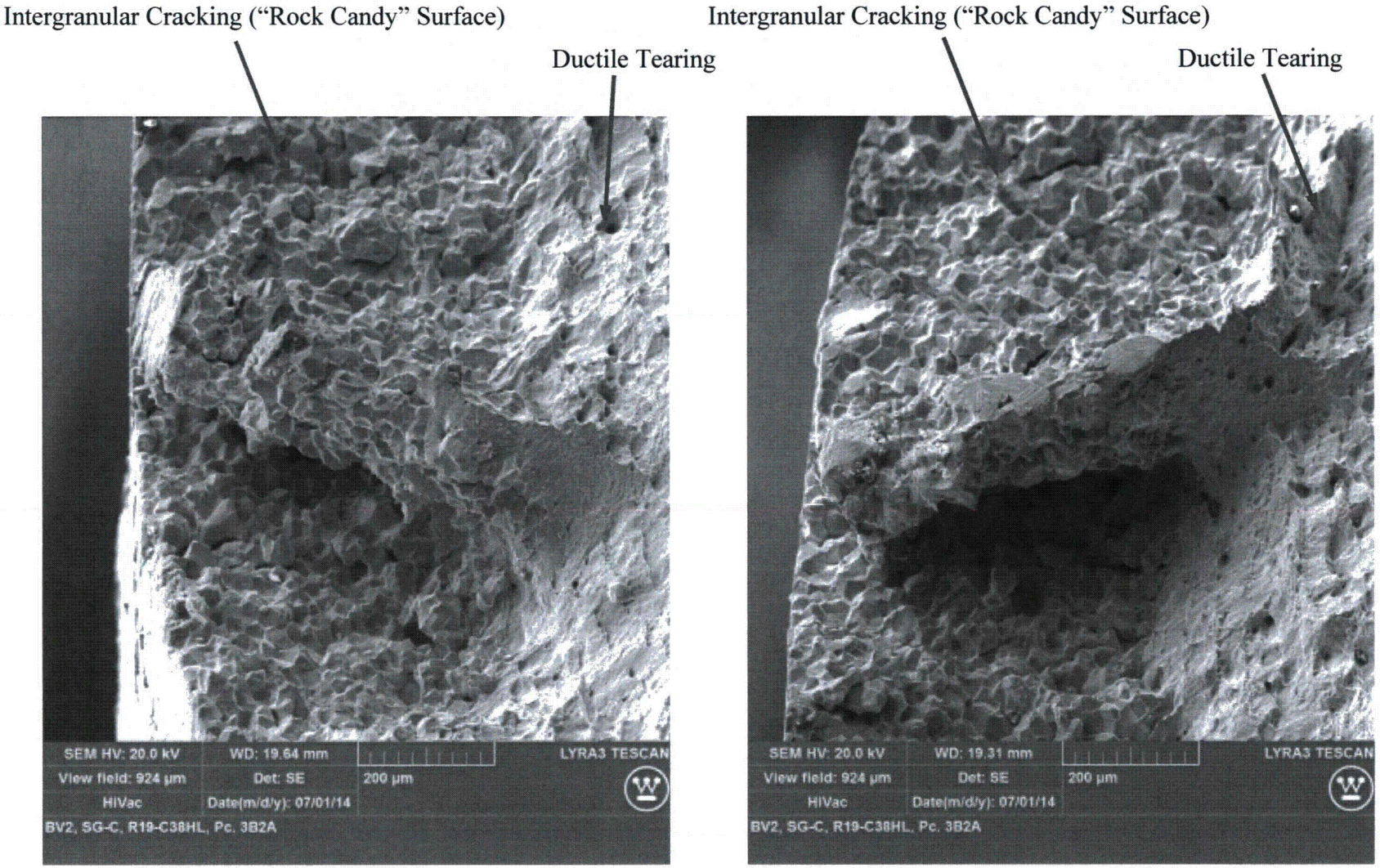

Figure 7-5: Example of R19C38-3B Burst Opening Fracture Surface (Near Top End of Crack)

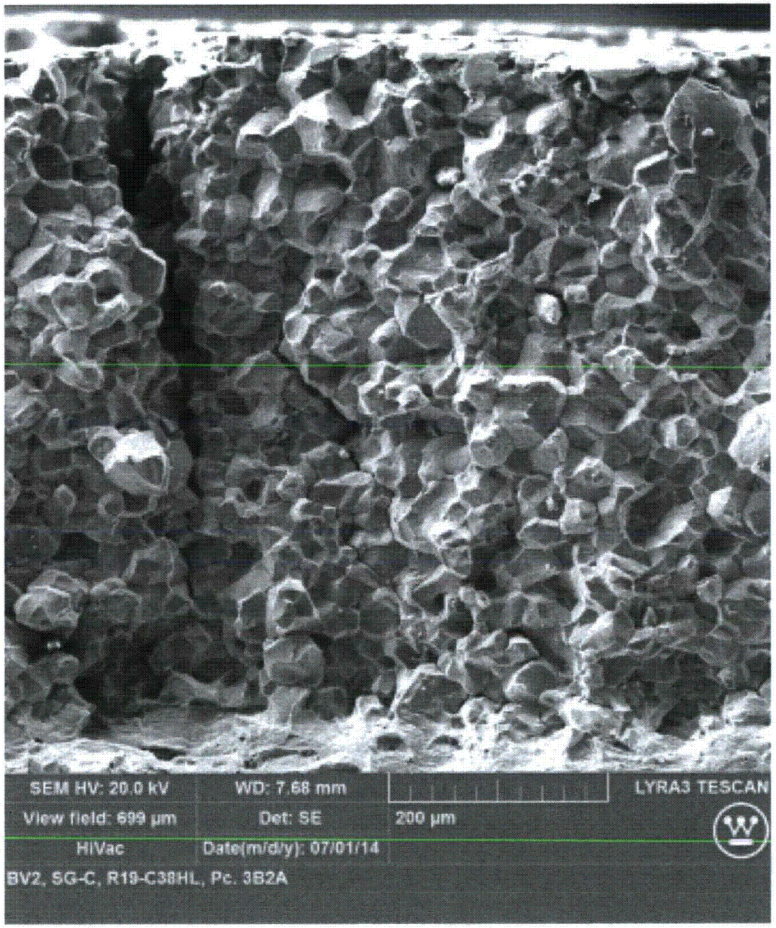

Figure 7-6: Example of R19C38-3B Burst Opening Fracture Surface (Center of Crack)

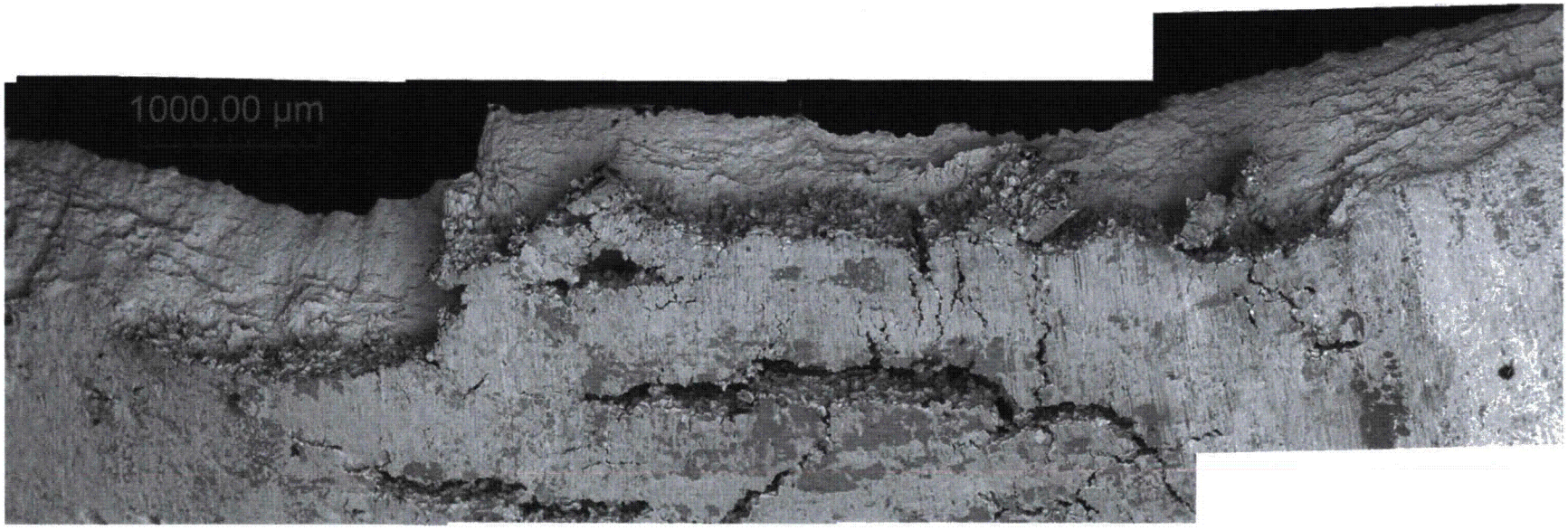

Figure 7-7: OD Surface of R19C38 02H, Adjacent to Burst Opening (Axial Direction is Horizontal)

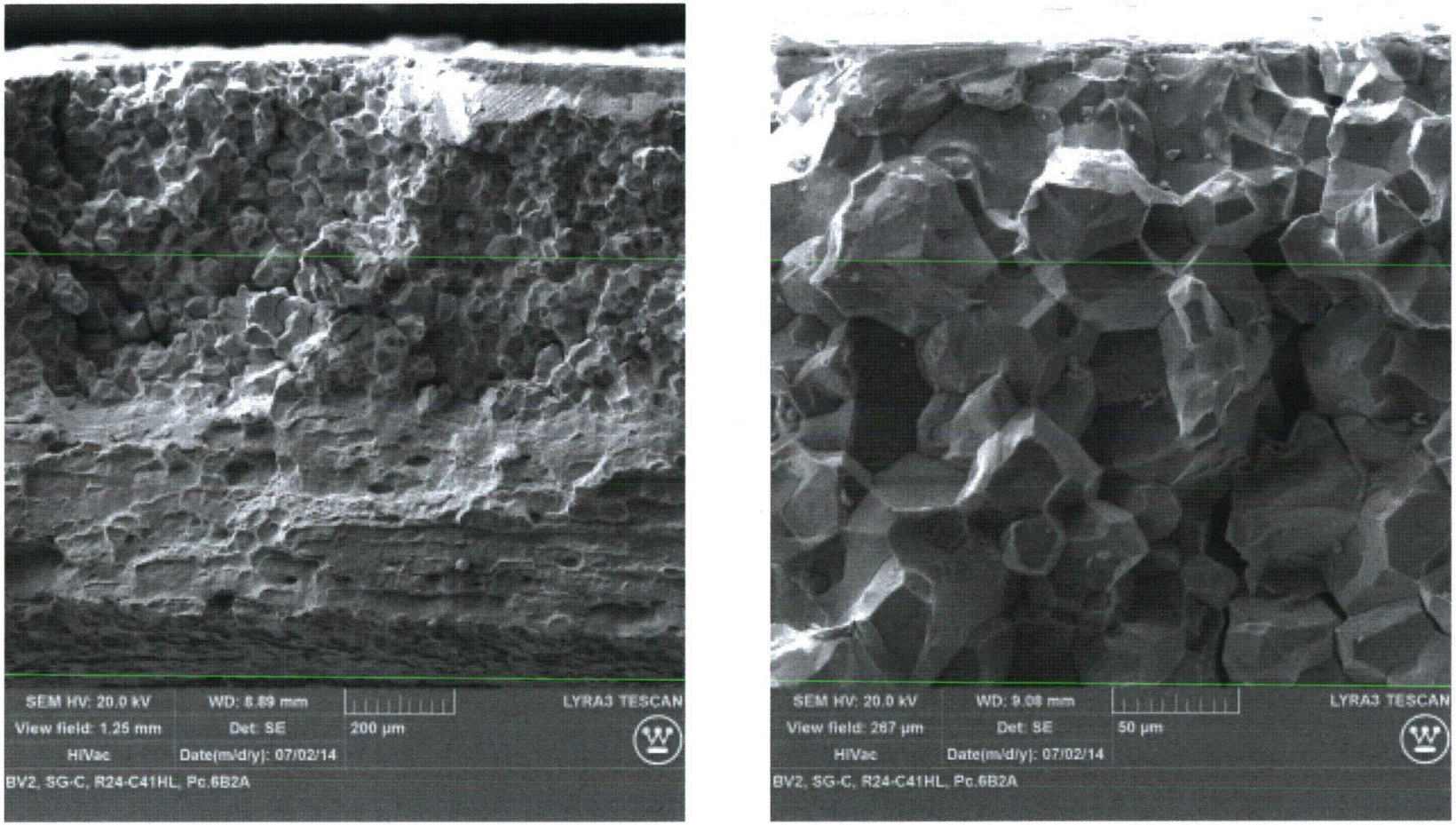

Figure 7-8: Example of R24C41-6B Burst Opening Fracture Surface

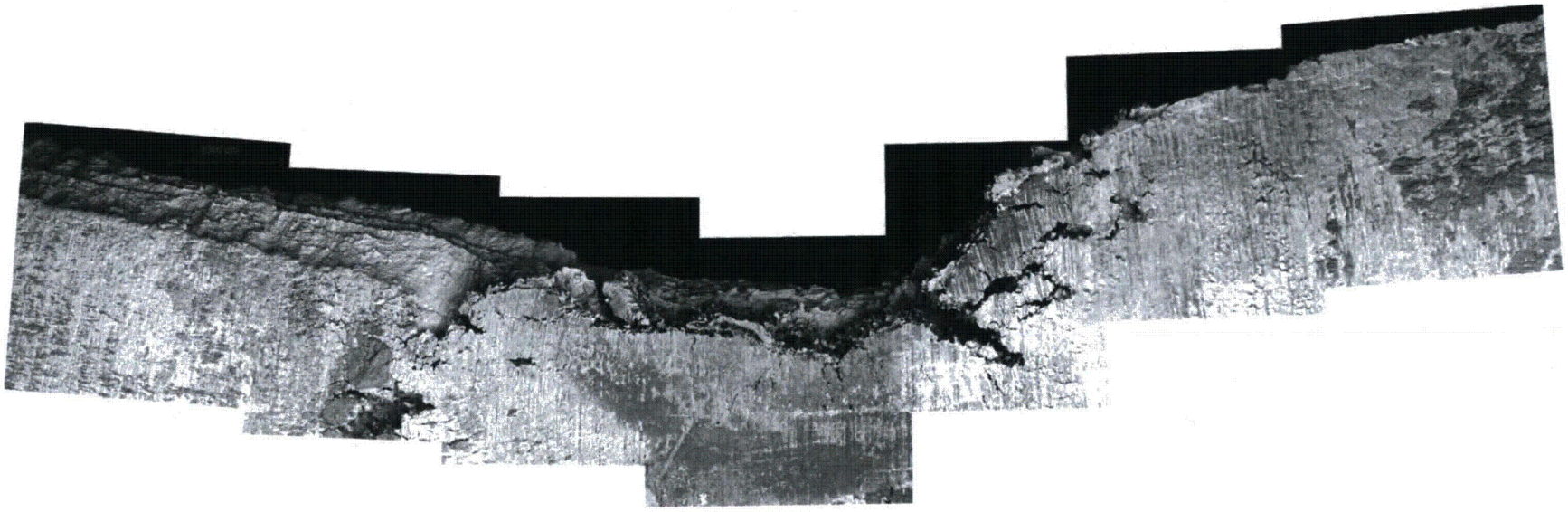

Figure 7-9: OD Surface of R24C41 04H, Adjacent to Burst Opening (Axial Direction is Horizontal)

8.0 METALLOGRAPHY OF CRACKS

8.1 Procedure

One transverse section was taken from each of the support plate regions. Table 8-1 summarizes the defect metallography samples. Table 8-2 provides a summary of the deepest cracks on each sample; these are discussed in the following sections.

The metallographic samples were mounted in epoxy to show the cracks in a transverse cross-section. Each mounted sample was ground with SiC papers, followed by diamond wheels using polishing oil, followed by diamond aerosol sprays, leaving the edge to be examined with a mirror finish. Samples were then examined and photographed after an electrolytic Nital etch. The electrolytic Nital etch was used to highlight the relationship between the cracks and the grain boundaries.

All of the images were taken on a Zeiss Observer Model D1M optical light microscope. Each image included a calibrated scale. Photographs were analyzed using the software program PAX-it (Version 7.8.0.0), which has a feature that allows the measurement of distances based on the calibrated scale on the image. Crack depths were measured using PAX-it. Depth measurements were converted to percent throughwall (%TW) by dividing by the nominal wall thickness.

8.2 R19C38 02H

Figure 8-1 shows a view of a transverse cross-sectional sample (3B2B) taken from the 02H TSP of R19C38. The gap in the circumference is the SEM sample (refer to the Figure 6-6 sectioning diagram). The left side of the burst opening is just to the left of the '2' mark in the figure.

At this elevation of the TSP, there were only two areas, other than the burst opening that showed any sign of corrosion; these are indicated by the number markers in Figure 8-1. The '1' marker is where the cracks at the 200° azimuthal location were identified (see Figure 5-14 and Figure 5-17). The number '2' marker is associated with the cracks near the 340° location (see Figure 5-14). Cracks near the 0° location are on the SEM sample and the cracks near the 280° location were very short and were not captured in this cross section.

Figure 8-2 shows a closer view of the cracks at the 200° location. The cracks have been widened by the swelling of the tube during the burst test. Cracking is intergranular without signs of IGA and are thus intergranular stress corrosion cracks (IGSCC). As these initiate from the outer surface, they are also ODSCC. The figure shows several cracks, two of which break the OD surface at this elevation and two cracks which break the OD surface at another elevation that is not shown in this view. The deepest of these (the middle crack) is 25.7%TW.

Figure 8-3 shows a crack at the 340° location, as well as the left side of the burst opening. The 340° crack is 22.9%TW and the crack depth of the burst opening is approximately 27%TW at this elevation. The figure also shows two other cracks which break the OD surface at another elevation that is not shown in this view.

8.3 R24C41 02H

Figure 8-4 shows a view of a transverse cross-sectional sample (3B2) taken from the 02H TSP of R24C41. As the burst occurred outside of the TSP region, the entire circumference is shown. The white circular marker "O" that is mounted inside the tube corresponds with the 0° location (since the view is in the down direction, azimuthal locations proceed in the counter-clockwise direction. This elevation was chosen to show the cracks at about the 170° location and the patch of shallow corrosion on both sides of 0° (see Figure 6-15 and Figure 5-18). The '1' marker is located at about 20°, the '2' marker is at about 160° and '3' marker is located at about the 340° location.

Figure 8-5 shows the 20° location of Marker '1'. It shows two shallow axial ODSCC, without any IGA. The maximum depth shown is 11.3%TW.

Figure 8-6 shows the 160° location of Marker '2'. It shows three shallow axial ODSCC, without any IGA. The maximum depth shown is 14.2%TW.

Figure 8-7 shows the 340° location of Marker '3'. It shows two shallow axial ODSCC, without any IGA. The maximum depth shown is 10.7%TW.

8.4 R24C41 03H

Figure 8-8 shows a view of a transverse cross-sectional sample (5B2) taken from the 03H TSP of R24C41. As the burst occurred outside of the TSP region, the entire circumference is shown. The "O" that is inside the tube corresponds with the 0° location (since the view is in the down direction, azimuthal locations proceed in the counter-clockwise direction). This elevation was chosen to show the cracks at the 180° location and the patch of shallow corrosion (see Figure 6-19 and Figure 5-20). The '1' marker is located at about 180°.

Figure 8-9 shows the cracks at the 180° location. The cracks are intergranular, but are shallow. These are only 2-4 grains deep. The deepest crack in this view is 4.4%TW.

8.5 R24C41 04H

Figure 8-10 shows a view of a transverse cross-sectional sample (6B2B) taken from the 04H TSP of R24C41. The gap in the circumference is the SEM sample (refer to the Figure 6-23 sectioning diagram). The left side of the burst opening is just to the right of the '1' mark in the figure, and the "O" that is inside the tube corresponds with the 0° location (since the view is in the down direction, azimuthal locations proceed in the counter-clockwise direction).

As the mid-plane of the visual observation map shows (Figure 5-23), there were several patches of cracks around the mid-plane of the 04H TSP. There were small cracks at the 80° location (Marker '1'), the 40° location (Marker '2'), and larger cracks in the 315°-360° range (Markers '3', '4' and '5').

Figure 8-11 shows the 80° location of Marker '1'. It shows several axial ODSCC cracks with a patch of shallow (<2 grains deep) IGA. The maximum crack depth shown is 16.4%TW.

Figure 8-12 shows the 40° location of Marker '2'. It shows three axial ODSCC cracks, without any IGA. The maximum crack depth shown is 23.2%TW. This location closely corresponds with the Ghent probe indication that was identified at the 29° location during the laboratory ECT (see Table 3-2).

Figure 8-13 shows the 350° location of Marker '3'. It shows several axial ODSCC cracks, without any IGA. The maximum crack depth shown is 35.2%TW.

Figure 8-14 shows the 325° location of Marker '4'. It shows several axial deep ODSCC cracks, without any IGA. The maximum crack depth shown is 40.8%TW.

Figure 8-15 shows the 305° location of Marker '5'. It shows several axial deep ODSCC cracks, without any IGA. The maximum crack depth shown is 45.4%TW.

Many of the cracks in the 305°-350° region approached the maximum crack depth in the burst fracture (48.6%TW). This region had a laboratory +Point/Ghent probe indication (at the 333°/336° locations, respectively) that likely corresponded with one of the field +Point indications (see Table 3-2). Consequently, another series of levels were examined to characterize the crack depths. The mounted sample was ground/polished and etched another eleven levels. The five largest cracks had depths measured along their lengths. Figure 8-16, which is a merger of Figure 5-24 and Figure 5-25, shows the cracks that were further characterized. Figure 8-17 provides a plot of the crack depths. The 350° orientation had a maximum depth of 46%TW at the 20 mil level (Figure 8-18).

Table 8-1: Defect Metallography Samples

Tube	TSP	Section	Mount#	View	Sectioning Diagram
R19C38	02H	3B2B	M3136	Transverse - Down	Figure 6-6
R24C41	02H	3B2	M3139	Transverse - Down	Figure 6-15
R24C41	03H	5B2	M3138	Transverse - Down	Figure 6-19
R24C41	04H	6B2B	M3137	Transverse - Down	Figure 6-23

Table 8-2: Maximum Crack Depth Measurement Results

Tube	Support	Azimuthal Orientation	Maximum Depth (%TW)	Other Depths (%TW)	Figure
R19C38	02H	200°	25.7		Figure 8-2
		340°	27.0	22.9	Figure 8-3
R24C41	02H	20°	11.3		Figure 8-5
		160°	14.2		Figure 8-6
		340°	10.7		Figure 8-7
	03H	180°	4.4		Figure 8-9
	04H	80°	16.4		Figure 8-11
		40°	23.2		Figure 8-12
		350°	35.2	See Figure 8-17	Figure 8-13
		325°	40.8		Figure 8-14
		305°	45.4		Figure 8-15
		335°	46.0		Figure 8-18

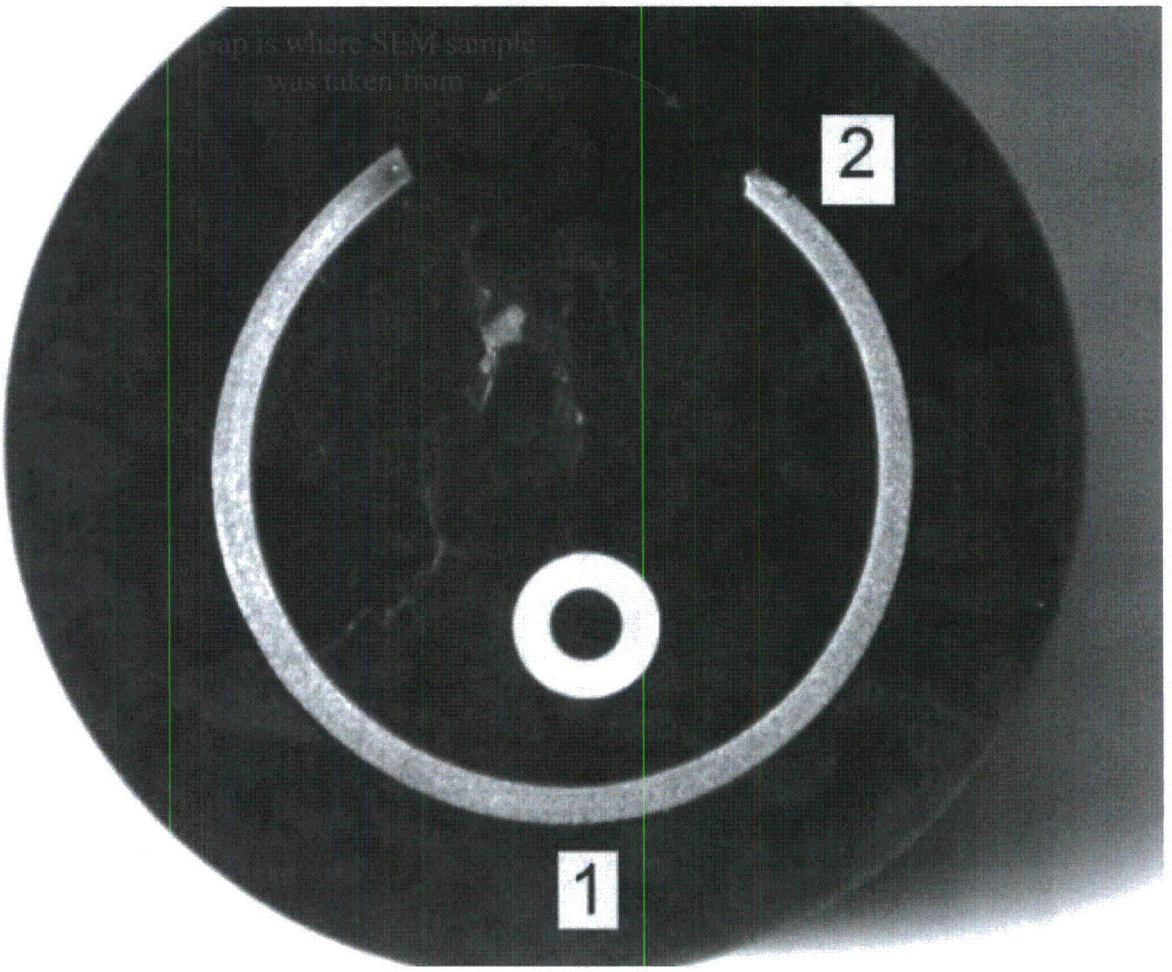

Figure 8-1: R19C38 02H - Overall View of Transverse Section

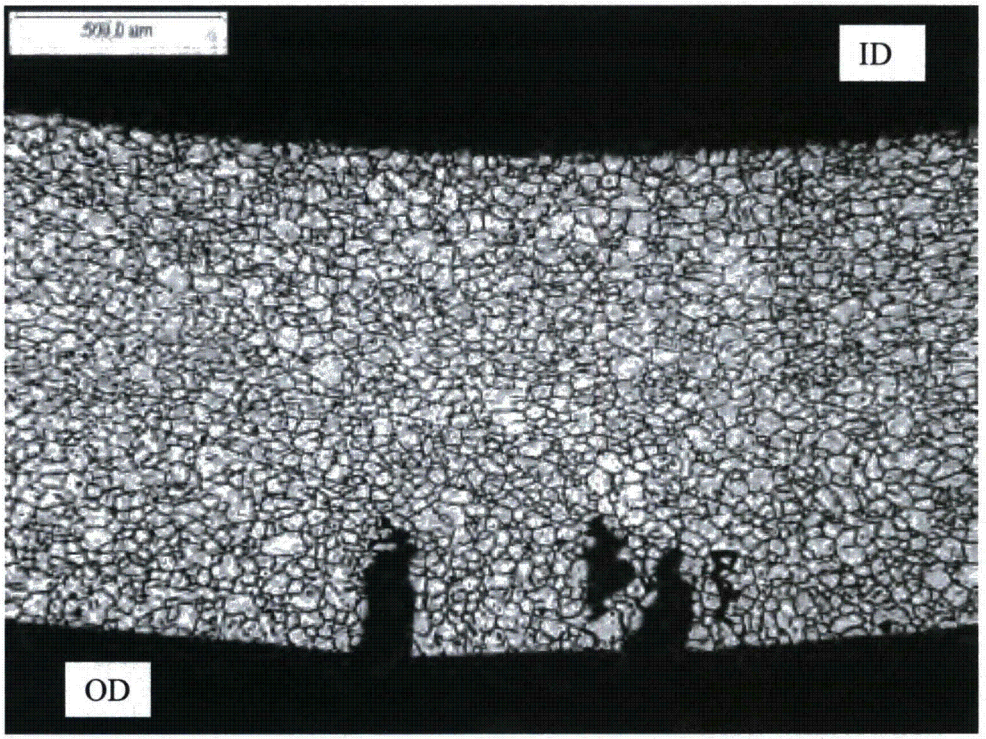

Figure 8-2: R19C38 02H, Transverse Section: Cracks at 200°

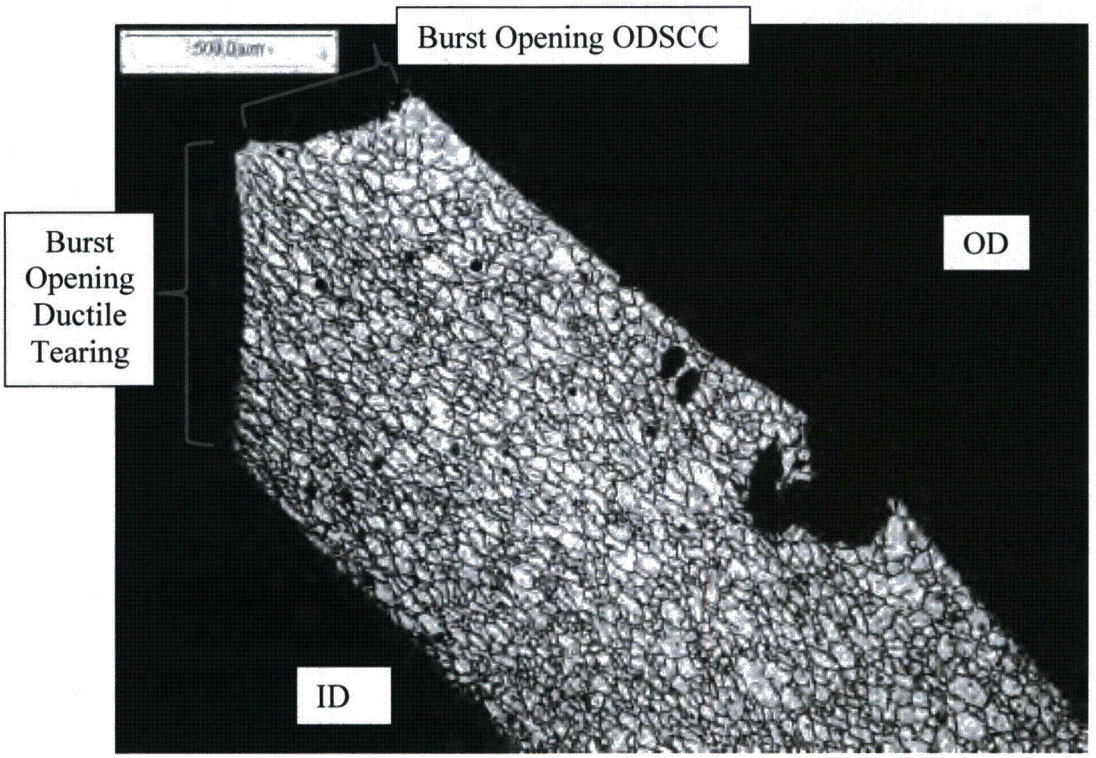

Figure 8-3: R19C38 02H, Transverse Section: Crack at 340°

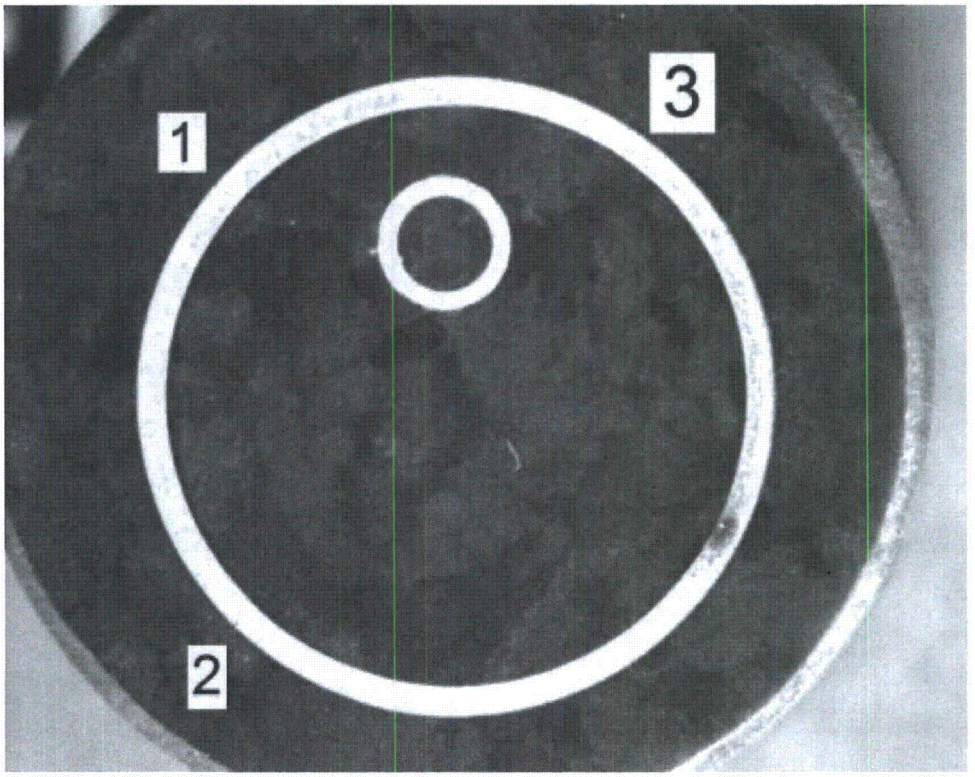

Figure 8-4: R24C41 02H - Overall View of Transverse Section

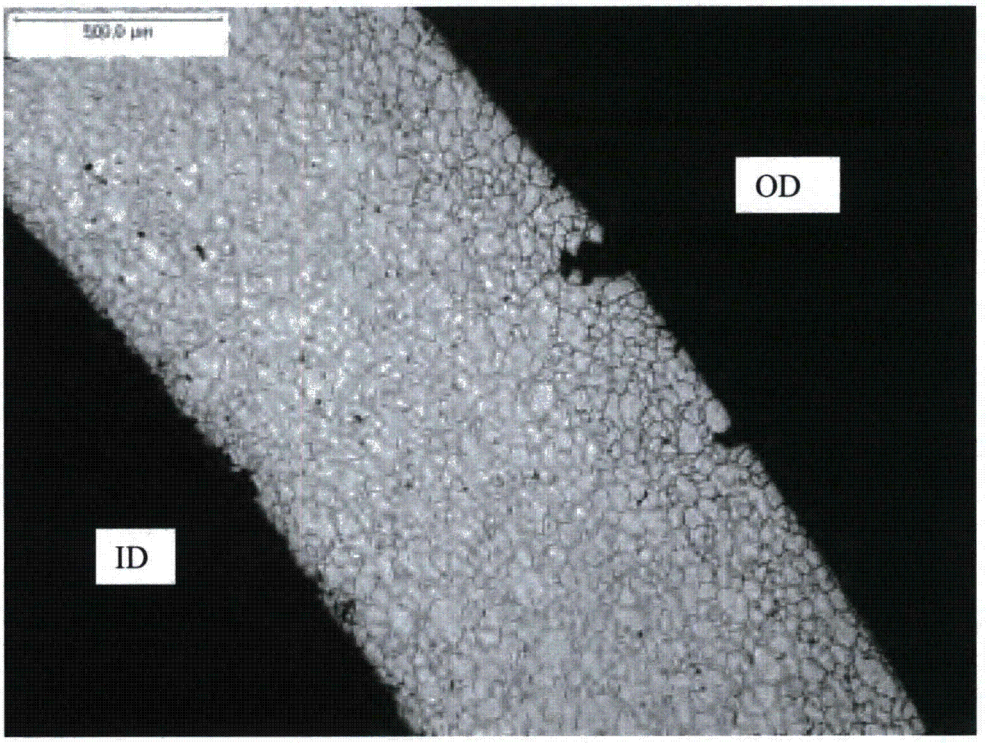

Figure 8-5: R24C41 02H, Transverse Section: Cracks at 20°

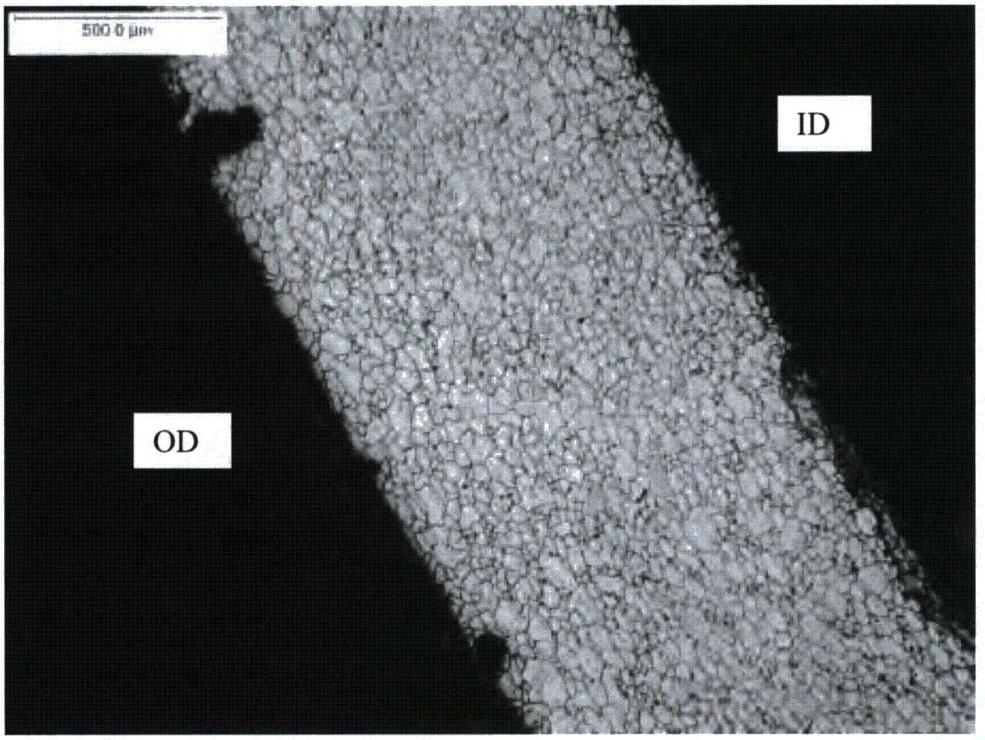

Figure 8-6: R24C41 02H, Transverse Section: Cracks at 160°

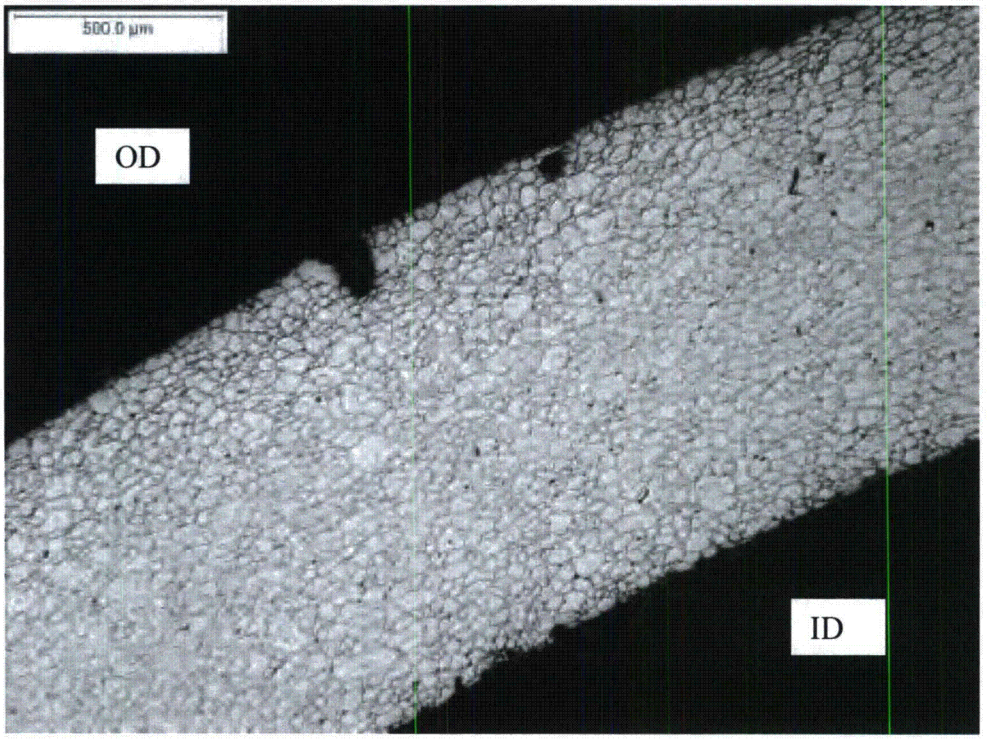

Figure 8-7: R24C41 02H, Transverse Section: Cracks at 340°

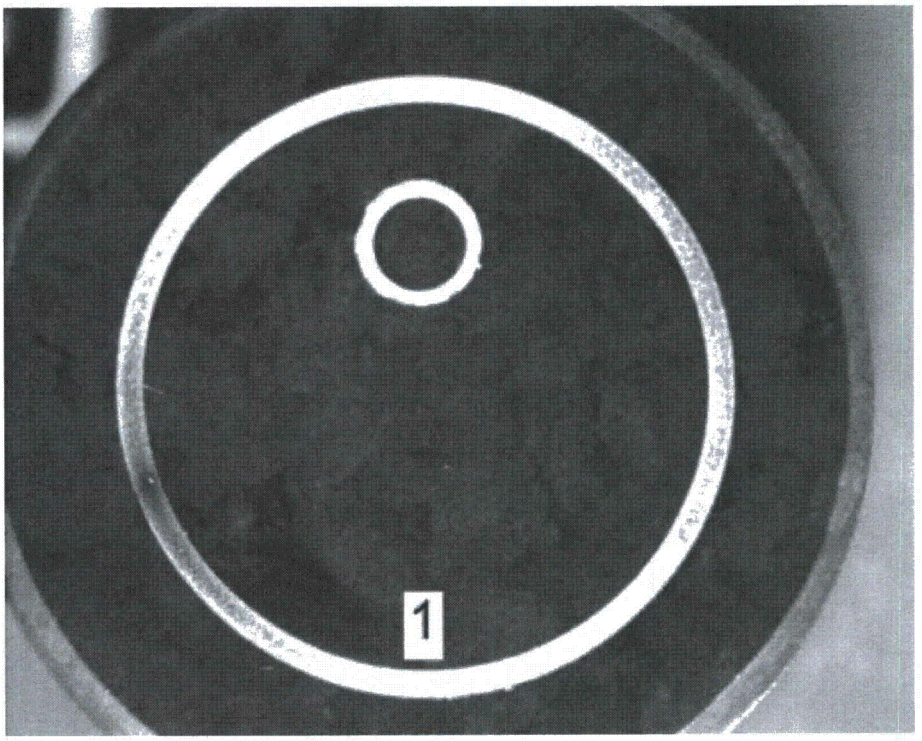

Figure 8-8: R24C41 03H - Overall View of Transverse Section

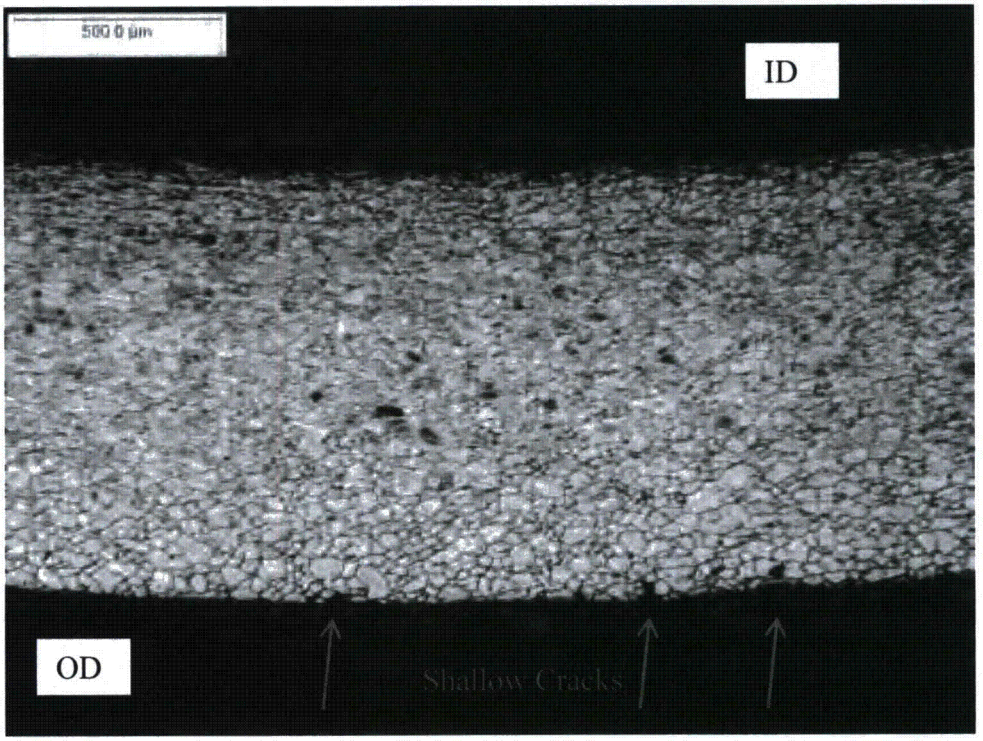

Figure 8-9: R24C41 03H, Transverse Section: Cracks at 180°

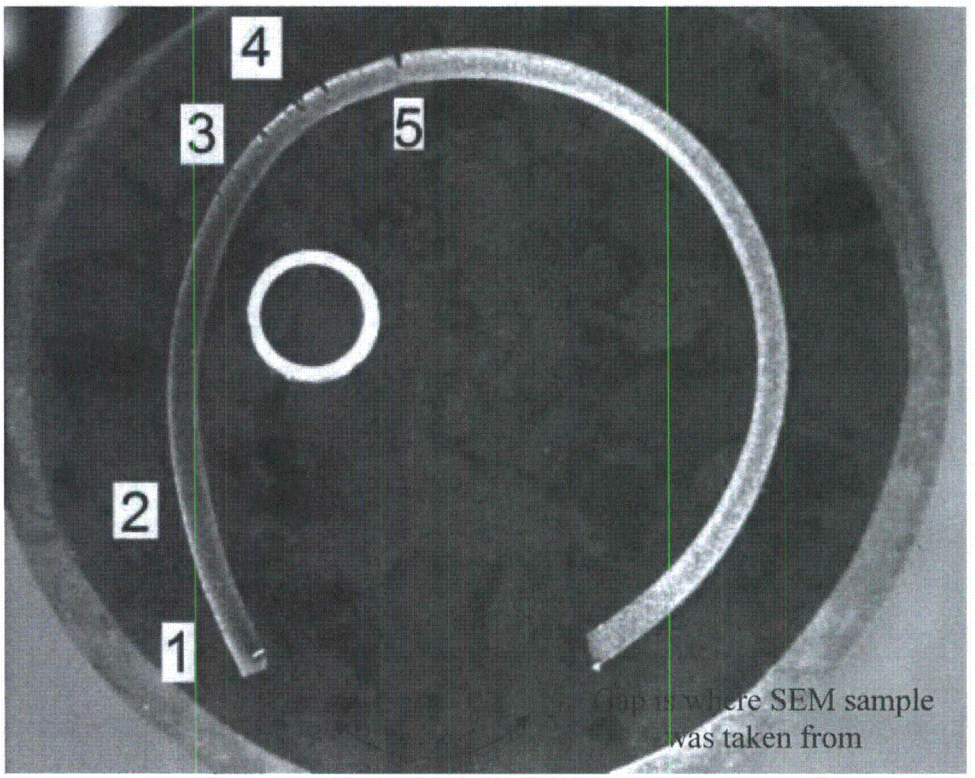

Figure 8-10: R24C41 04H - Overall View of Transverse Section

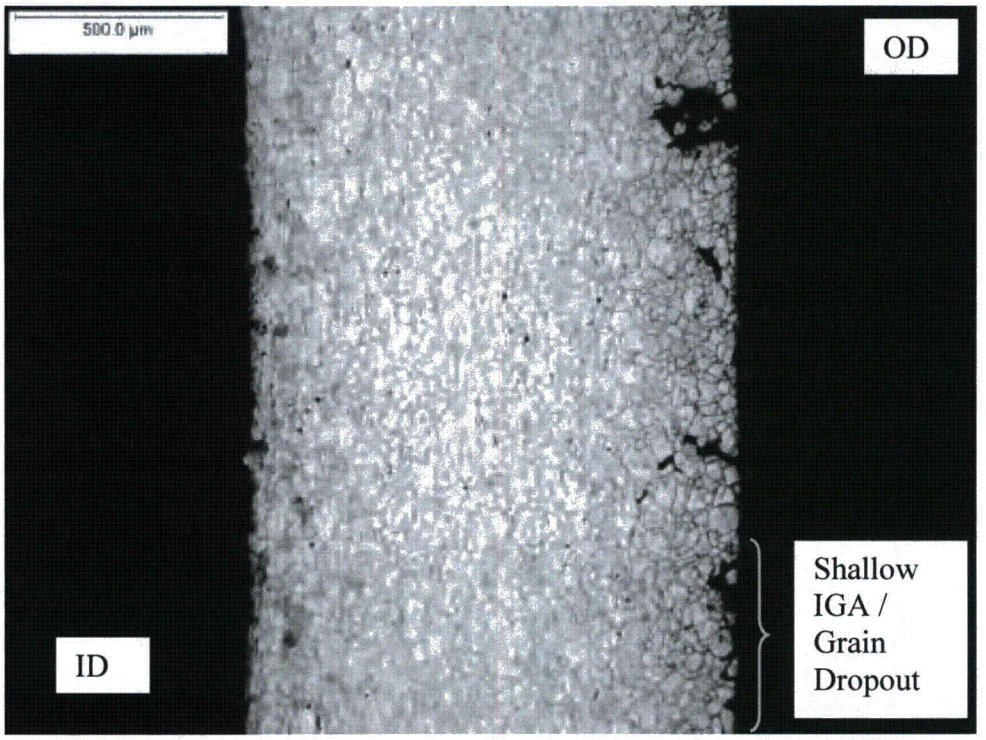

Figure 8-11: R24C41 04H, Transverse Section: Cracks at 80°

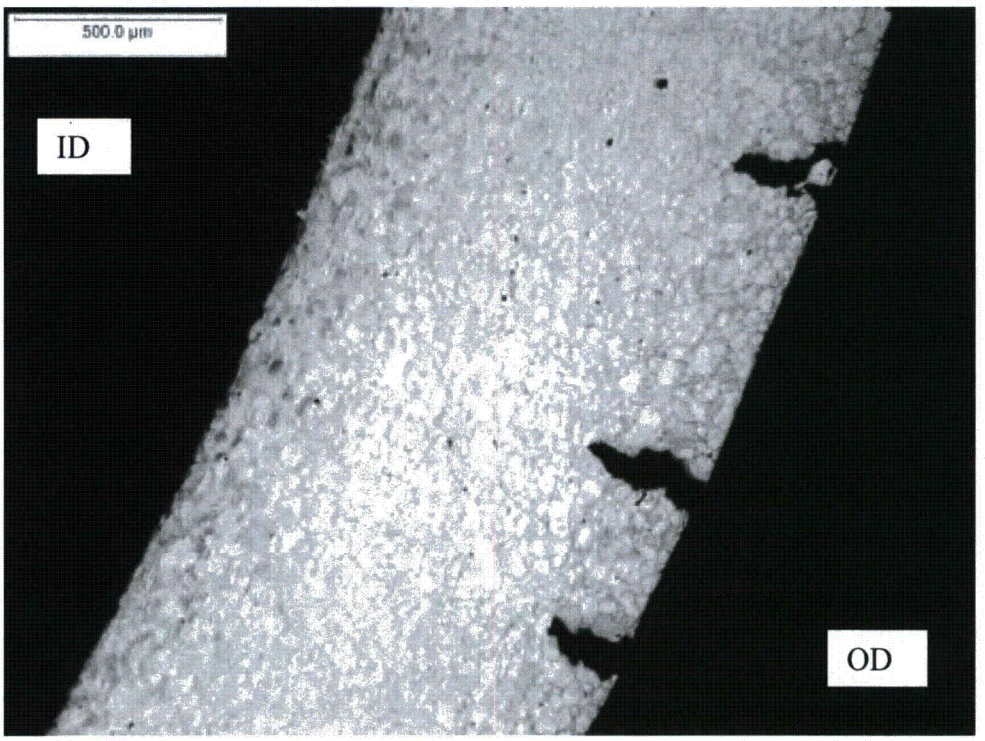

Figure 8-12: R24C41 04H, Transverse Section: Cracks at 40°

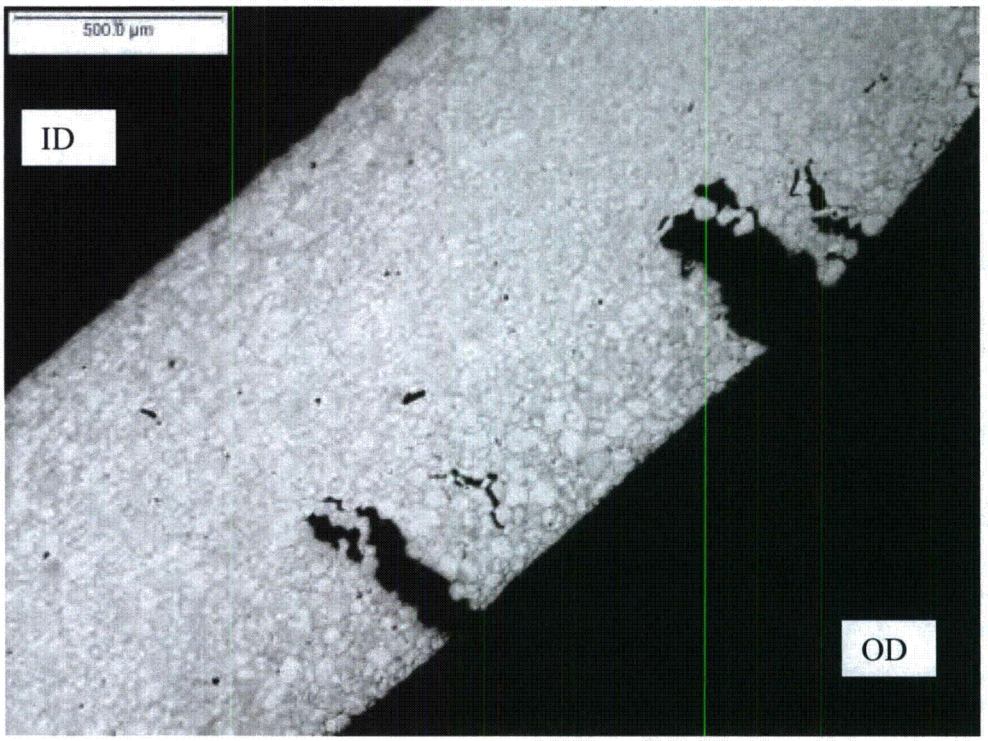

Figure 8-13: R24C41 04H, Transverse Section: Cracks at 350°

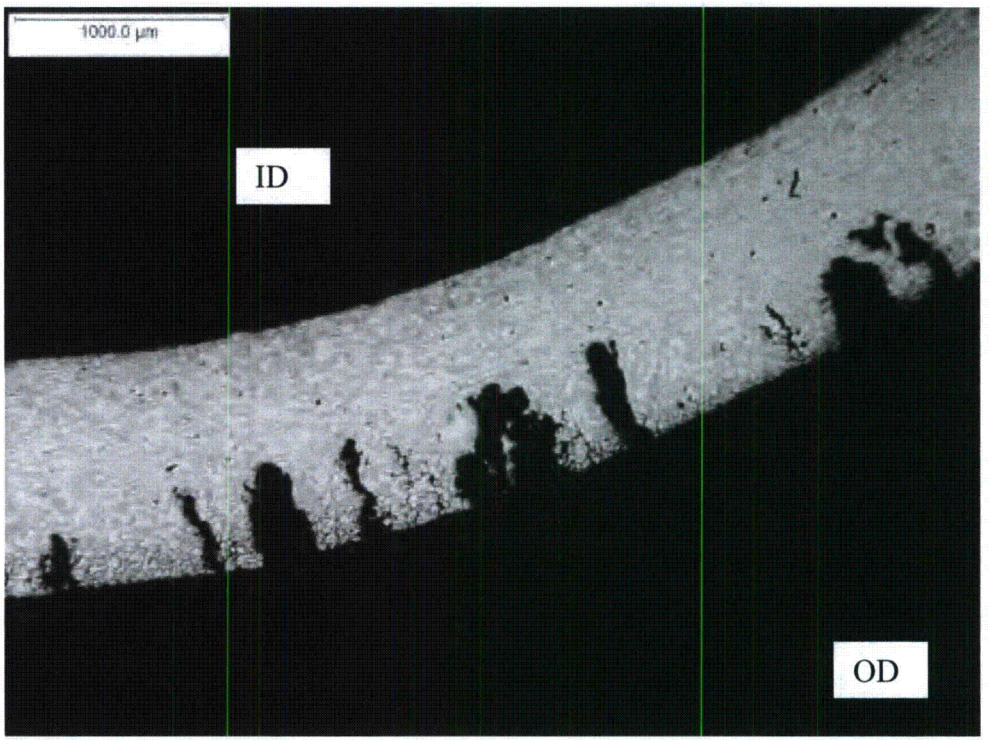

Figure 8-14: R24C41 04H, Transverse Section: Cracks at 325°

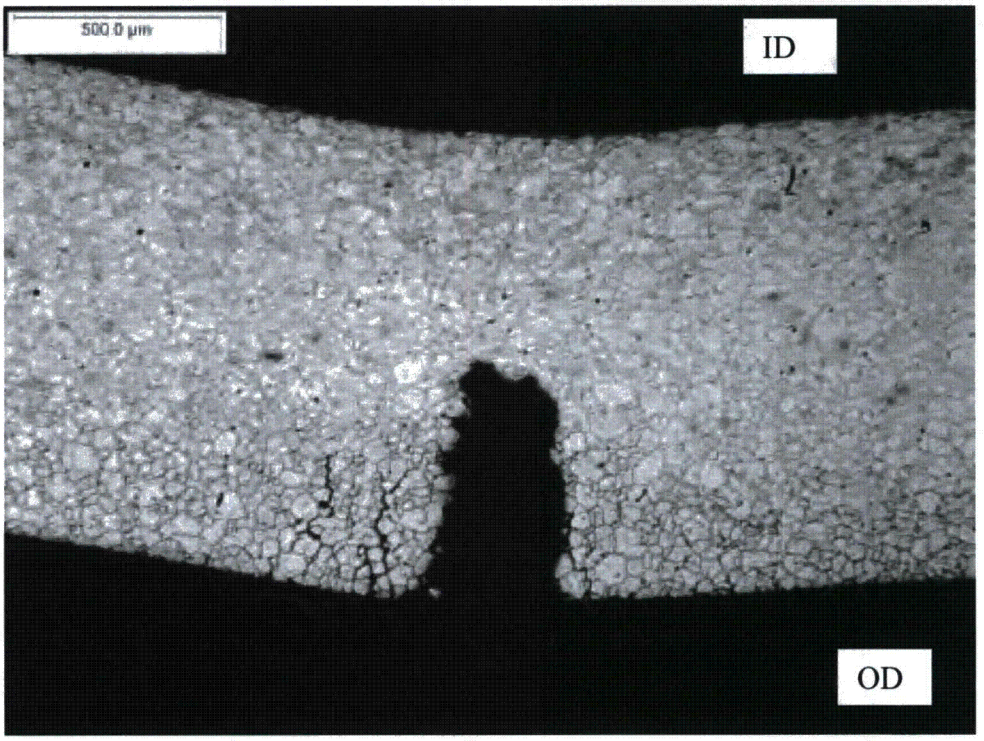

Figure 8-15: R24C41 04H, Transverse Section: Cracks at 305°

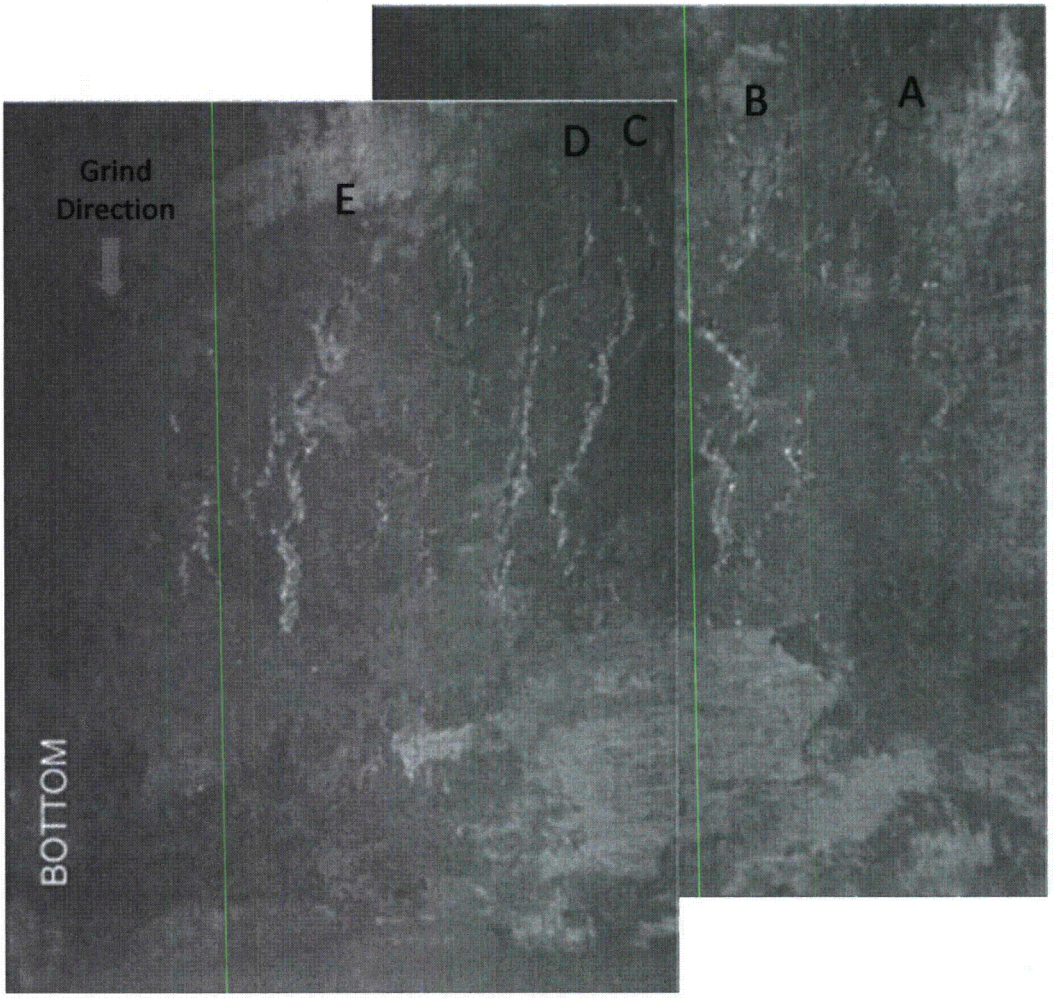

Figure 8-16: Cracks Further Characterized by Metallography (305°-350°)

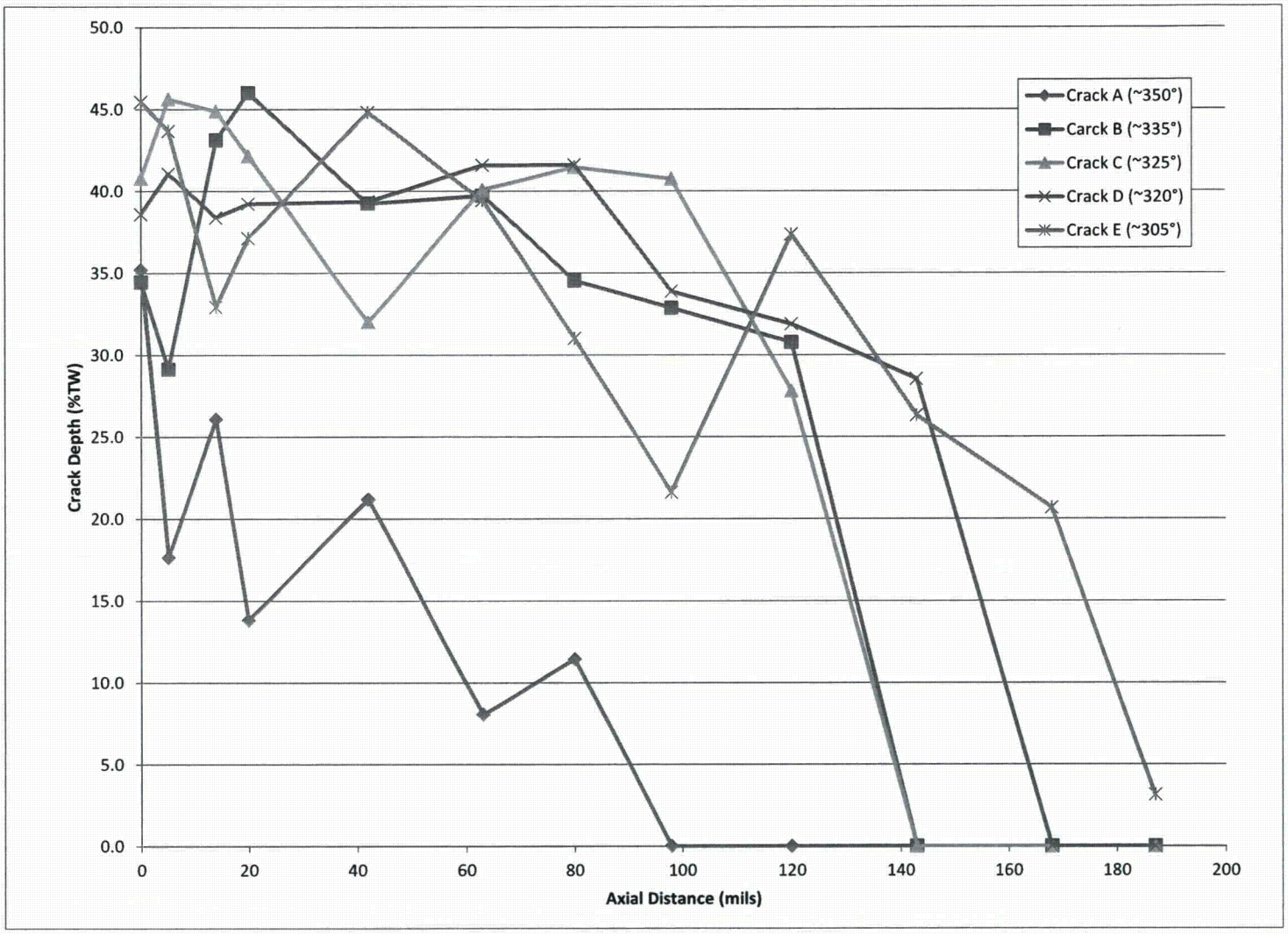

Figure 8-17: R24C41 04H Crack Depth Profiles Between 305°-350°

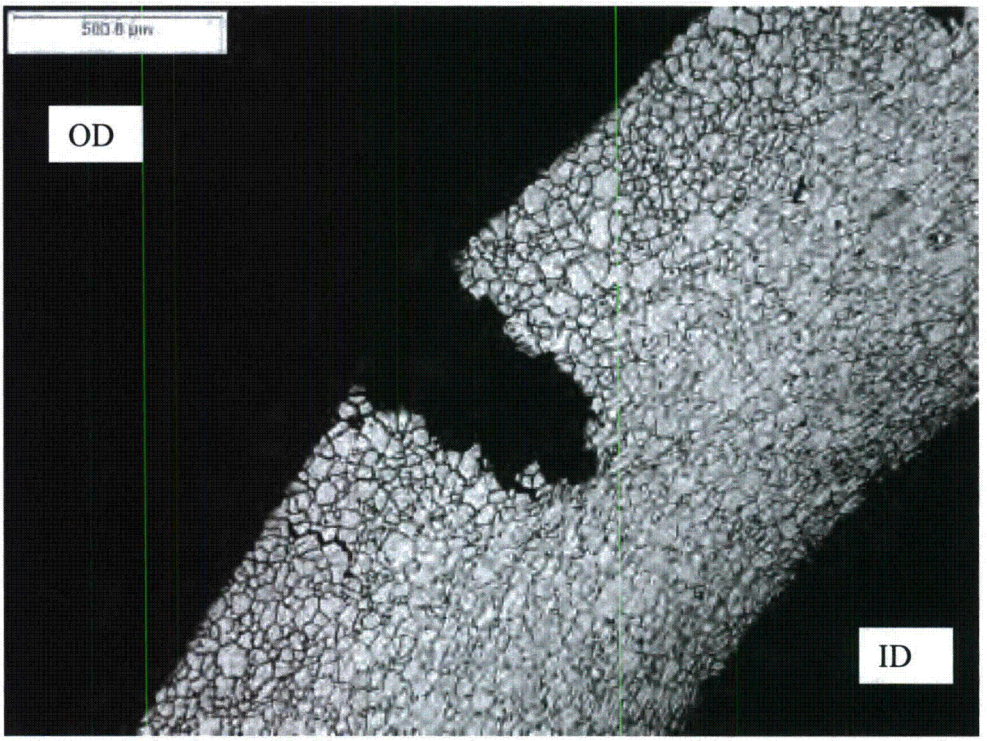

Figure 8-18: R24C41 04H, Transverse Section: Crack at 335°, 20 mil Axial Location

9.0 MATERIAL CHARACTERIZATION

9.1 Tensile Test

Mechanical properties of tubes R19C38 and R24C41 were determined by room temperature tensile tests of full cross-section tubular specimens. A 12-inch long sample was taken from a freespan region of each tube: section R19C38-4C (see Figure 6-7) and R24C41-7C (see Figure 6-24).

Tensile testing was performed in accordance with the Reference 25 work instructions and ASTM E8 test methods (Reference 26). Tests were performed on an Instron 5900 Series material testing system. An Epsilon Technology extensometer (part number 3542L-0350-200T-ST) and a 3.50 inch gauge length were used in the tests.

Both full cross section tubular specimens were fitted with snug-fitting stainless steel plugs (mandrels) that were in accordance with ASTM Standard Method E8 (Reference 26). Crosshead speeds of 0.075 inch/minute through the yield point and 0.75 inch/minute beyond the yield point were used during testing.

Figure 9-1 provides the engineering stress-strain curves for both tubes in the lower strain region, to show the yield point. Figure 9-2 provides the entire stress-strain curves for both tubes. The results of the tensile tests are provided in Table 9-1. Included in Table 9-1 are the tensile test results of the tube pulled from Beaver Valley Unit 1 in 2002 (Reference 27), the two tubes pulled from Beaver Valley Unit 1 in 1992 (Reference 28), the three tubes pulled from Beaver Valley Unit 1 in 1995 (Reference 29) and the average and standard deviation of the Reference 30 database for 7/8" tubes. As the table shows, R19C38 and R24C41 both have relatively low yield and ultimate tensile strengths in comparison with other pulled tubes, but are within a standard deviation of the database average. The yield strength of both tubes is higher than the tube that was pulled in 2002 from Beaver Valley Unit 1.

9.2 Bulk Chemistry

The chemical composition of the base metal of each tube was determined by a quantitative chemical analysis of a one inch section from both pulled tubes. Bulk chemical composition of the material was assessed to determine if the material met Alloy 600 specifications, which is the material for which GL 95-05 applies (Reference 1). Sample R19C38-3A5 was taken from tube R19C38 (see Figure 6-4) and sample R24C41-3A5 was taken from tube R24C41 (see Figure 6-14). The radioactive contamination of each section was removed by several cycles of immersion in a room temperature solution of 35% HNO_3 + 4% HF (by volume), plus surface abrasion with silicon carbide wheels. Quantitative analysis was performed using a combination of x-ray fluorescence, inductively coupled plasma, inert gas fusion, and combustion methods (Reference 31).

The results of the chemical analyses are provided in Table 9-2. The composition of the tube is within the limits set by specification ASME SB167 (1977) (Reference 32). R19C38 and R24C41 have nearly identical compositions.

The carbon content of the pulled tubes was 0.017 - 0.018 wt%. This matches the lower end of the range of carbon content (0.018 – 0.029 wt%) found in five tubes that were pulled from a Model D4 steam generator for laboratory examination in 1996, having tubes manufactured just before the Beaver Valley Unit 2 tubes. It is concluded that the Beaver Valley Unit 2 tubes have a composition that is within ASME specifications for Alloy 600, and the tubes have a carbon content that is within the range of Westinghouse produced mill annealed Alloy 600 tubing.

9.3 Microstructure Analysis

9.3.1 Procedure

The microstructure of both pulled tubes was examined to determine the grain size and the general distribution of the carbide precipitation. From tube R19C38, section 3A2 was taken from a freespan location (see Figure 6-4) above 02H that had not been burst tested. Section 3A2, a ½-inch long section, was then cut axially to expose a longitudinal view for metallography, sample 3A2A (section 3A2B was not used).

Likewise, from tube R24C41, section 3A2 was taken from a freespan location (see Figure 6-14) above 02H that had not been burst tested. Section 3A2, a ½-inch long section, was then cut axially to expose a longitudinal view for metallography, sample 3A2A (section 3A2B was not used).

The samples were mounted in epoxy to show a longitudinal view. Mounted samples were examined for carbide precipitation by SEM following polishing and etching in a 2% bromine-methanol solution. This etchant reveals both carbides and grain boundaries at the same time, allowing for a direct assessment of the amount of grain boundary carbide precipitation and the level of intragranular carbides. The etched samples were then examined with a Zeiss Supra Field Emission Scanning Electron Microscope. Three areas were examined on each sample, and each area was documented at three different magnifications.

Samples were examined for grain size rating per the intercept method of ASTM E112 (Reference 33).

9.3.2 Results

Figure 9-3 through Figure 9-5 show a representative example of the carbide distribution and grain boundaries from R19C38, at three levels of magnification. Likewise, Figure 9-6 through Figure 9-8 show a representative example of the carbide distribution and grain boundaries from R24C41, at three levels of magnification.

The grain boundaries of the material are the linear features, as shown in Figure 9-5. The grain boundaries form cells that surround the grains of the material. Carbides are shown as the small white dots in the figures. The carbides may occur in the same location as the grain boundaries (intergranular carbides) or may be intragranular, as shown in Figure 9-5. The microstructure for both tubes is similar. The microstructure of both tubes shows few grain boundary carbides; most grain boundaries had no carbides. Nearly all carbides were

intragranular. Such a carbide distribution may be described as a discontinuous network of carbides, as there is no correspondence between carbides and grain boundaries. As Figure 9-4 and Figure 9-7 show, the carbides form linear features that are independent of the grain boundaries. These are carbides that were present on the grain boundaries of a prior grain boundary structure.

Figure 9-3 and Figure 9-6 were used to measure the average grain size for tubes R19C38 and R24C41, respectively. There are a considerable number of annealing twins present in both microstructures. Annealing twin boundaries are not counted as grain boundaries. The average grain size for tube R19C28 is ASTM 7.2 and the average grain size for tube R24C41 is 7.0. These values indicate that the grain size for these tubes is coarser than the average for Westinghouse Alloy 600 7/8 inch OD mill annealed tubing. For example, Beaver Valley Unit tubes pulled for examination in 1995 had grain sizes of ASTM 8.0-11.0 (Reference 29). The coarser grain size is consistent with the lower yield strength properties and lower hardness readings observed.

9.4 Microhardness Testing

9.4.1 Procedure

Microhardness tests are used to provide information such as general hardness, verification of specific heat treatment, and random hardness variations.

The mounted samples used in the microstructure analysis of Section 9.3 (one from each tube) were ground and polished to remove the etch. Five sets of Vickers microhardness measurements were obtained from the mid-wall and near the OD of each sample.

The Vickers microhardness tests were performed in accordance to the Reference 34 work instructions on a Tukon Microhardness Tester. Vickers microhardness is determined by dividing the applied kg-force load by the surface area of the indentation in square millimeters, computed from the mean of the measured diagonals of the indentation. A 500-g load was used for the measurements on a polished transverse cross-section.

9.4.2 Results

Table 9-3 summarizes the microhardness results. The results show a consistent microhardness across the tube wall. The average microhardnesses (166-181 HV500) are similar (164-170 HV500) to other pulled tubes in Westinghouse experience that were mill annealed Alloy 600 and were pulled using relatively low pull forces. Other pulled tubes, such as those from Beaver valley Unit 1 (Reference 29), had higher average microhardnesses (184-204 HV500).

9.5 Sensitization Assessment

9.5.1 Procedure

During the manufacturing of the Alloy 600 tubing, carbon that has been dissolved during the final mill annealing operation and has been retained in solid solution, may precipitate to form (primarily) intergranular chromium carbides. Short-range diffusion of chromium to the grain boundaries in order to effect the precipitation of intergranular $M_{23}C_6$ can result in a Cr-depleted region adjacent to the grain boundaries. This condition is typically referred to as "sensitization," and is a condition that renders the material to become susceptible to intergranular attack in aggressive oxidizing chemical environments (but not generally in PWR primary water).

For mill annealed tubing, the only intergranular carbides that form do so during the cooling transient from peak temperature to about 1000°F. Negligible precipitation would be expected.

The extent of grain boundary carbide precipitation is controlled by: alloy composition (in particular carbon and chromium), final mill annealing temperature relative to carbon content, diffusivity of carbon during cooling from mill annealing, grain size, and the availability of dissolved carbon for precipitation at the grain boundaries.

Westinghouse has adopted a modified version of the Huey test (ASTM A262 Practice C – Reference 35) as the principal tool for the evaluation of grain boundary chromium depletion in Alloy 600. The test was modified to a single 48-hr exposure in boiling 25 wt% nitric acid. This modification was necessary to enhance the sensitivity of the test for detecting chromium depletion in nickel alloys. Modified Huey testing of the Beaver Valley tubes was performed in accordance with the approved work instructions (Reference 36).

Two 0.5-inch samples were taken from each tube for sensitization testing. These were tested so as to identify any significant variations, possibly from failures in annealing. From R19C38, the two samples were 3A3 (see Figure 6-4) and 4A2 (see Figure 6-8). From R24C41, the two samples were 3A3 (see Figure 6-14) and 7A2 (see Figure 6-25).

9.5.2 Results

The results of the 25 wt % HNO_3 modified Huey tests are summarized in Table 9-4. The pulled tubes showed weight losses of 28-33 mg/dm^2/day. These results are less than that associated with a sensitized condition (200 mg/dm^2/day) as stated in Westinghouse work instructions (Reference 36).

The Modified Huey results do not indicate any inconsistencies in annealing or other heat treatments. The results (28-33 mg/dm^2/day) are at the low end of the range (17-103 mg/dm^2/day) of other pulled tubes in Westinghouse experience that were Westinghouse supplied mill annealed Alloy 600 tubing.

9.6 Material Characterization Conclusions

The low density of intergranular carbide precipitation suggests that few carbides were precipitated on cooling from the mill annealing temperature. The fact that the grain size is the larger than average for Westinghouse mill annealed tubing is indicative of grain growth during the mill annealing treatment being relatively unimpeded by the presence of a large number undissolved carbides. The material has a relatively coarse grain size consistent with the relatively low carbon content and the range of mill annealing temperatures used at the Blairsville tube mill. For a single phase face-centered cubic material, the strength and hardness properties are typically dictated by the grain size due the Hall-Petch relationship. The slightly larger than average grain size is consistent with the slightly lower than average yield strength and hardness.

The relationship between the location of the carbides and the grain boundaries is an important factor in characterizing a nickel alloy's susceptibility to intergranular stress corrosion cracking. Material with an elevated resistance to stress corrosion cracking tends to have low strength, coarse grains, few intragranular carbides and a semi-continuous to continuous network of intergranular carbides. These Beaver Valley Unit 2 tubes have low strength, coarse grains, and few intragranular carbides but no semi-continuous network of intergranular carbides. Without an intentional thermal treatment, these carbides would have to precipitate and grow during slow cooling from the mill annealing temperature through the carbide precipitation range. Slow cooling was not the practice at the Westinghouse tube mill.

The material characteristics of the pulled Beaver Valley Unit 2 tubes are consistent with Westinghouse supplied mill annealed Alloy 600 tubing that is applicable to the Alternative Repair Criteria (Reference 1).

Table 9-1: Tensile Test Results

Tube	0.2% Offset Yield Strength (KSI)	Ultimate Tensile Strength (KSI)	Percent Elongation	Maximum Load Observed (lb_f)	Tensile Strain at Yield (in/in)
R19C38	49.4	98.9	41.9	13,385	0.00327
R24C41	51.1	98.9	44.3	12,938	0.00314
Beaver Valley Unit 1 (R15C62) (Reference 27)	48.5	105.0	37.8		
Beaver Valley Unit 1 (R11C48) (Reference 28)	55.6	104.4	41.0		
Beaver Valley Unit 1 (R16C60) (Reference 28)	61.0	111.0	41.0		
Beaver Valley Unit 1 (R10C48) (Reference 29)	65.7	115.7	29.3		
Beaver Valley Unit 1 (R22C38) (Reference 29)	63.0	111.6	29.8		
Beaver Valley Unit 1 (R28C42) (Reference 29)	58.5	106.1	32.0		
Average for 7/8" tubes (Reference 30 Database)	57.5 $\sigma = 9.9$	104.8 $\sigma = 7.2$	not reported		

Table 9-2: Chemical Composition of Bulk Material (Composition in wt%)

Element	R19C38	R24C41	SB167 (1977) Specification[1]	Notes
Co	0.04	0.04		
Cr	15.22	15.25	14.0-17.0	Both in spec
Cu	0.30	0.30	0.5 max	Both in spec
Fe	7.38	7.40	6.0-10.0	Both in spec
Mg	0.02	0.02		
Mn	0.17	0.17	1.0 max	Both in spec
Mo	0.07	0.07		
Nb	0.05	0.04		
Ni	75.88	75.84	72.0 min	Both in spec
Si	0.16	0.16	0.5 max	Both in spec
Ti	0.26	0.26		
V	0.03	0.02		
Al	0.37	0.38		
Pb	0.00003	0.00012		
C	0.018	0.017	0.15 max	Both in spec
S	<0.001	0.001	0.015 max	Both in spec
N	0.0082	0.0070		

Note 1: Reference 32

Table 9-3: Microhardness Summary

Tube	Point	Vickers Hardness Value (HV500)	
		Mid-Wall	Near OD
R19C38	1	166	167
	2	161	177
	3	171	180
	4	169	167
	5	162	171
	Average	166	172
R24C41	1	177	181
	2	170	178
	3	162	180
	4	171	184
	5	174	180
	Average	171	181

Table 9-4: Summary of Modified Huey Results

Tube	Sample	Weight loss, mg/dm^2 /day
R19C38	3A3	27.65
R19C38	4A2	31.23
R24C41	3A3	33.19
R24C41	7A2	27.71

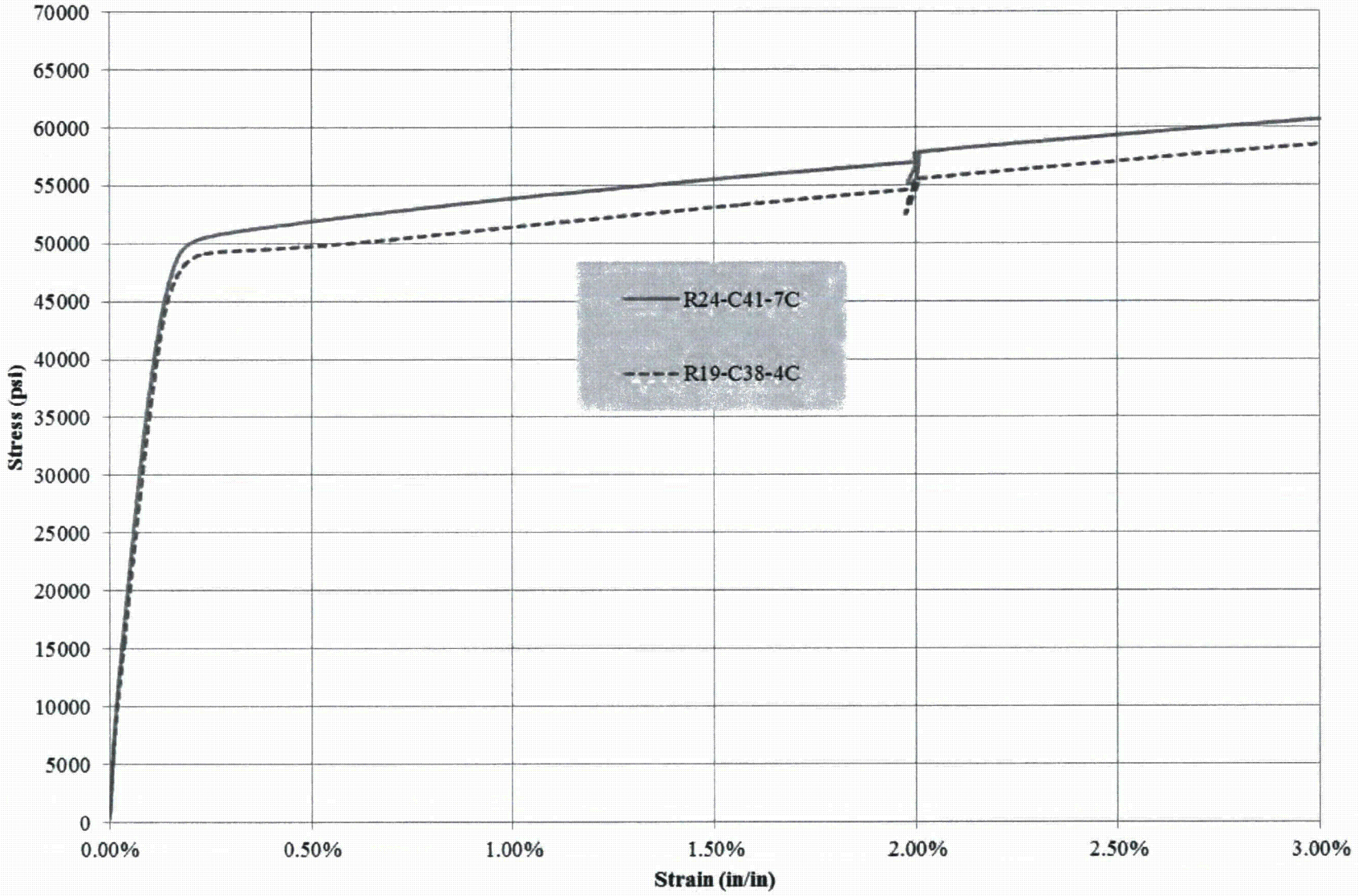

Figure 9-1: Stress-Strain Curves (Low Strain)

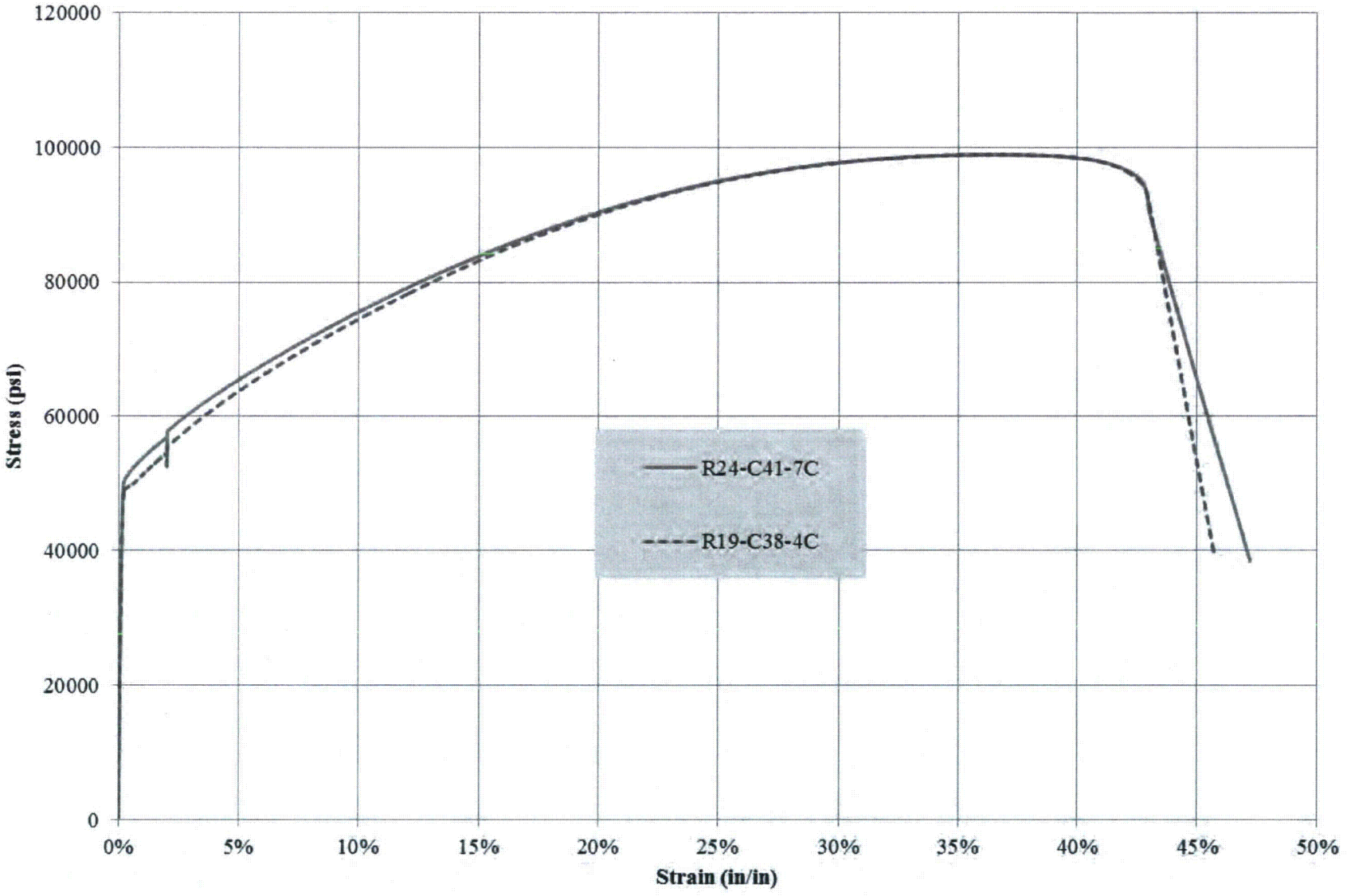

Figure 9-2: Stress-Strain Curves (All)

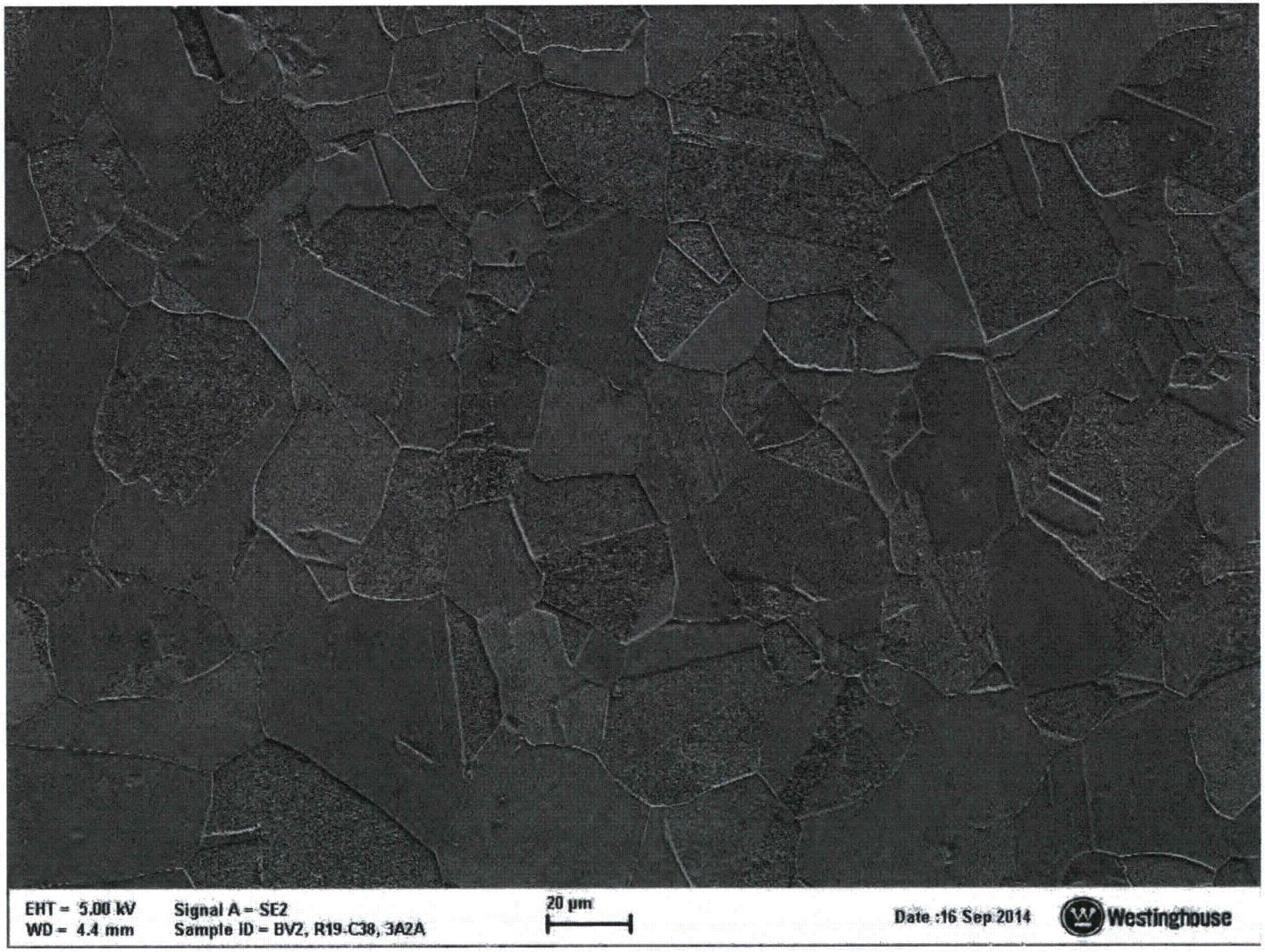

Figure 9-3: General Microstructure of Tube R19C38 (Low Magnification View)

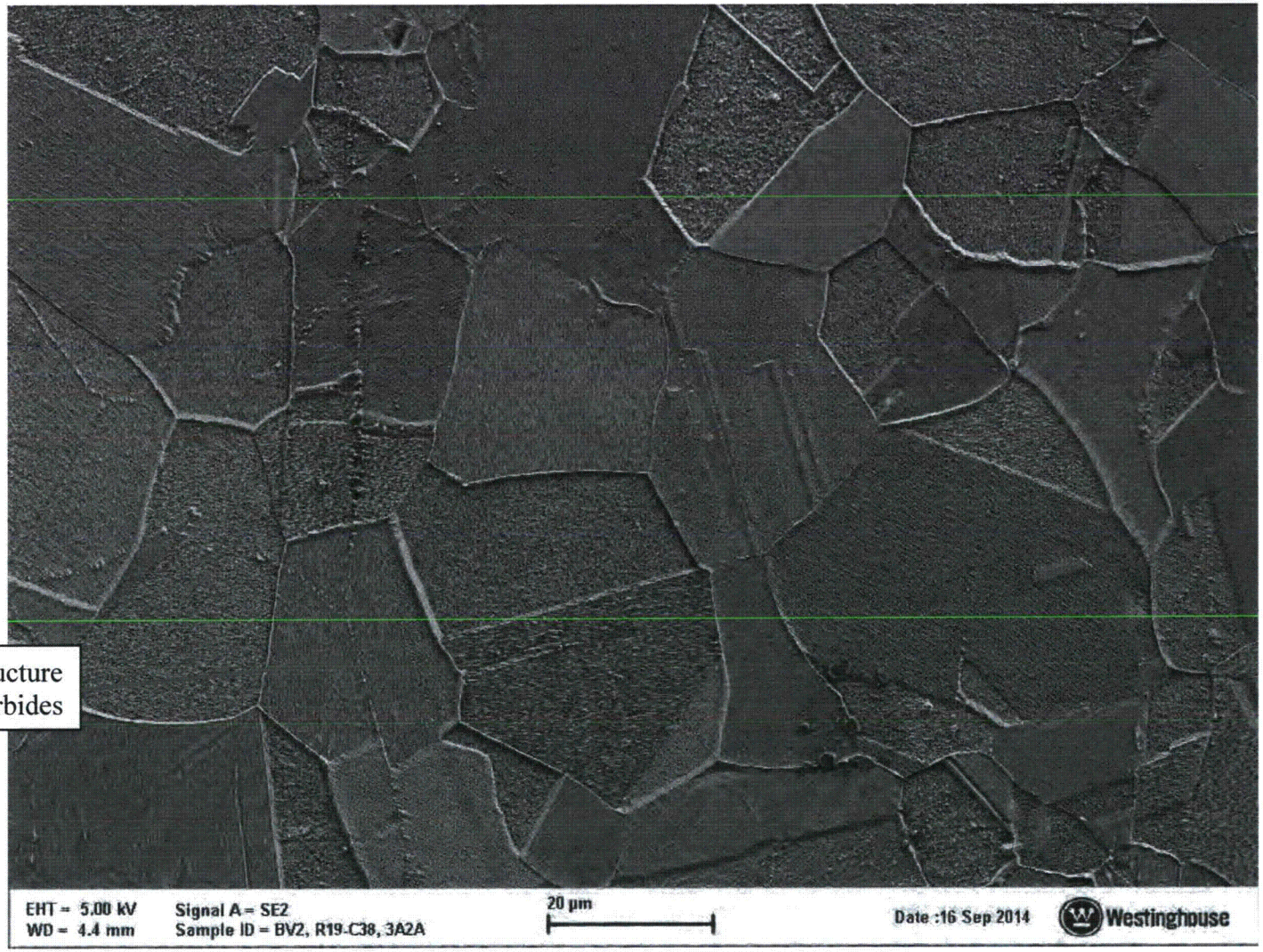

Figure 9-4: General Microstructure of Tube R19C38 (Medium Magnification View)

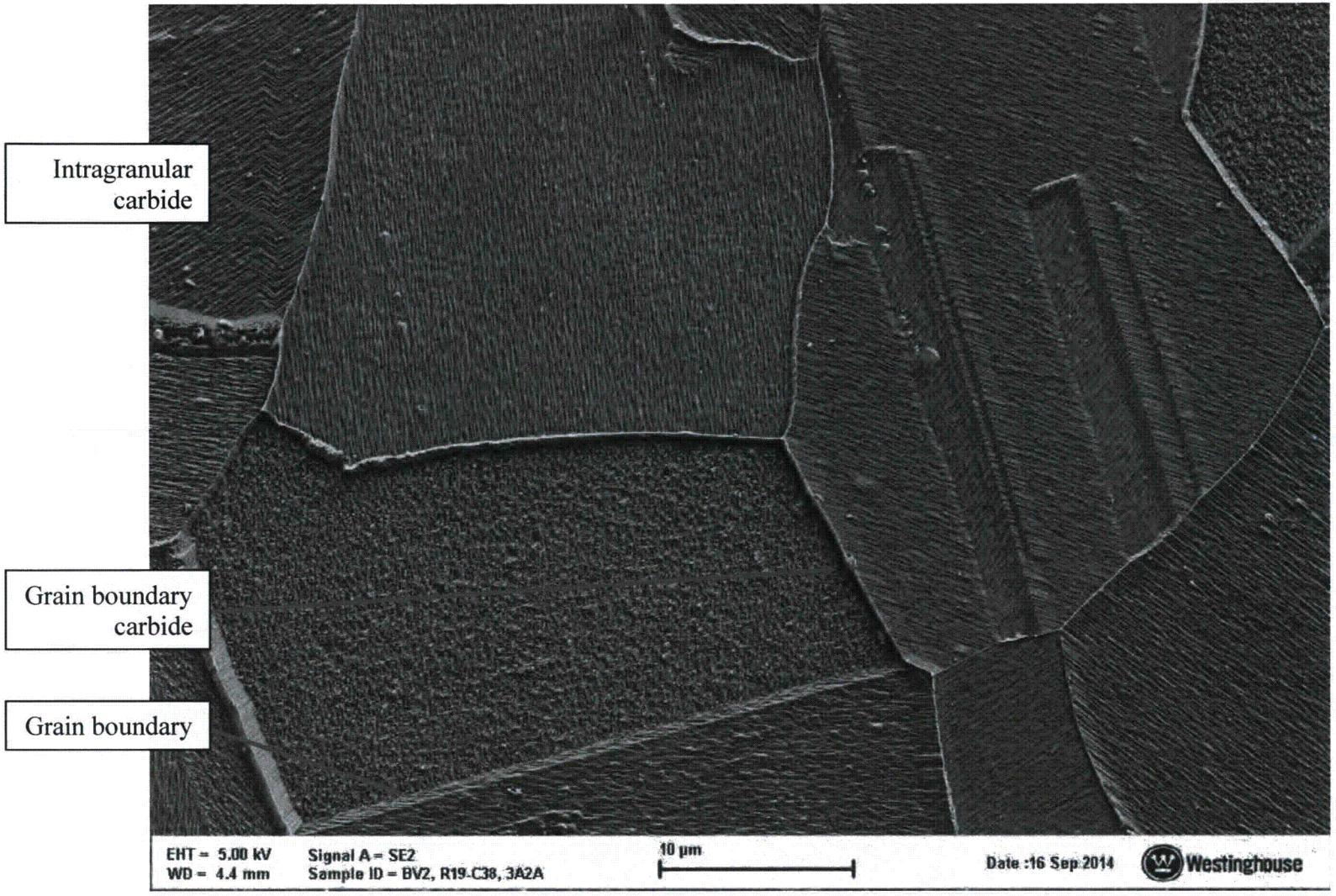

Figure 9-5: General Microstructure of Tube R19C38 (High Magnification View)

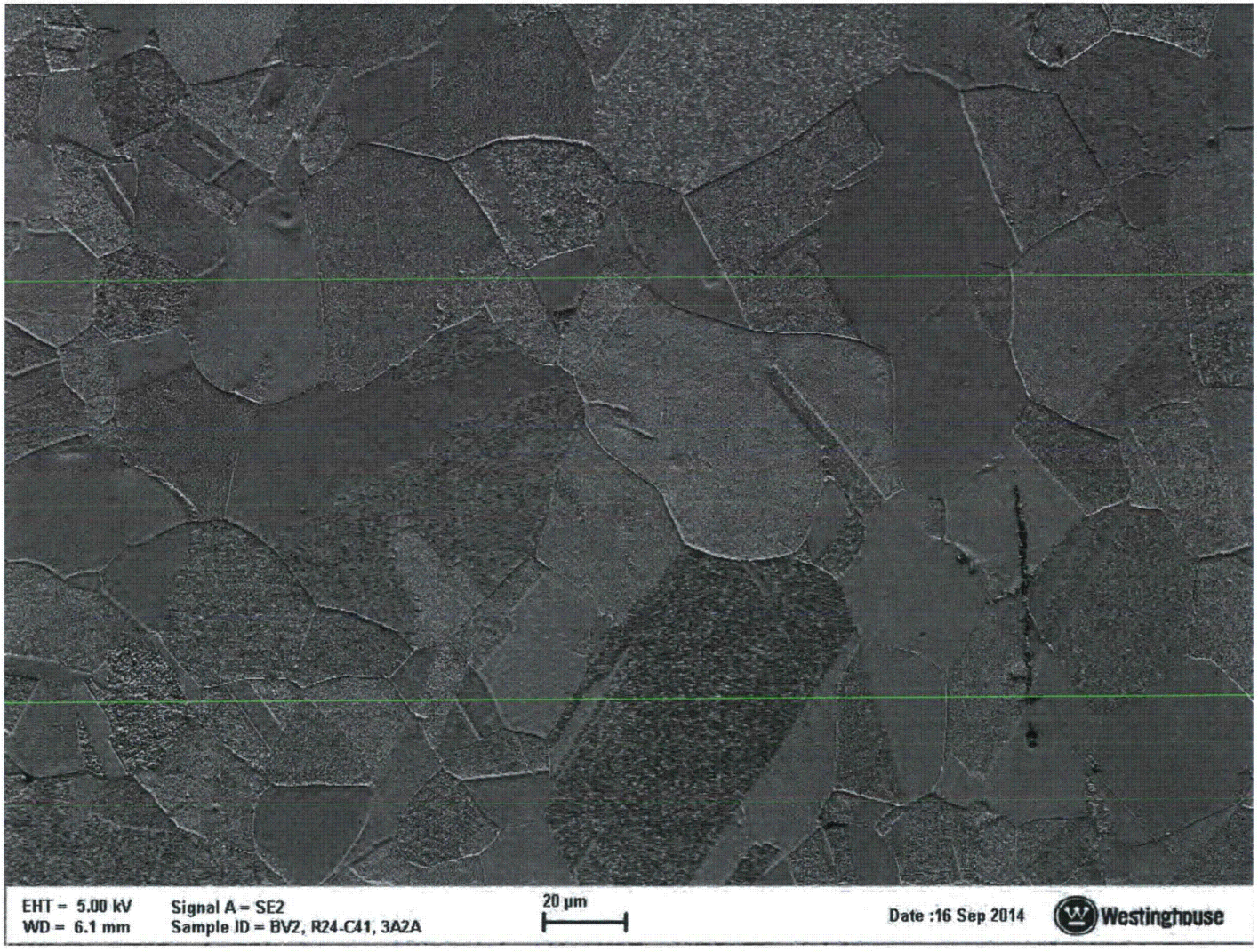

Figure 9-6: General Microstructure of Tube R24C41 (Low Magnification View)

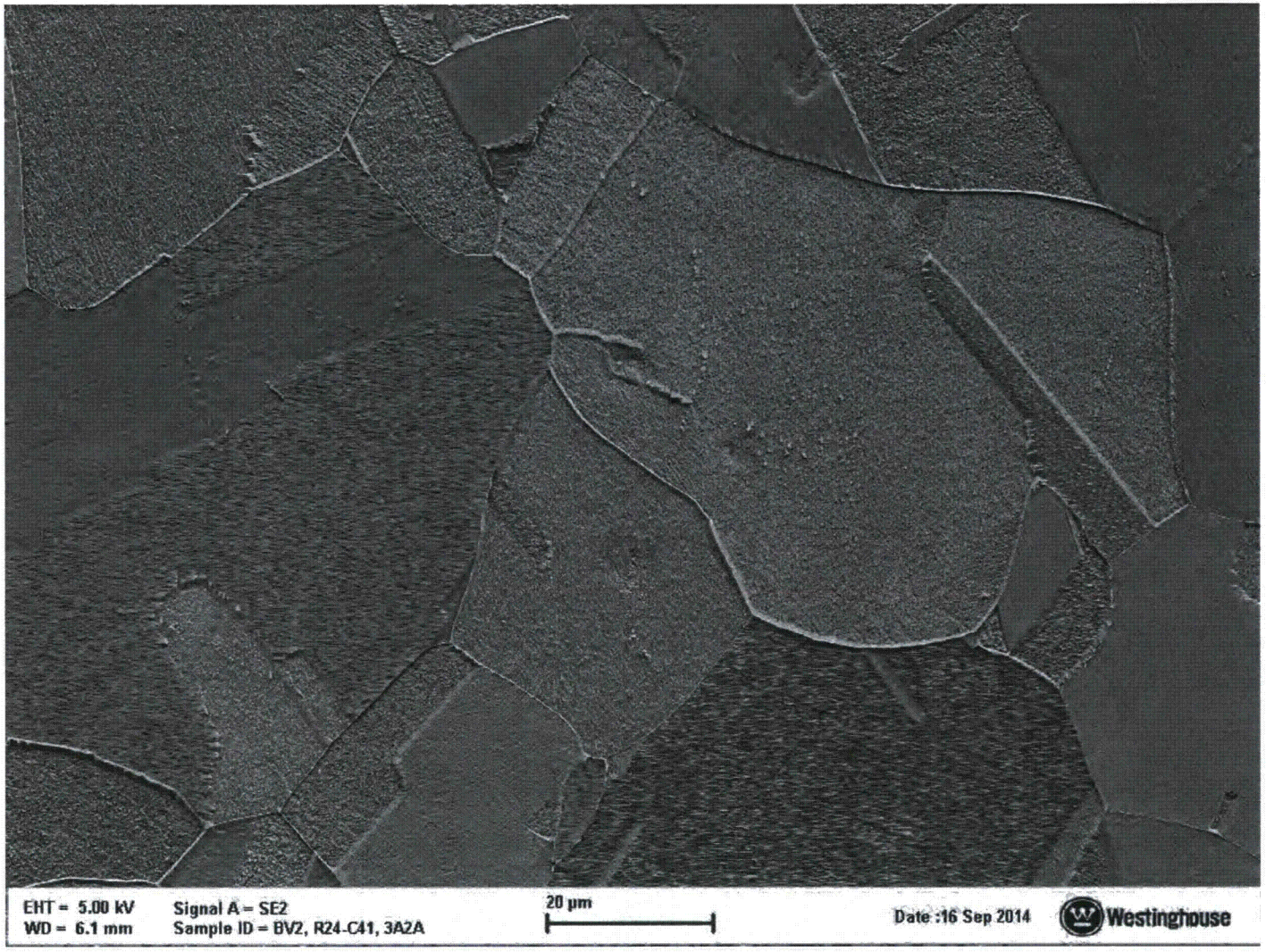

Figure 9-7: General Microstructure of Tube R24C41 (Medium Magnification View)

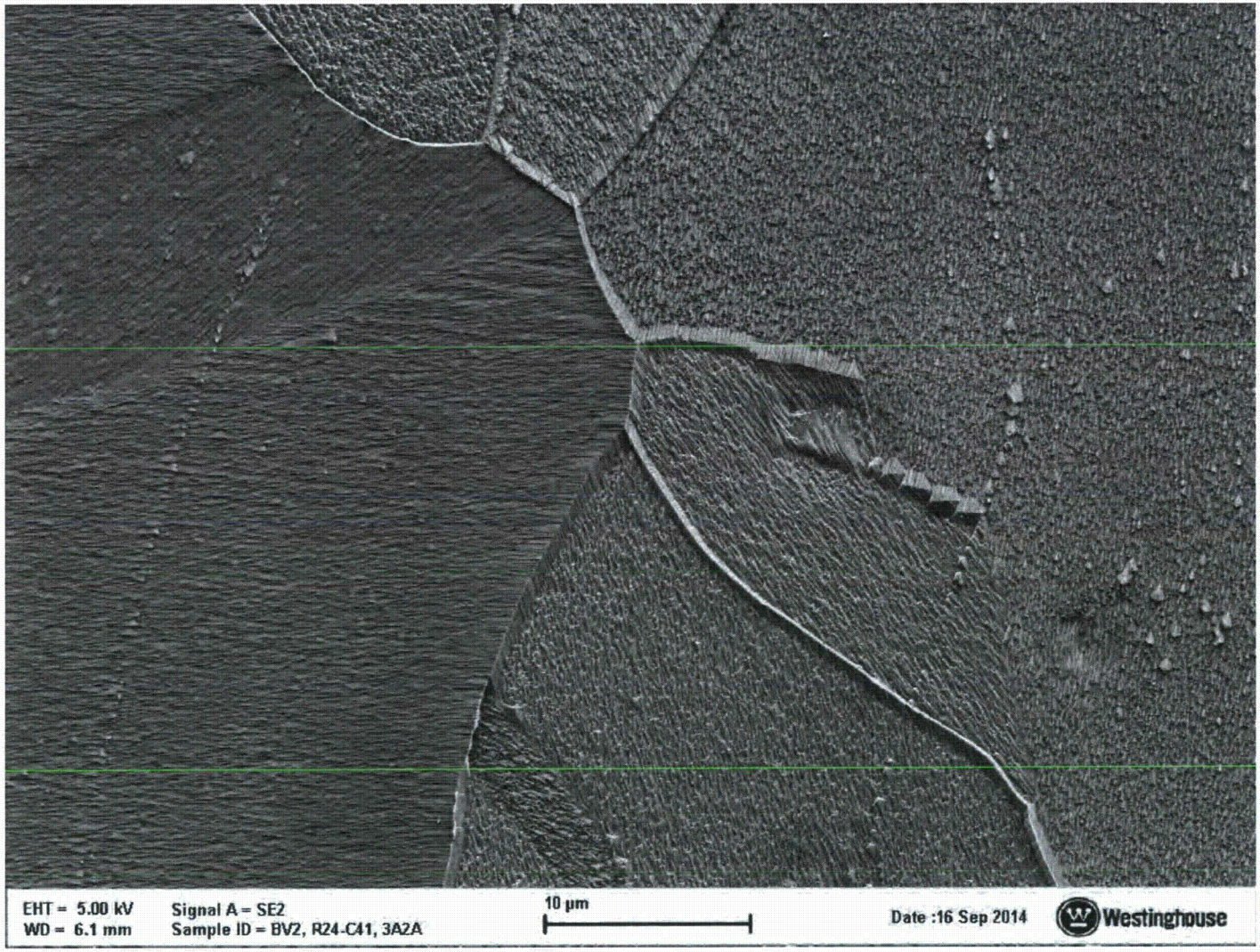

Figure 9-8: General Microstructure of Tube R24C41 (High Magnification View)

10.0 EDS ANALYSIS OF SURFACES AND DEPOSITS

In conjunction with the performance of the SEM fractography, discussed in Section 7.0, Energy Dispersive X-ray Spectroscopy (EDS) was performed to characterize the elemental composition of surface oxides and outer surface deposits remaining on the surfaces of the areas that were examined by SEM.

In addition, TSP deposits that spalled off the tube during the expansion of the tube diameter during burst testing were collected for analysis by SEM/EDS.

A TESCAN LYRA Scanning Electron Microscope was used in conjunction with an Oxford Instruments Energy Dispersive Spectroscopy System for the analysis. EDS is an integral part of the SEM instrument. EDS provided a semi-quantitative elemental analysis using AZtec software. Analyses were conducted at 20 keV at a working distance of 9.3 mm. The results in this section are provided for information only and are not a GL 95-05 reporting requirement.

10.1 SEM/EDS Analysis of Burst Opening Surfaces

EDS analyses were performed on selected areas of each of the two burst openings that had degradation (see sample R19C38-3B2A from 02H in the Figure 6-6 sectioning diagram and sample R24C41- 6B2A from 04H in the Figure 6-23 sectioning diagram).

On the fracture surface of each sample, both the crack surfaces and the ductile tearing surfaces were examined. As the ductile tearing is a surface that opened as a result of the burst test, EDS analysis of the ductile surfaces represents an analysis of the base metal.

The OD surfaces of the two TSP region were also examined. The OD surfaces that were examined were adjacent to the cracking.

Figure 10-1, Figure 10-2 and Figure 10-3 show three areas of the R19C38-02H burst opening fracture surfaces that were examined by SEM/EDS. The boxes indicate the areas that were examined. The results of the R19C38-02H fracture surface EDS analyses are summarized in Table 10-1. The elements identified on the ductile surfaces are approximately the same as the bulk chemistry results shown in Table 9-2. The crack surface analyses did not identify any unusual or deleterious elements, such as copper, lead or sulfur.

Figure 10-4 and Figure 10-5 show the OD surface adjacent to the R19C38-02H cracking in low and high magnification views. The belt polish marks are evident in the higher magnification view as the vertically-oriented features on the OD surface. Much of the OD surface is free of hydrothermal deposits in these views, but there are remnants of deposits (or thick oxide) in patches on the surface. The analyses performed on the low magnification view were all spot analyses, as indicated by the white dots in Figure 10-4. In the higher magnification view the analyses were performed in area scans, as indicated by the boxes in Figure 10-5. The results of the R19C38-02H OD surface EDS analyses are summarized in Table 10-2. The analyses performed on areas 18 and 19 are bare OD surfaces. Spots 12-16 were collected from areas that had remnants of deposits. These areas showed a relatively high concentration of iron, as would

be expected. They also showed moderate levels of deposit binding agents (Al, Si, Mg, and Ca). Small concentrations of copper, sulfur and barium were also identified, but not consistently.

Figure 10-6 shows an areas of the R24C41-04H burst opening fracture surface that was examined by SEM/EDS. The boxes indicate the areas that were examined. The results of the R24C41-04H fracture surface EDS analyses are summarized in Table 10-3. The elements identified on the ductile surface are approximately the same as the bulk chemistry results shown in Table 9-2. The crack surface analyses did not identify any unusual or deleterious elements, such as copper, lead or sulfur.

Figure 10-7 shows the OD surface adjacent to the R24C41-04H cracking. The belt polish marks are evident in Figure 10-7 as the vertically oriented features on the OD surface. Much of the OD surface is bare in this view, but there are remnants of deposits (or thick oxide) in patches on the surface. Table 10-4 summarizes the results of the EDS examination of the areas in Figure 10-7. Large-to-moderate levels of deposit binding agents (Al, Si, Mg, and Ca) were identified in the deposits. Copper was identified in all but one of the areas. Sulfur and phosphorus were found in some of the areas. Barium was identified in a relatively high amount in two locations, prompting further examination for confirmation.

10.2 SEM/EDS Analysis of Spalled Deposits

Lightweight tape was wrapped around three TSP regions (R19C38-02H, R24C41-03H and R24C41-04H) before burst testing. As the burst test caused the tube diameter to swell, the deposits in the TSP regions popped off the tube. Most of this spalled deposit was retained on the tape. The deposits on the tape were subsequently examined by SEM and EDS.

Figure 10-9 shows the deposit surface that was pressed against the tube surface of R19C38 in the 02H TSP region. The deposits have provided a replica of the tube surface: the circumferential belt polish marks on the tube surface are shown (as a negative) as the vertical lines in the deposit surface. Figure 10-9 also shows a likely scratch in the tube that would have been created during installation (the horizontal feature that passes through the bottom of the Spectrum 3 box).

Figure 10-10 and Figure 10-11 shows the deposit surfaces that were pressed against the tube surfaces of R24C41 in the 03H and 04 TSP regions, respectively. Circumferential belt polish mark replications are clearly evident as the nearly vertical parallel lines in the deposit surface.

The presence of the replicated circumferential belt polish marks is significant as they show that this was the deposit that was pressed directly against the tube surface.

Table 10-6 provides a summary of the EDS analyses that were performed on the spalled deposits from R19C38 in the 02H TSP region. The results show some deposit binding agents (Si and Al), but no unusual or deleterious elements. These results are somewhat similar to the OD surface analyses summarized in Table 10-2.

Table 10-7 and Table 10-8 provide summaries of the EDS analyses that were performed on the spalled deposits from R24C41 in the 03H and 04H TSP regions. The results show some deposit binding agents (Si and Al). Copper was identified in five of the six areas examined on the 03H

deposits and on one of the six areas examined on the 04H deposits. Sulfur was also identified in three of the twelve areas.

Table 10-1: Results of EDS Analyses Performed on R19C38-02H Fracture Surfaces

	Spectrum 1	Spectrum 8	Spectrum 10	Spectrum 2	Spectrum 7	Spectrum 11
Element	Crack Surface	Crack Surface	Crack Surface	Ductile Surface	Ductile Surface	Ductile Surface
C				6.62		
O	10.63	1.26	4.88		5.98	1.33
Al	0.57	0.61	2.60	0.81	0.63	0.72
Si	2.79	0.35		0.29	1.33	0.31
Ca	0.12					
Ti	0.23	0.47		0.30	0.29	0.47
Cr	13.97	15.83	18.89	15.09	15.05	15.76
Fe	6.74	7.70	10.69	7.50	7.42	7.85
Ni	64.96	73.78	62.94	69.39	69.30	73.56
Total	100.01	100.00	100.00	100.00	100.00	100.00

Spectra 1 and 2 – See Figure 10-1
Spectra 7 and 8 - See Figure 10-2
Spectra 10 and 11 - See Figure 10-3

Table 10-2: Results of EDS Analyses Performed on R19C38-02H OD Surfaces

	Spectrum 12	Spectrum 13	Spectrum 14	Spectrum 15	Spectrum 16	Spectrum 18	Spectrum 19	Spectrum 17	Spectrum 20	Spectrum 21
Element	Deposit Remnant	Deposit Remnant	Deposit Remnant	Deposit Remnant	Deposit Remnant	Bare OD Surface	Bare OD Surface	Mixed Surface	Mixed Surface	Mixed Surface
C		16.90		9.41	11.93					
O	1.50	22.92	26.59	10.81	13.42	3.39		11.70	14.37	12.81
Mg		0.65								
Al	4.94	4.44	6.32	6.36	4.21	2.54	2.62	4.30	2.14	2.42
Si	2.95	9.84	10.23	10.22	5.76	0.34		1.05	0.60	0.63
S		0.20								
Ca	1.34	7.38	9.86	14.15	7.37				0.45	0.28
Ti									0.40	0.31
Cr			1.20	1.02	0.58	11.77	13.00	13.09	17.22	17.28
Mn	3.85	2.27	1.45	1.76	1.83			0.91		0.78
Fe	83.25	33.79	39.36	41.81	51.81	6.26	6.59	9.37	10.75	11.13
Ni	2.16	1.59	4.97	2.71	2.10	75.70	77.79	59.60	54.07	54.36
Cu					0.98					
Ba				1.75						
Total	99.99	99.98	99.98	100.00	99.99	100.00	100.00	100.02	100.00	100.00

Spectra 12-17 – See Figure 10-4
Spectra 18-21 - See Figure 10-5

Table 10-3: Results of EDS Analyses Performed on R24C41-04H Fracture Surface

	Spectrum 22	Spectrum 23	Spectrum 24
Element	Crack Surface	Crack Surface	Ductile Surface
O	14.05	9.55	
Mg			
Al	0.65	0.82	0.72
Si	2.43	1.64	0.35
Ca			
Ti	0.20		0.54
Cr	13.2	14.10	16.13
Mn	0.41		
Fe	6.85	7.27	8.02
Ni	62.2	66.61	74.24
Total	99.99	99.99	100.00

Spectra 22-24 – See Figure 10-6

Table 10-4: Results of EDS Analyses Performed on R24C41-04H OD Surface

	Spectrum 37	Spectrum 38	Spectrum 39	Spectrum 40	Spectrum 41	Spectrum 42	Spectrum 43
Element	Deposit Remnant	Partial Deposit	Partial Deposit	Partial Deposit	Deposit Remnant	Deposit Remnant	Bare OD Surface
C	1.28	1.39	1.61		2.23	1.93	1.77
O	10.42	10.94	12.73	10.68	17.17	12.30	3.19
Mg	1.85	1.02	0.91	0.73	1.74	1.79	
Al	5.03	3.62	2.50	4.30	5.92	30.09	6.60
Si	4.50	4.03	3.92	4.51	17.29	4.20	0.52
P	0.19	0.48	0.47				
S	1.05		0.17			0.30	
Ca	0.77	1.72	1.76	0.41		1.02	
Ti	0.89	0.73	0.58	0.36		1.69	
Cr	11.45	14.04	14.47	13.39	3.25	0.48	12.76
Mn	1.42	1.87	1.75	1.49	1.86	8.40	0.86
Fe	23.38	21.41	20.27	12.22	11.13	30.52	7.00
Ni	30.40	36.84	36.17	41.52	39.41	2.14	63.43
Cu	1.09	1.90	2.68	10.40		3.77	3.88
Ba	6.27					1.38	
Total	99.99	99.99	99.99	100.01	100.00	100.01	100.01

Spectra 37-43 – See Figure 10-7

Table 10-5: Results of EDS Analyses Performed on R24C41-04H OD Surface Detailed Area

	Spectrum 45	Spectrum 46	Spectrum 47	Spectrum 48
Element	Light Shaded Particle	Light Shaded Particle	Light Shaded Particle	Dark OD Deposit
C		1.82	1.75	1.70
O	9.62	11.41	12.71	15.81
Mg		0.31		2.62
Al	1.35	4.47	1.32	5.22
Si	0.49	1.00	0.53	8.60
S	8.32	9.98	12.37	0.24
Ca	0.41	0.34		0.57
Ti				0.78
Cr				14.78
Mn				1.77
Fe	18.30	6.02	1.93	25.34
Ni	4.03	1.98	1.65	22.57
Mo		1.98		
Ba	57.49	60.69	67.74	
Total	100.01	100.00	100.00	100.00

Spectra 45-48 – See Figure 10-8

Table 10-6: R19C38-02H Spalled TSP Deposit EDS Analysis Results

	Spectrum 3	Spectrum 4	Spectrum 5	Spectrum 6	Spectrum 7
Element[1]	Area Scan	Area Scan	Area Scan	Point Scan	Point Scan
C	8.18				
Al	1.44	1.20	1.22	1.29	0.96
Si	0.48	0.54		0.72	0.48
Ti	1.73	1.70	1.83	0.88	0.51
Cr	11.17	23.71	23.40	18.81	17.21
Mn	1.11	1.31	1.47	0.88	
Fe	49.50	39.13	41.83	21.65	22.23
Ni	26.39	32.41	30.24	55.76	58.61
Total	100.00	100.00	99.99	99.99	100.00

Spectra 3-7 – See Figure 10-9

Note 1: Results do not include oxygen. Oxygen removed to provide emphasis to other elements.

Table 10-7: R24C41-03H Spalled TSP Deposit EDS Analysis Results

	Spectrum 8	Spectrum 9	Spectrum 10	Spectrum 11	Spectrum 12	Spectrum 13
Element[1]	Area Scan	Area Scan	Area Scan	Point Scan	Point Scan	Point Scan
C		8.49	9.15	14.94		12.72
Al	1.35	1.07	1.21	1.23	1.02	1.55
Si	0.60			0.82		1.16
S						0.49
Ti	1.38	1.34	1.27	0.63	0.79	0.87
Cr	24.18	18.49	14.41	14.44	5.20	18.73
Mn	1.47	1.11	1.79	0.93	2.84	1.99
Fe	36.22	36.05	41.93	26.14	70.46	25.07
Ni	34.80	31.28	27.89	39.05	11.82	33.85
Cu		2.16	2.34	1.82	7.86	3.57
Total	100.00	99.99	99.99	100.00	99.99	100.00

Spectra 8-13 – See Figure 10-10

Note 1: Results do not include oxygen. Oxygen removed to provide emphasis to other elements.

Table 10-8: R24C41-04H Spalled TSP Deposit EDS Analysis Results

	Spectrum 14	Spectrum 15	Spectrum 16	Spectrum 17	Spectrum 18	Spectrum 19
Element[1]	Area Scan	Area Scan	Area Scan	Point Scan	Point Scan	Point Scan
C		7.85			8.50	14.52
Al	0.91	0.88	1.46	0.92	1.53	0.66
Si	0.57		0.53			
Ti	1.18	1.25	1.47	0.43	0.67	0.65
Cr	13.09	14.51	18.57	14.46	3.11	2.02
Mn	1.24	1.05	1.49	1.00	0.97	2.29
Fe	54.42	45.47	42.85	20.83	71.17	67.47
Ni	28.58	28.99	33.64	62.36	14.06	6.34
Cu						6.06
Total	99.99	100.00	100.01	100.00	100.01	100.01

Spectra 14-19 – See Figure 10-11

Note 1: Results do not include oxygen. Oxygen removed to provide emphasis to other elements.

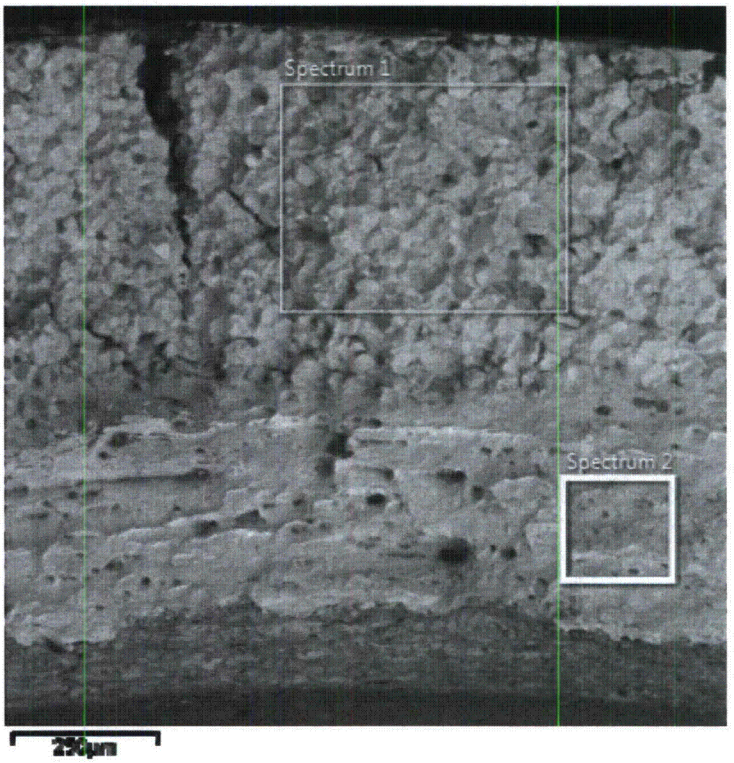

Figure 10-1: R19C38-02H Burst Opening – Crack Area 1 for EDS Analysis

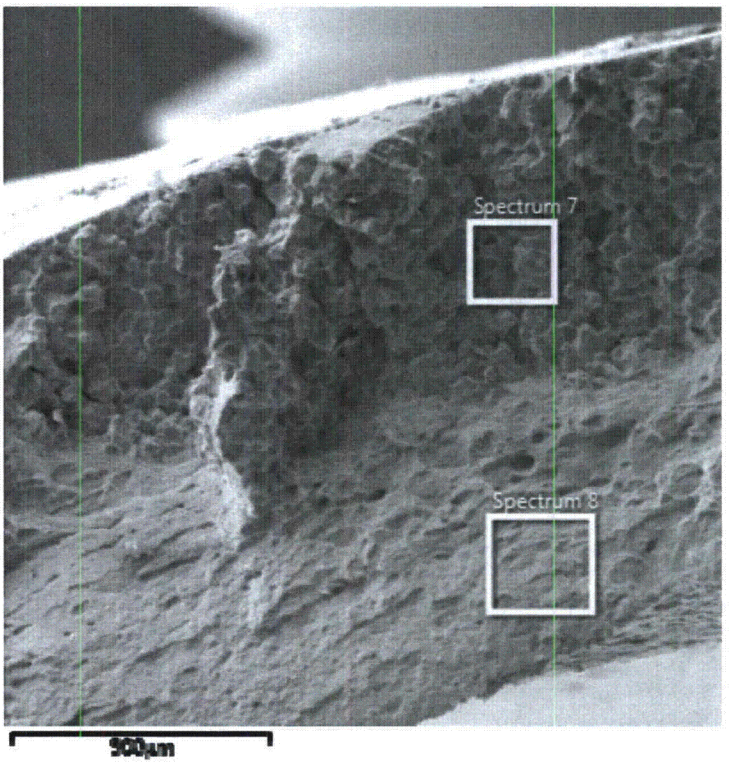

Figure 10-2: R19C38-02H Burst Opening – Crack Area 2 for EDS Analysis

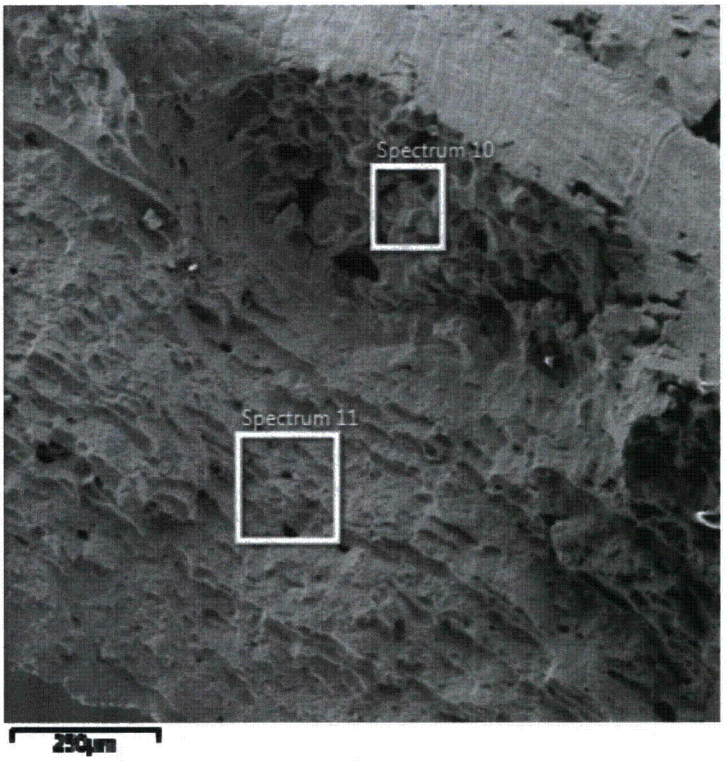

Figure 10-3: R19C38-02H Burst Opening – Crack Area 3 for EDS Analysis

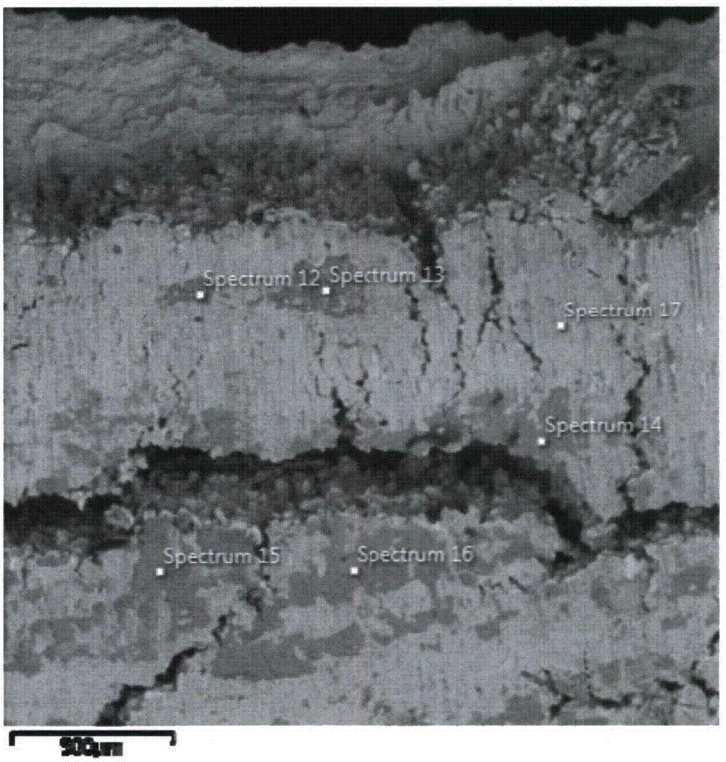

Figure 10-4: R19C38-02H Burst Opening – OD Surface Area 1 for EDS Analysis

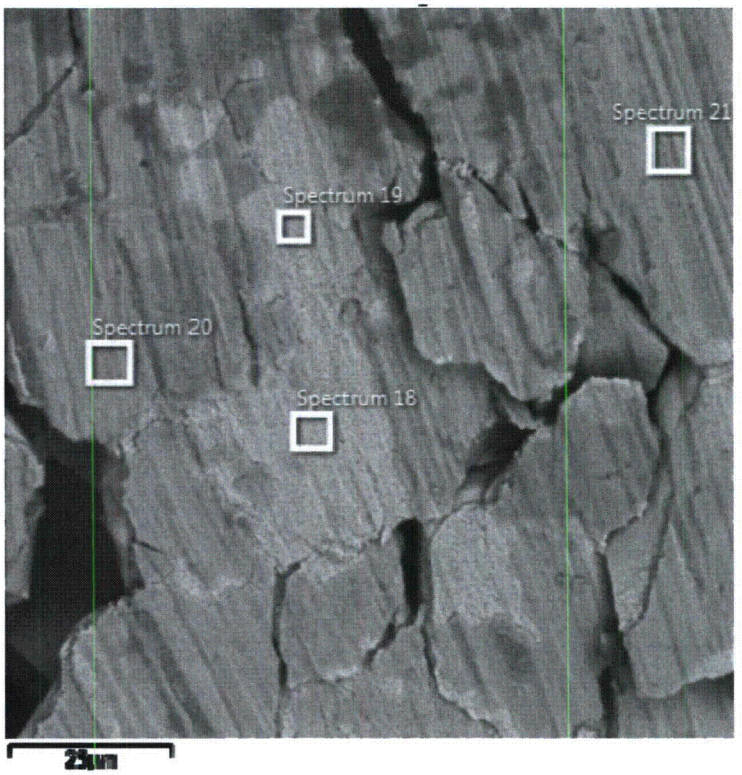

Figure 10-5: R19C38-02H Burst Opening – OD Surface Area 2 for EDS Analysis

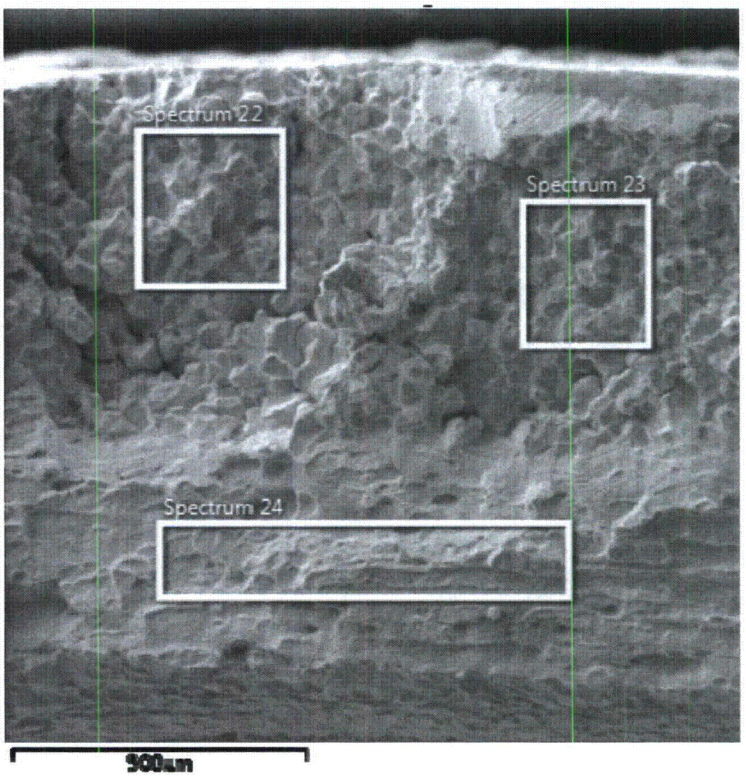

Figure 10-6: R24C41-04H Burst Opening – Crack Area for EDS Analysis

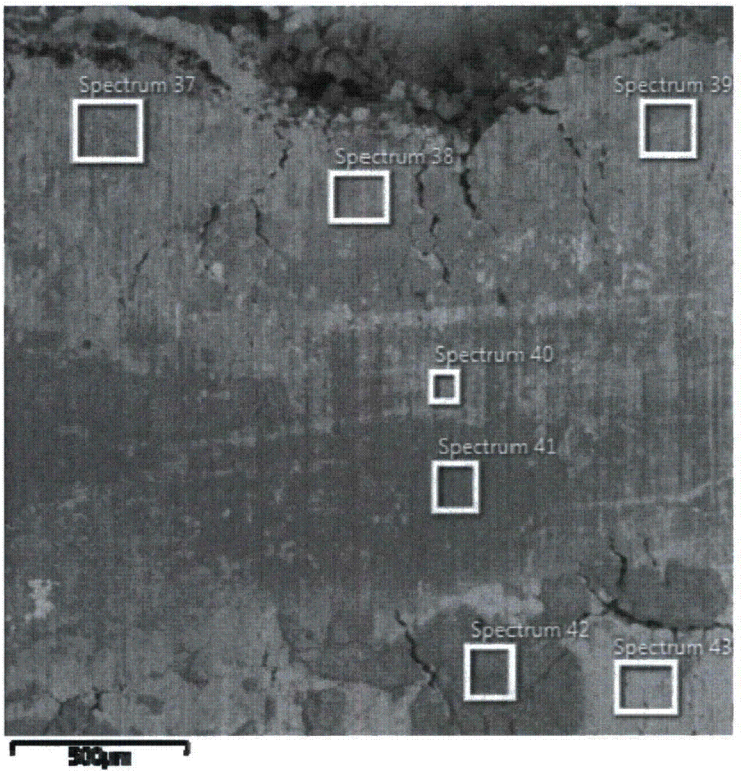

Figure 10-7: R24C41-04H Burst Opening – OD Surface Area 1 for EDS Analysis

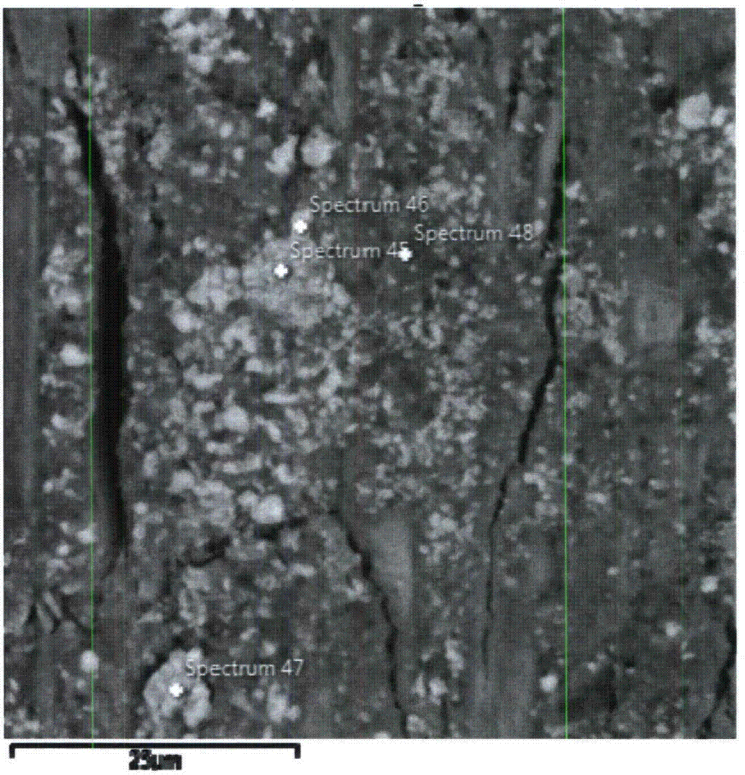

Figure 10-8: R24C41-04H Burst Opening – OD Surface Area 2 for EDS Analysis

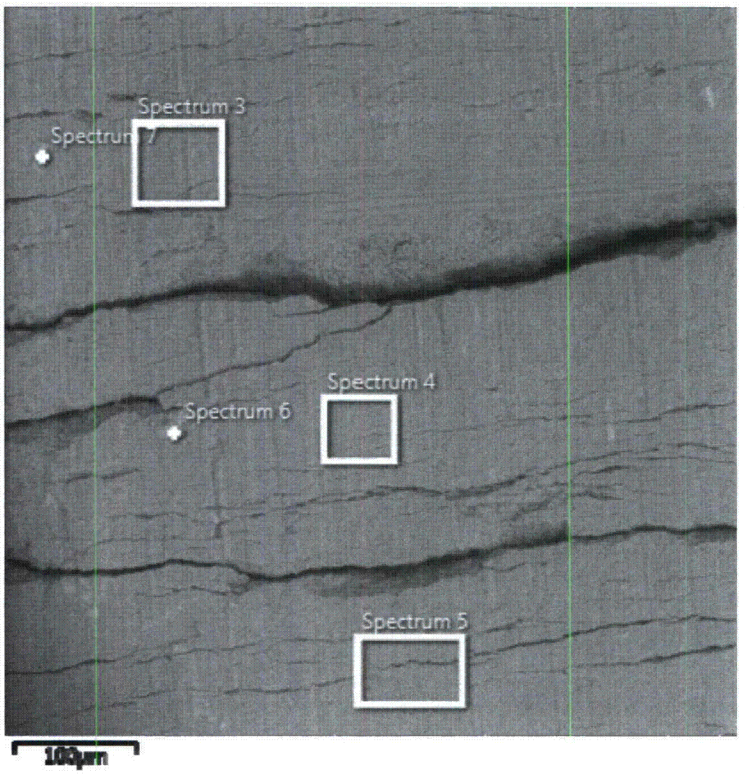

Figure 10-9: R19C38-02H Spalled Deposits – View of Surface Next to Tube

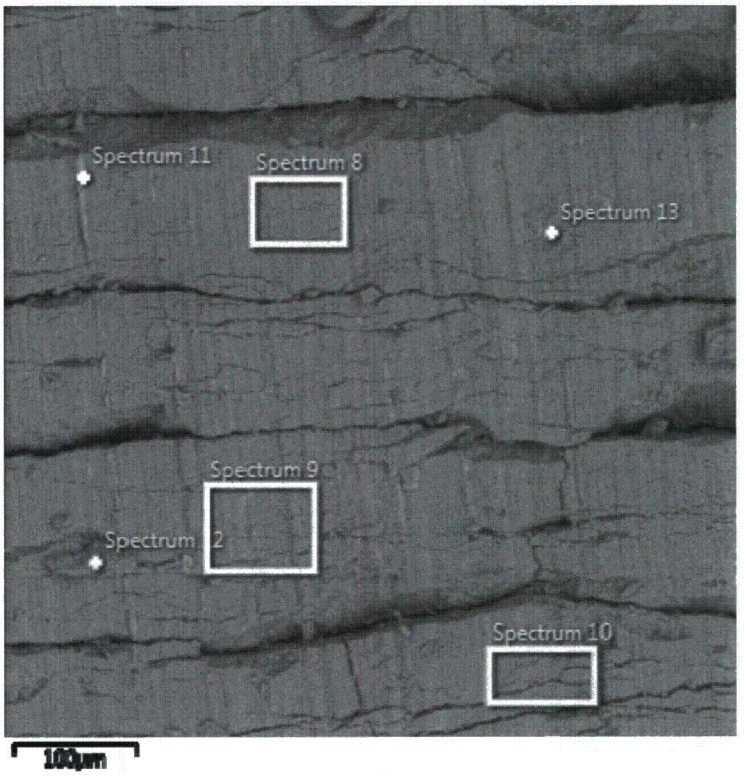

Figure 10-10: R24C41-03H Spalled Deposits – View of Surface Next to Tube

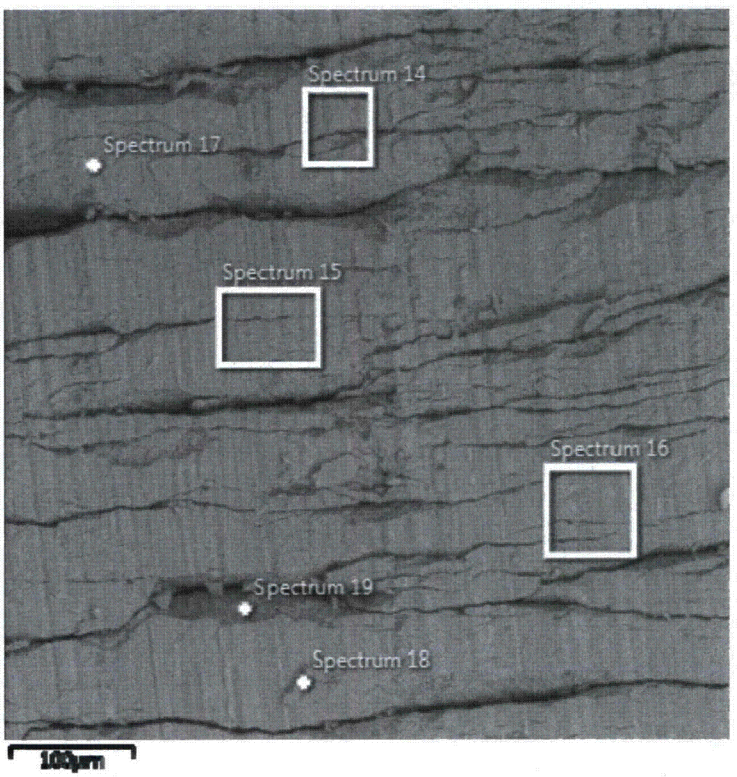

Figure 10-11: R24C41-04H Spalled Deposits – View of Surface Next to Tube

11.0 DISCUSSION / CONCLUSIONS

11.1 Characterization of Corrosion

SEM and metallography examinations confirmed that localized corrosion morphology in the TSP regions was predominantly axially-orientated ODSCC with a few small and shallow patches of IGA. Cellular corrosion was not observed. The observed degradation is in accordance with the morphology criteria provided in Section 1.a of GL 95-05 (Reference 1). The observed degradation is consistent with the current GL 95-05 database (Reference 30).

All four TSP regions that were pulled for laboratory examination had some degree of degradation in the form of stress corrosion cracking. There was no degradation found outside of the TSP regions.

The two TSP regions that had confirmed bobbin coil indications (R19C38-02H and R24C41-04H) had the deepest cracking. The R19C38-02H TSP had a maximum crack depth of 49.9%TW. The R24C41-04H TSP had a maximum crack depth of 48.6%TW located within the burst fracture, but there was another region of multiple axial cracks that were nearly as deep (maximum measured depth of 46.0%TW).

The two TSP regions that did not have confirmed bobbin coil indications (R24C41-02H and R24C41-03H) had shallower cracks. The R24C41-02H TSP had a maximum crack depth of 14.2%TW. The R24C41-03H TSP had a maximum crack depth of 4.4%TW.

11.2 Characterization of Tubing Material

Tensile testing, material chemistry evaluations, microstructure analyses, microhardness testing and sensitization assessment all demonstrated that both tubes are typical of Westinghouse mill annealed Alloy 600. The characteristics of the pulled Beaver Valley Unit 2 tubes are consistent with those in the Alternative Repair Criteria (ARC) database (Reference 30).

Tensile test results showed that the yield strength and ultimate tensile strength of both tubes are low, but well within a standard deviation of the ARC database (Reference 30) for 7/8" tubes.

11.3 Tube Integrity

Room temperature leak screening was conducted at pressures up to and including SLB pressure. None of the tubes that were pulled for laboratory examination leaked.

Room temperature burst tests were conducted on all of the TSP regions provided. All of the TSP regions had burst pressures far in excess of 3NOP. The lowest burst pressure was 9678 psig.

Table 11-1 presents a comparison of the field ECT calls and the laboratory results. The table shows that both bobbin and +Point provided excellent characterization of the degradation.

Figure 11-1 presents the ARC database (Reference 30) plot of the ligament-corrected burst pressure vs. bobbin amplitude. The Beaver Valley Unit 2 tubes, including the unconfirmed DSI

of R24C41-02H, are indicated on the plot. It is important to note that the raw burst pressure data from the Beaver Valley Unit 2 tubes is indicated. The figure shows that the Beaver Valley Unit 2 raw burst pressures fall above the regression line for ligament-corrected burst pressures.

The degradation assessment (Reference 18) notes that bobbin coil technique ETSS I28411 was used for detection of axial ODSCC at TSP intersections and +Point technique ETSS I28424 was used for confirmation. The probabilities of detection for these techniques are shown in Figure 11-2 and Figure 11-3, respectively. Figure 11-2 shows that the probability of detection for the 14.2%TW maximum depth of the crack in R24C41-02H is greater than 20% for bobbin, while Figure 11-3 shows that probability of detection is nearly zero for the +Point technique. This is consistent with the reported field results. Figure 11-2 shows a probability of detection of nearly zero for the 4.4%TW crack depth of R24C41-03H, which is also consistent with the report field results.

Table 11-1 shows that the +Point probe accurately characterized the degradation in R19C38-02H and R24C41-04H as two areas of cracking. As the depth profile of Figure 7-3 shows, the degradation consisted of a bottom region of cracking with a lot of ligaments, and an upper region of cracking with few ligaments. This is consistent with the +Point report of a larger top SAI and a smaller bottom SAI. Similarly for R24C41-04H, there were two regions of cracking and the field eddy current data indicated two SAIs.

11.4 Conclusion

Section 4c of Attachment 1 of GL 95-05 (Reference 1) provides criteria for examination and testing of the removed tube sections. The leak and burst testing performed under this program meet these criteria. None of the degradation from these pulled tubes leaked at SLB pressure. All of the TSP regions had burst pressures far in excess of 3NOP.

Subsequent to burst testing, the intersections were to be destructively examined to confirm that the degradation morphology is consistent with the assumed morphology for ODSCC at the tube-to-TSP intersections. Section 1a of Attachment 1 of GL 95-05 (Reference 1) provides the definition of the assumed morphology for ODSCC. The degradation morphology of the Beaver Valley ODSCC was shown to be consistent with GL 95-05 assumed morphology for ODSCC at the tube-to-TSP intersections. The dominant degradation mechanism affecting tube burst and leakage properties was axially-oriented ODSCC.

In addition, it was demonstrated that material and mechanical characteristics of the pulled Beaver Valley Unit 2 tubes are consistent with Westinghouse mill annealed Alloy 600 tubing.

The testing performed on the pulled tubes, and the results of the tests, satisfy the Alternative Repair Criteria of Reference 1.

Table 11-1: Comparison of Field Sizing and Lab Results

Tube TSP	Pre-Pull Field Eddy Current		Laboratory Characterization		
	Bobbin Coil IND / Volts	+Point IND / Volts	Crack Description	Maximum Depth (%TW)	Burst (psi)
R19C38 02H	DSI / 0.62v	SAI (Top&Bot) SAI(Top) / 0.25v SAI(Bot) / 0.15v	Burst opening had an upper and a lower region of corrosion. The upper region was ~5%TW deeper with fewer ligaments. Multiple short shallow axial cracks occurring in groups all around the circumference	49.9	9678
R24C41 02H	DSI / 1.19v	NDF	Multiple short axial cracks, all in one closely spaced region	14.2	10,741 Burst in freespan
R24C41 03H	NDD	NI	Two closely spaced shallow short axial cracks	4.4	10,733 Burst in freespan
R24C41 04H	DSI / 0.47v	SAI (2 Reported) SAI(1) / 0.23v SAI(2) / 0.09v	Burst opening had a single ¼ inch long crack. 100° from the burst opening were multiple parallel axial cracks of nearly equal maximum depth	48.6 (90°) 46.0 (350°)	9678

DSI – Distorted Support Indication
NDF - No Degradation Found
NDD - No Detectable Degradation
NI - Not Inspected
SAI- Signal Axial Indication

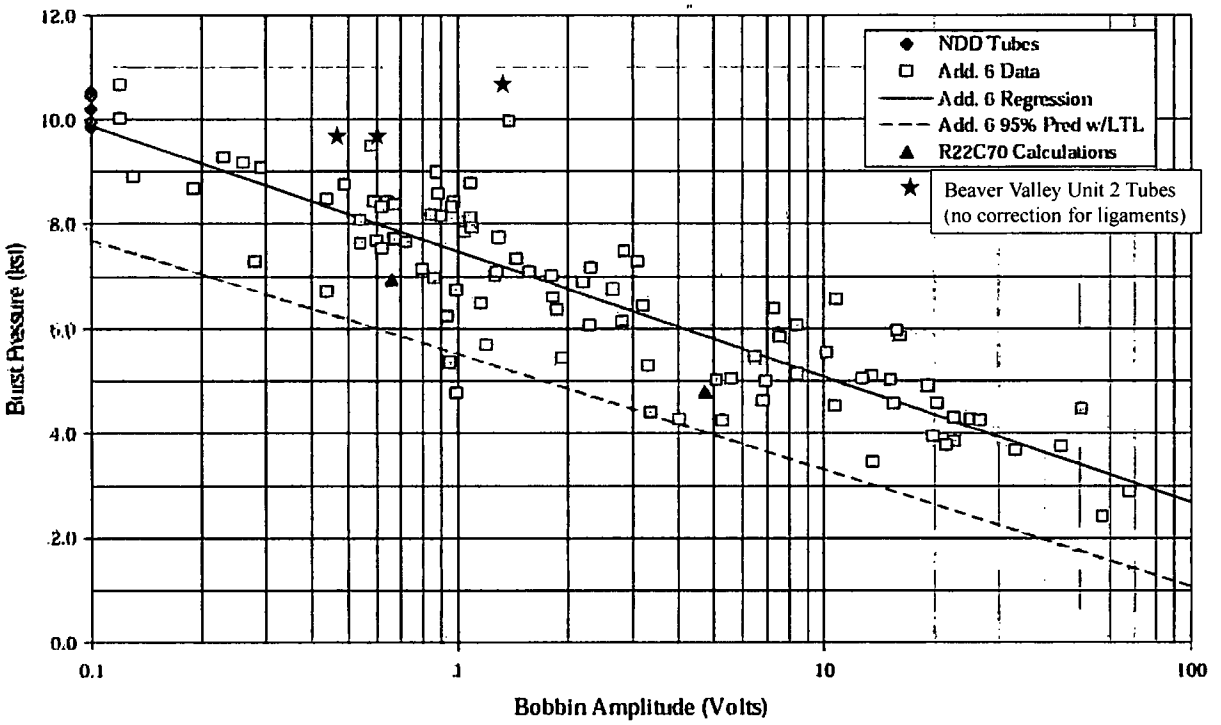

Figure 11-1: ARC Database: Burst Pressure vs. Volts for 7/8" OD Alloy 600 SG Tubes

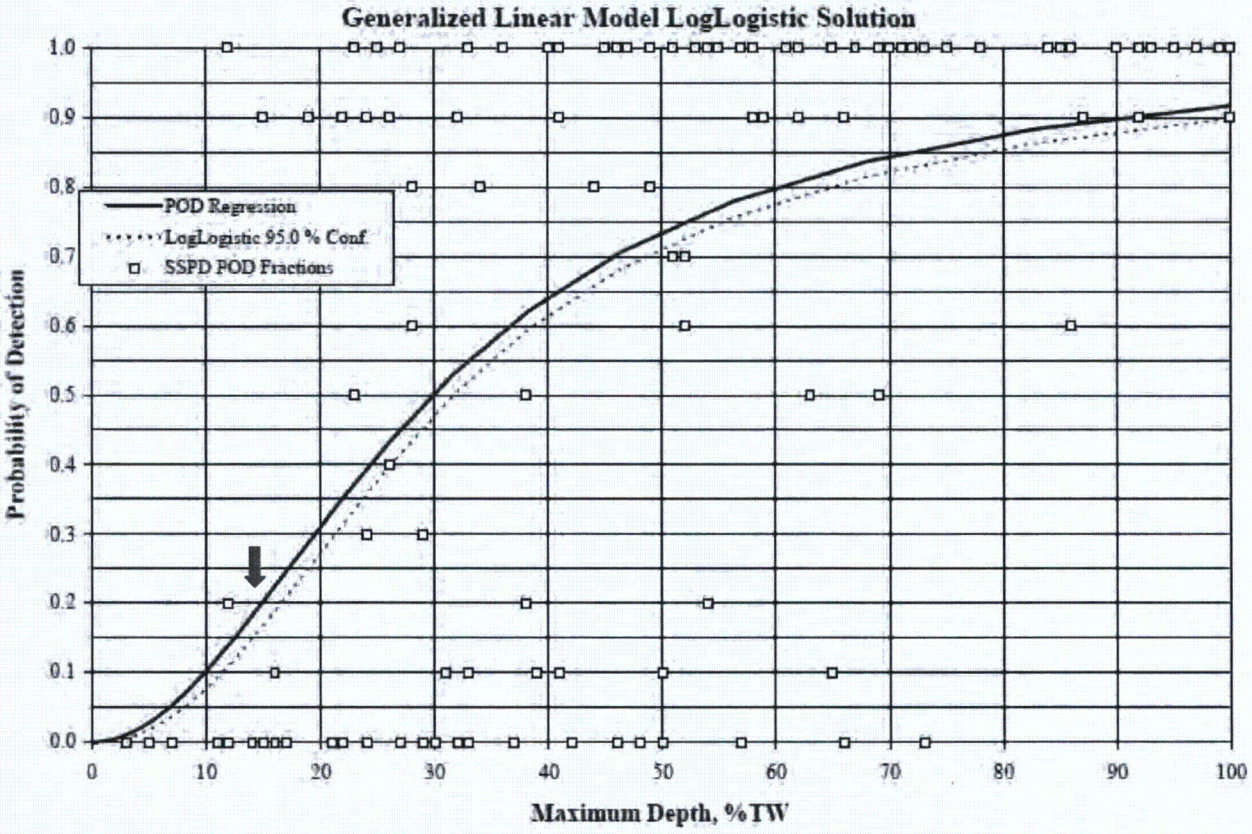

Figure 11-2: Detection Probability for Bobbin Coil Technique ETSS I28411

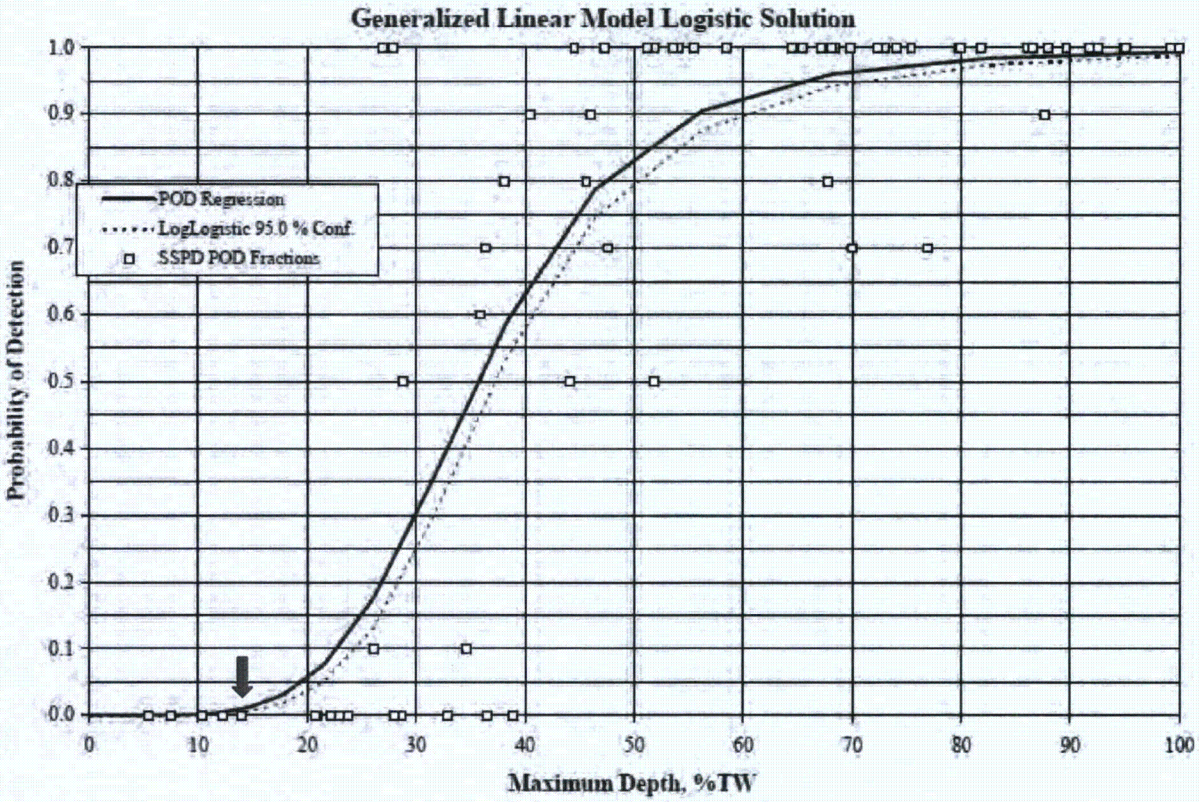

Figure 11-3: Detection Probability for +Point Technique ETSS I28424

12.0 REFERENCES

1. NRC Generic Letter 95-05, "Voltage-Based Repair Criteria for Westinghouse Steam Generator Tubes Affected by Outside Diameter Stress Corrosion Cracking," USNRC Office of Nuclear Reactor Regulation, August 3, 1995.
2. "Beaver Valley Unit 2 End-of-Cycle 17 Analysis and Prediction for End-of-Cycle 18 Voltage-Based Repair Criteria 90-Day Report," SG-SGMP-14-17, Revision 1, July 2014.
3. "Industry Recommended Steam Generator Tube Pull Program," NRC Adams Accession Number ML003678700, January 28, 2000.
4. FENOC Task Authorization, P.O. 47320244, February 28, 2014.
5. Attachment 1 to "Westinghouse Offer to Provide the Steam Generator Services for Beaver Valley Unit 2 (DMW) 2R17 in the Spring of 2014," LTR-AMER-MKG-13-599, Revision 4, March 6, 2014.
6. "Interim Report: Examination of Steam Generator Tubes Removed from Beaver Valley Unit 2," SG-CCOE-14-1, Revision 0, July 2014.
7. "Beaver Valley Unit 2 Post-Tube Pull Eddy Current Testing (ECT) Results," LTR-SGMP-14-49, June 23, 2014.
8. "Beaver Valley Unit 2 Model 51M Steam Generator Secondary Side Tube Support Plate Elevations for Eddynet Confirmation," DLC-98-768 / NSD-CPM-98-142, August 25, 1998.
9. "Beaver Valley Power Station Unit 2 2R17 Steam Generator Condition Monitoring Evaluation," SG-SGMP-14-14, Revision 0, May 2014.
10. "Transmittal of LTR-CCOE-14-54 'Pulled Tubes Receipt'," FENOC-14-41, June 3, 2014.
11. [ ]^{a,c}
12. Starrett Dial Caliper Model 120-A, S/N 06295903, Equipment #30009308, Calibration Record #0010775617, Exelon Power Labs. Test Date 8/14/13, Calibration Due Date 8/14/14.
13. "Bobbin 24 IPS ETSS," DMW-02-14, Revision 0, March 2014.
14. "3 Coil +PT ETSS," DMW-05-14, Revision 0, March 2014.
15. "Ghent G3/G4 ETSS," DMW-12-14, Revision 0, March 2014.
16. "Beaver Valley Power Station Unit 2 Steam Generator Examination Guidelines," ISIE1-8, Revision 15, April 2014.
17. "Beaver Valley Unit 2 Post-Tube Pull Non-Destructive Examination (NDE) Eddy Current Instructions," LTR-SGMP-14-44, Revision 1, June 20, 2014.
18. "Beaver Valley Power Station Unit 2 2R17 Refueling Outage Steam Generator Degradation Assessment," SG-SGMP-14-4, March 2014.
19. "Steam Generator Program Guidelines," NEI 97-06 Revision 3, March 2011.

20. "Steam Generator Management Program: Steam Generator Integrity Assessment Guidelines," Revision 3. EPRI, Palo Alto, CA: 2009. 1019038.

21. [ ]a,c

22. "Steam Generator Tubing Burst Testing and Leak Rate Testing Guidelines," Revision 0. EPRI, Palo Alto, CA: 2002. 1006783.

23. [ ]a,c

24. "Steam Generator Information Report," LTR-SGDA-11-189, Revision 0, August 2011.

25. [ ]a,c

26. "Standard Test Methods for Tension Testing of Metallic Materials," ASTM E8/E8M-13a, 2013.

27. "Beaver Valley Unit 1 Steam Generator Tube Examination," SG-SGDA-02-19, Revision 0, December 2002.

28. "Post Service Examination of Tubes R11C48 and R16C60 from a Beaver Valley-1 Steam Generator," TR-MCC-191, Revision 0, April 1992.

29. "Examination of Beaver Valley Unit 1 Hot Leg Steam Generator Tubes," 95-5TE2-BVRTB-R1, September 1995.

30. "Steam Generator Tubing Outside Diameter Stress Corrosion Cracking at Tube Support Plates Database for Alternate Repair Limits," Addendum 7 to NP-7480-L Database. EPRI, Palo Alto, CA: 2008. 1018047.

31. Dirats Laboratories, Report Number R589753, August 28, 2014.

32. "Specification for Nickel-Chromium-Iron Alloy (UNS N06600) Seamless Pipe and Tube," SB-167, ASME Boiler and Pressure Vessel Code, ANSI/ASME BPV-II, 1977.

33. "Standard Test Methods for Determining Average Grain Size," ASTM E112-13, October 1, 2013.

34. [ ]a,c

35. "Detecting Susceptibility to Intergranular Attack in Austenitic Stainless Steel," ASTM A262-14, July 1, 2014.

36. [ ]a,c

APPENDIX A - CRACK DEPTH PROFILE DATA

R19C38 – 02H (Sample 3B2A)

Axial Position Above Bottom End of Sample (mils)	Crack Depth (%TW)	Ligament Orientation Compared to Crack Face	Ligament Uncorroded Area ($mils^2$)	Ligament Depth (%TW)
0	0.0			
4.86	0.0			
6.65	11.2			
11.01	14.4			
15.97	17.5			
21.09	23.3			
26.51	29.2			
31.12	33.0			
36.03	30.8			
40.62	30.9			
45.53	32.5			
50.43	39.8			
55.48	38.4			
60.48	39.7			
65.76	44.2			
70.73	44.0			
75.98	43.8			
80.68	38.1			
85.39	34.4			
90.84	23.1	Out of Plane	123.65	13
95.18	9.2			
99.64	15.2			
104.67	20.8			
109.58	21.6			
114.50	12.0			
118.82	0.0			
123.75	0.0			
129.04	20.6	In-Plane	37.44	14
133.97	26.2			
138.39	32.3			
143.26	36.4			
148.04	31.5			

Axial Position Above Bottom End of Sample (mils)	Crack Depth (%TW)	Ligament Orientation Compared to Crack Face	Ligament Uncorroded Area ($mils^2$)	Ligament Depth (%TW)
153.15	20.0			
157.93	8.2			
163.08	26.0	In-Plane	68.80	19
168.21	26.6			
173.01	34.5			
177.81	36.7			
182.41	34.5			
187.10	33.3			
192.07	28.1	Out of Plane	275.32	24
197.00	24.1			
202.01	0.0			
211.93	0.0			
216.56	16.0			
221.40	22.2	Out of Plane	14.42	15
226.41	26.4			
231.59	24.8			
236.24	17.0			
240.87	11.4			
245.64	0.0			
394.82	0.0			
399.52	11.7			
404.38	11.7	Out of Plane	26.56	10
410.13	8.4			
414.63	0.0			
429.26	0.0			
434.96	25.1			
439.82	27.5			
444.83	27.1			
449.65	29.2			
454.69	26.6			
458.87	26.0			
463.61	27.3			
468.80	28.3			
473.31	29.4			
477.89	30.2			

Axial Position Above Bottom End of Sample (mils)	Crack Depth (%TW)	Ligament Orientation Compared to Crack Face	Ligament Uncorroded Area ($mils^2$)	Ligament Depth (%TW)
482.86	29.8			
487.71	31.4			
493.02	31.6			
497.57	31.9			
502.68	30.6			
507.67	39.2	Out of Plane	128.28	19
512.44	42.5			
517.51	37.7			
522.78	35.6			
528.03	32.5			
532.56	29.2			
537.32	28.5			
542.48	31.5			
547.86	31.6			
553.20	36.1			
558.14	36.8			
562.98	39.6			
567.92	41.6			
573.36	44.2			
578.49	42.9			
583.21	46.9			
587.93	48.0			
592.75	46.6			
597.06	49.4			
602.70	48.4			
607.72	49.9			
612.75	48.7			
617.46	48.5			
622.30	47.7			
626.90	47.8			
631.99	43.0			
637.29	39.1	Out of Plane	32.72	11
642.06	41.8			
646.66	41.1			
651.75	43.6			

Axial Position Above Bottom End of Sample (mils)	Crack Depth (%TW)	Ligament Orientation Compared to Crack Face	Ligament Uncorroded Area ($mils^2$)	Ligament Depth (%TW)
656.65	42.8			
661.71	43.6			
666.78	41.4			
671.96	38.1			
675.92	40.6			
681.31	41.9			
686.43	44.6	Out of Plane	29.27	18
692.12	41.9			
697.11	31.7			
701.86	18.6			
706.95	0.0			
876.50	0.0			
994.91	0.0			
1123.15	0.0			
1208.99	0.0			

R24C41 – 04H (Sample 6B2A)

Axial Position Above Bottom End of Sample (mils)	Crack Depth (%TW)	Ligament Orientation Compared to Crack Face	Ligament Uncorroded Area ($mils^2$)	Ligament Depth (%TW)
0.00	0.0			
163.20	0.0			
299.25	0.0			
454.50	0.0			
483.33	0.0			
487.24	6.0			
492.40	13.8			
497.75	13.9			
502.61	16.7			
507.67	20.2	Out of Plane	40.33	14
512.59	22.1			
517.48	22.9			
522.81	24.3			
527.86	22.2			
532.35	22.3			
537.78	25.9			
543.18	28.0			
548.00	33.5			
553.37	32.5			
558.67	20.2			
563.34	30.0			
568.61	37.6			
573.76	43.4			
579.08	42.7			
584.05	40.3			
589.03	40.2			
594.22	41.9			
598.88	43.0			
603.65	44.7			
608.52	43.6			
614.99	40.2			
619.55	48.1			
624.54	48.4			
629.75	48.6			

Axial Position Above Bottom End of Sample (mils)	Crack Depth (%TW)	Ligament Orientation Compared to Crack Face	Ligament Uncorroded Area (mils^2)	Ligament Depth (%TW)
634.57	46.5			
640.38	46.7			
645.34	46.0			
650.81	42.7			
655.64	43.6			
660.57	44.9			
665.22	46.4			
669.91	37.8	Out of Plane	18.14	19
675.37	35.7			
680.82	39.1			
685.83	38.1			
691.28	31.7			
696.97	17.8			
702.07	17.2			
706.74	21.2			
711.95	17.0			
717.11	15.2			
722.37	14.9			
727.86	14.2			
732.92	13.1	Out of Plane	16.31	13
738.29	15.7			
742.83	12.2			
747.99	11.8			
753.63	0.0			
898.54	0.0			
1038.66	0.0			
1154.26	0.0			
1229.63	0.0			
1325.34	0.0			

Enclosure B
L-15-091

Affidavit for Examination of Steam Generator Tubes Removed from Beaver Valley Unit 2, Proprietary Information Notice, and Copyright Notice

(6 Pages Follow)

CAW-15-4153
March 30, 2015

AFFIDAVIT

COMMONWEALTH OF PENNSYLVANIA:

ss

COUNTY OF BUTLER:

I, James A. Gresham, am authorized to execute this Affidavit on behalf of Westinghouse Electric Company LLC (Westinghouse), and that the averments of fact set forth in this Affidavit are true and correct to the best of my knowledge, information, and belief.

James A. Gresham, Manager
Regulatory Compliance

(1) I am Manager, Regulatory Compliance, Westinghouse Electric Company LLC (Westinghouse), and as such, I have been specifically delegated the function of reviewing the proprietary information sought to be withheld from public disclosure in connection with nuclear power plant licensing and rule making proceedings, and am authorized to apply for its withholding on behalf of Westinghouse.

(2) I am making this Affidavit in conformance with the provisions of 10 CFR Section 2.390 of the Commission's regulations and in conjunction with the Westinghouse Application for Withholding Proprietary Information from Public Disclosure accompanying this Affidavit.

(3) I have personal knowledge of the criteria and procedures utilized by Westinghouse in designating information as a trade secret, privileged or as confidential commercial or financial information.

(4) Pursuant to the provisions of paragraph (b)(4) of Section 2.390 of the Commission's regulations, the following is furnished for consideration by the Commission in determining whether the information sought to be withheld from public disclosure should be withheld.

(i) The information sought to be withheld from public disclosure is owned and has been held in confidence by Westinghouse.

(ii) The information is of a type customarily held in confidence by Westinghouse and not customarily disclosed to the public. Westinghouse has a rational basis for determining the types of information customarily held in confidence by it and, in that connection, utilizes a system to determine when and whether to hold certain types of information in confidence. The application of that system and the substance of that system constitute Westinghouse policy and provide the rational basis required.

Under that system, information is held in confidence if it falls in one or more of several types, the release of which might result in the loss of an existing or potential competitive advantage, as follows:

(a) The information reveals the distinguishing aspects of a process (or component, structure, tool, method, etc.) where prevention of its use by any of

Westinghouse's competitors without license from Westinghouse constitutes a competitive economic advantage over other companies.

(b) It consists of supporting data, including test data, relative to a process (or component, structure, tool, method, etc.), the application of which data secures a competitive economic advantage, e.g., by optimization or improved marketability.

(c) Its use by a competitor would reduce his expenditure of resources or improve his competitive position in the design, manufacture, shipment, installation, assurance of quality, or licensing a similar product.

(d) It reveals cost or price information, production capacities, budget levels, or commercial strategies of Westinghouse, its customers or suppliers.

(e) It reveals aspects of past, present, or future Westinghouse or customer funded development plans and programs of potential commercial value to Westinghouse.

(f) It contains patentable ideas, for which patent protection may be desirable.

(iii) There are sound policy reasons behind the Westinghouse system which include the following:

(a) The use of such information by Westinghouse gives Westinghouse a competitive advantage over its competitors. It is, therefore, withheld from disclosure to protect the Westinghouse competitive position.

(b) It is information that is marketable in many ways. The extent to which such information is available to competitors diminishes the Westinghouse ability to sell products and services involving the use of the information.

(c) Use by our competitor would put Westinghouse at a competitive disadvantage by reducing his expenditure of resources at our expense.

(d) Each component of proprietary information pertinent to a particular competitive advantage is potentially as valuable as the total competitive advantage. If competitors acquire components of proprietary information, any one component may be the key to the entire puzzle, thereby depriving Westinghouse of a competitive advantage.

(e) Unrestricted disclosure would jeopardize the position of prominence of Westinghouse in the world market, and thereby give a market advantage to the competition of those countries.

(f) The Westinghouse capacity to invest corporate assets in research and development depends upon the success in obtaining and maintaining a competitive advantage.

(iv) The information is being transmitted to the Commission in confidence and, under the provisions of 10 CFR Section 2.390, it is to be received in confidence by the Commission.

(v) The information sought to be protected is not available in public sources or available information has not been previously employed in the same original manner or method to the best of our knowledge and belief.

(vi) The proprietary information sought to be withheld in this submittal is that which is appropriately marked in SG-CCOE-14-4-P, Revision 1, "Examination of Steam Generator Tubes Removed from Beaver Valley Unit 2" (Proprietary), for submittal to the Commission, being transmitted by the FirstEnergy Nuclear Operating Company letter and Application for Withholding Proprietary Information from Public Disclosure, to the Document Control Desk. The proprietary information as submitted by Westinghouse is that associated with steam generator manufacturing parameters and test setup methodology, and may be used only for that purpose.

(a) This information is part of that which will enable Westinghouse to:

(i) Provide steam generator design, testing and licensing defense services to utilities worldwide.

(b) Further this information has substantial commercial value as follows:

(i) Westinghouse plans to sell the use of similar information to its customers for the purpose of offering steam generator design, testing and licensing defense services.

(ii) Westinghouse can sell support and defense of industry guidelines and acceptance criteria for plant-specific applications.

(iii) The information requested to be withheld reveals the distinguishing aspects of a methodology which was developed by Westinghouse.

Public disclosure of this proprietary information is likely to cause substantial harm to the competitive position of Westinghouse because it would enhance the ability of competitors to provide similar steam generator design, testing and licensing defense services for commercial power reactors without commensurate expenses. Also, public disclosure of the information would enable others to use the information to meet NRC requirements for licensing documentation without purchasing the right to use the information.

The development of the technology described in part by the information is the result of applying the results of many years of experience in an intensive Westinghouse effort and the expenditure of a considerable sum of money.

In order for competitors of Westinghouse to duplicate this information, similar technical programs would have to be performed and a significant manpower effort, having the requisite talent and experience, would have to be expended.

Further the deponent sayeth not.

PROPRIETARY INFORMATION NOTICE

Transmitted herewith are proprietary and non-proprietary versions of documents furnished to the NRC in connection with steam generator manufacturing parameters and test setup methodology, and may be used only for that purpose.

In order to conform to the requirements of 10 CFR 2.390 of the Commission's regulations concerning the protection of proprietary information so submitted to the NRC, the information which is proprietary in the proprietary versions is contained within brackets, and where the proprietary information has been deleted in the non-proprietary versions, only the brackets remain (the information that was contained within the brackets in the proprietary versions having been deleted). The justification for claiming the information so designated as proprietary is indicated in both versions by means of lower case letters (a) through (f) located as a superscript immediately following the brackets enclosing each item of information being identified as proprietary or in the margin opposite such information. These lower case letters refer to the types of information Westinghouse customarily holds in confidence identified in Sections (4)(ii)(a) through (4)(ii)(f) of the Affidavit accompanying this transmittal pursuant to 10 CFR 2.390(b)(1).

COPYRIGHT NOTICE